Chapter 4
Special Topics

4.1 Deep Potentials Falling off Faster than $1/r^2$ Asymptotically

As already discussed in Chap. 2, the characteristic features of scattering by a potential, in particular at near-threshold energies, depend crucially on whether its fall-off at large distances is faster or slower than $1/r^2$. In contrast to long-range Coulombic potentials, which support infinite Rydberg series of bound states if the Coulombic tail is attractive, potentials falling off faster than $1/r^2$ support at most a finite number of bound states. A special situation arises if the potential falls off faster than $1/r^2$, while being so deep that the number of bound states is very large. In this case, there is a range of energies around threshold, excluding the immediate near-threshold regime, where semiclassical approximations are quite accurate and able to describe the systematics of scattering phase shifts and bound-state energy progressions. In the immediate near-threshold regime, however, quantum mechanical effects, as typically expressed in Wigner's threshold law, are dominant. An accurate treatment of deep potentials falling off faster than $1/r^2$ must include a reliable account of this extreme quantum regime in the immediate vicinity of the threshold.

Since the transition between the semiclassical regime away from threshold and the extreme quantum regime at threshold is most easily demonstrated for the bound states below threshold, we start with the theory of near-threshold quantization in Sect. 4.1.1. Above-threshold continuum states are treated in the subsequent subsections on quantum reflection (Sect. 4.1.2) and scattering (Sect. 4.1.3). The treatment in Sects. 4.1.1 to 4.1.3 is restricted to the case of vanishing angular momentum. The implications of nonvanishing angular momentum are explained in Sect. 4.1.4.

4.1.1 Near-Threshold Quantization

Consider a potential $V(r)$ which falls off faster than $1/r^2$ at large distances and is so deeply attractive at small distances that it supports a large, albeit finite number

H. Friedrich, *Scattering Theory*, DOI 10.1007/978-3-662-48526-2_4

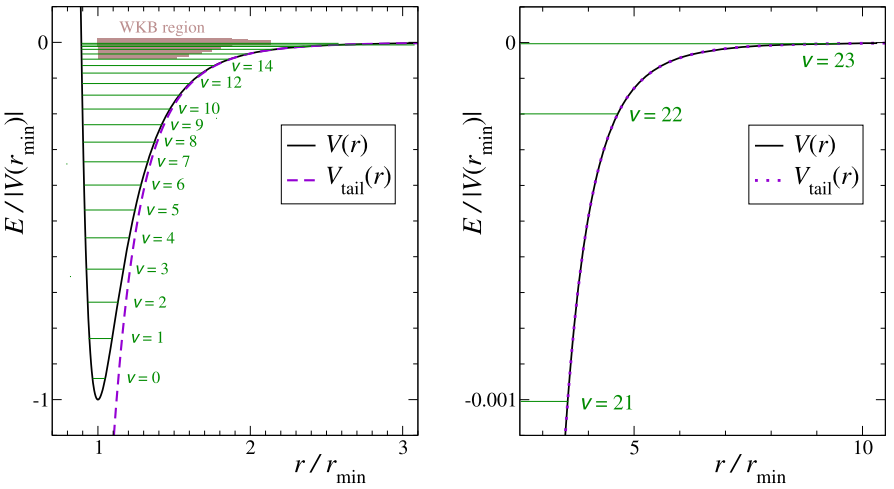

Fig. 4.1 Deep potential falling off faster than $1/r^2$ at large distances. The example is actually the Lennard–Jones potential (2.298) with $B_{\mathrm{LJ}} = 10^4$, which supports 24 bound states, $\upsilon = 0, 1, 2, \ldots, 23$. The brown shaded area in the left-hand panel schematically indicates where the WKB approximation is accurate at near-threshold energies

of bound states. An example with 24 bound states is shown in Fig. 4.1. Since such potentials typically describe the interatomic interaction in diatomic molecules, we adopt the molecular physics notation and use the letter "υ" for "vibrational" to label the bound states. The potential in Fig. 4.1 actually corresponds to the Lennard–Jones potential (2.298) already discussed in Sect. 2.6.5, and the dimensionless parameter B_{LJ}, which is defined by Eq. (2.299) and determines the quantum mechanical properties of the potential, is $B_{\mathrm{LJ}} = 10^4$ in the present case. The theory below is, however, very general and does not rely on any special properties of the potential, except that it should be deep and fall off faster than $1/r^2$ at large distances.

In the bound-state regime, the total energy is negative and related to the asymptotic inverse penetration depth κ by

$$E = -\frac{\hbar^2\kappa^2}{2\mu}. \tag{4.1}$$

Since the potential is deep, a total energy near threshold implies that the kinetic energy is large in a region of r-values between the inner classical turning point $r_{\mathrm{in}}(E)$ and the outer classical turning point $r_{\mathrm{out}}(E)$. This justifies the assumption, that there is a "WKB region" between $r_{\mathrm{in}}(E)$ and $r_{\mathrm{out}}(E)$, where the condition formulated as Eq. (2.141) in Sect. 2.4.1 is well fulfilled, so the solution of the radial Schrödinger equation is accurately given by the WKB representation,

$$u(r) \propto \frac{1}{\sqrt{p(E;r)}} \cos\left[\frac{1}{\hbar}\int_{r_{\mathrm{in}}(E)}^{r} p\big(E;r'\big)\mathrm{d}r' - \frac{\phi_{\mathrm{in}}(E)}{2}\right]. \tag{4.2}$$

For vanishing angular momentum, the local classical momentum (2.136) is

$$p(E;r) = \sqrt{2\mu\big[E - V(r)\big]}; \tag{4.3}$$

it is real and positive in the classically allowed region $V(r) < E$. The phase $\phi_{\rm in}(E)$ is the reflection phase at the classical turning point $r_{\rm in}(E)$, as introduced in Sect. 2.4.2, see Eq. (2.145). Reflection phases are chosen to be $\frac{\pi}{2}$ in conventional WKB theory [11, 55], but allowing them to depend on energy makes it possible to use WKB wave functions to derive results which are highly accurate, or even exact, far away from the semiclassical limit [35]. The condition that the right-hand side of (4.2) accurately represents the exact wave function $u(r)$ for r-values in the WKB region defines $\phi_{\rm in}(E)$.

An alternative and equally valid WKB representation of $u(r)$ is obtained by choosing the outer classical turning point $r_{\rm out}(E)$ as point of reference:

$$u(r) \propto \frac{1}{\sqrt{p(E;r)}} \cos\left[\frac{1}{\hbar}\int_r^{r_{\rm out}(E)} p\big(E;r'\big)\mathrm{d}r' - \frac{\phi_{\rm out}(E)}{2}\right], \tag{4.4}$$

and $\phi_{\rm out}(E)$ is the reflection phase at $r_{\rm out}(E)$. Compatibility of (4.2) and (4.4) requires that the argument of the cosines be equal modulo π, up to a sign, for all r-values in the WKB region. This leads to a quantization condition for the bound-state energies E_υ:

$$\frac{1}{\hbar}\int_{r_{\rm in}(E_\upsilon)}^{r_{\rm out}(E_\upsilon)} p(E_\upsilon;r)\mathrm{d}r = \upsilon\pi + \frac{\phi_{\rm in}(E_\upsilon)}{2} + \frac{\phi_{\rm out}(E_\upsilon)}{2}, \quad \upsilon \text{ integer.} \tag{4.5}$$

If we take both reflection phases to be equal to $\frac{\pi}{2}$, then the right-hand side of (4.5) becomes $(\upsilon + \frac{1}{2})\pi$, as in the conventional Bohr-Sommerfeld quantization rule [55].

At threshold, $E = 0$, the condition (4.5) with integer υ is fulfilled only if there is a bound state exactly at threshold. For the general case, we write

$$\frac{1}{\hbar}\int_{r_{\rm in}(0)}^{\infty} p(E=0;r)\mathrm{d}r = \upsilon_{\rm D}\pi + \frac{\phi_{\rm in}(0)}{2} + \frac{\phi_{\rm out}(0)}{2}, \tag{4.6}$$

where $\upsilon_{\rm D}$ is the *threshold quantum number*, which is in general non-integer. The present theory is especially suited for the description of diatomic molecules or molecular ions, where the bound-to-continuum threshold is the dissociation threshold, hence the subscript "D".

Subtracting Eq. (4.5) from (4.6) yields the *quantization rule*,

$$\upsilon_{\rm D} - \upsilon = F(E_\upsilon), \tag{4.7}$$

with the *quantization function* $F(E)$ given by

$$F(E) = \frac{1}{\pi\hbar}\left[\int_{r_{\text{in}}(0)}^{\infty} p(0;r)\mathrm{d}r - \int_{r_{\text{in}}(E)}^{r_{\text{out}}(E)} p(E;r)\mathrm{d}r\right] - \frac{\phi_{\text{in}}(0)-\phi_{\text{in}}(E)}{2\pi} - \frac{\phi_{\text{out}}(0)-\phi_{\text{out}}(E)}{2\pi}. \tag{4.8}$$

By definition, $F(E)$ vanishes at threshold,

$$F(E=0) = 0. \tag{4.9}$$

Since the bound-state energies form a discrete finite set, it is always possible to find a smooth function $F(E)$ with (4.9) such that (4.7) is fulfilled at all bound-state energies E_υ. The explicit expression (4.8) is trivially valid, if we allow appropriate values of $\phi_{\text{in}}(E)$ and $\phi_{\text{out}}(E)$. If, at a given energy E, there is a WKB region between the inner and outer classical turning points where the WKB approximation is sufficiently accurate, then the reflection phases $\phi_{\text{in}}(E)$ and $\phi_{\text{out}}(E)$ can be determined precisely via (4.2) and (4.4), respectively.

The leading near-threshold energy dependence of the quantization function (4.8) is a property of the large-distance behaviour of the potential. To be specific, we assume that the potential is accurately given at large distances by a reference potential, the "tail potential" $V_{\text{tail}}(r)$,

$$V(r) \overset{r \text{ large}}{\sim} V_{\text{tail}}(r). \tag{4.10}$$

As reference potential, $V_{\text{tail}}(r)$ is defined for all $r > 0$, but it only represents the true interaction for large distances. The phrase "r large" over the "$\sim$" sign in (4.10) has been chosen deliberately in order to emphasize that, in general, it is not just the leading asymptotic behaviour of $V(r)$ that is important. The radial Schrödinger equation with the reference potential $V_{\text{tail}}(r)$ alone and vanishing angular momentum reads

$$-\frac{\hbar^2}{2\mu}\frac{\mathrm{d}^2u}{\mathrm{d}r^2} + V_{\text{tail}}(r)u(r) = Eu(r). \tag{4.11}$$

Being an approximation to the full potential at large distances, the reference potential $V_{\text{tail}}(r)$ falls off faster than $1/r^2$ for $r \to \infty$. At small distances, the full interaction is not well described by the reference potential $V_{\text{tail}}(r)$, and its precise form is usually not well known anyhow. In the following we choose $V_{\text{tail}}(r)$ such that it diverges to $-\infty$ more rapidly than $-1/r^2$ for $r \to 0$. This has the advantage that the WKB representations of the solutions of (4.11), at any energy E, become increasingly accurate for decreasing r and are, in fact, exact in the limit $r \to 0$. This can be confirmed by verifying that the quantality function (2.139) vanishes for $r \to 0$ when the potential is more singular than $1/r^2$ in this limit.

As for the repulsive inverse-power potentials discussed in Sect. 2.4.2, the proximity to the semiclassical or anticlassical limits can be estimated via the value of a typical classically defined action in units of $\hbar$. Such a classical action is provided by

the product of the momentum-like quantity $\hbar\kappa$ and the outer classical turning point $r_{\rm out}(E)$, which is the same for the full interaction and for the reference potential $V_{\rm tail}(r)$ at near-threshold energies and diverges to infinity at threshold,

$$r_{\rm out}(E) \overset{\kappa\to 0}{\longrightarrow} \infty. \tag{4.12}$$

The typical action $\hbar\kappa r_{\rm out}(E)$ in units of $\hbar$ is thus $\kappa r_{\rm out}(E)$, a quantity that has been called the "reduced classical turning point" [85]. With $r^2 V_{\rm tail}(r) \overset{r\to\infty}{\longrightarrow} 0$ it follows from (4.12) that

$$\begin{aligned} \big|V_{\rm tail}\big(r_{\rm out}(E)\big)\big| r_{\rm out}(E)^2 = \frac{\hbar^2\kappa^2}{2\mu} r_{\rm out}(E)^2 \overset{\kappa\to 0}{\longrightarrow} 0 \\ \Longrightarrow \quad \kappa r_{\rm out}(E) \overset{\kappa\to 0}{\longrightarrow} 0. \end{aligned} \tag{4.13}$$

The threshold $E = 0$ represents the anticlassical or extreme quantum limit of the Schrödinger equation (4.11). For the singular attractive reference potential $V_{\rm tail}(r)$, the outer classical turning point moves towards the origin for $E \to -\infty$,

$$r_{\rm out}(E) \overset{\kappa\to\infty}{\longrightarrow} 0, \tag{4.14}$$

and with $r^2 V_{\rm tail}(r) \overset{r\to 0}{\longrightarrow} -\infty$ it follows that

$$\big|V_{\rm tail}\big(r_{\rm out}(E)\big)\big| r_{\rm out}(E)^2 = \frac{\hbar^2\kappa^2}{2\mu} r_{\rm out}(E)^2 \overset{\kappa\to\infty}{\longrightarrow} \infty \quad \Longrightarrow \quad \kappa r_{\rm out}(E) \overset{\kappa\to\infty}{\longrightarrow} \infty. \tag{4.15}$$

The semiclassical limit of the Schrödinger equation (4.11) is at $\kappa \to \infty$, i.e. for large binding energies. How close the semiclassical limit is approached in a realistic potential well depends on its depth.

The quantization function (4.8) contains a contribution $F_{\rm tail}(E)$, which is determined solely by the reference potential $V_{\rm tail}(r)$,

$$\begin{aligned} F_{\rm tail}(E) = \lim_{r_{\rm in}\to 0} \frac{1}{\pi\hbar}\left[\int_{r_{\rm in}}^{r_{\rm out}(0)} p_{\rm tail}(0;r)\mathrm{d}r - \int_{r_{\rm in}}^{r_{\rm out}(E)} p_{\rm tail}(E;r)\mathrm{d}r\right] \\ - \frac{\phi_{\rm out}(0) - \phi_{\rm out}(E)}{2\pi}, \end{aligned} \tag{4.16}$$

where $p_{\rm tail}$ is the local classical momentum defined with $V_{\rm tail}(r)$,

$$p_{\rm tail}(E;r) = \sqrt{2\mu\big[E - V_{\rm tail}(r)\big]}. \tag{4.17}$$

As the inner classical turning point $r_{\rm in}$ tends to zero, the action integrals in (4.16) actually diverge, but their difference remains well defined in the limit. The tail part (4.16) of the quantization function contains no contribution from the inner reflection phases, because the wave functions become independent of energy for $r \to 0$ so the difference $\phi_{\rm in}(0) - \phi_{\rm in}(E)$ vanishes for $r_{\rm in} \to 0$.

In addition to the tail contribution $F_{\text{tail}}(E)$, the quantization function contains a contribution $F_{\text{sr}}(E)$ arising from the deviation of the full interaction from the reference potential $V_{\text{tail}}(r)$ at small distances:

$$F(E) = F_{\text{tail}}(E) + F_{\text{sr}}(E). \tag{4.18}$$

Since the full quantization function $F(E)$ vanishes at threshold according to (4.9), and since $F_{\text{tail}}(E = 0)$ is obviously zero, the same must hold for $F_{\text{sr}}(E = 0)$. Furthermore, $F_{\text{sr}}(E)$ is defined in the short-range region of the potential, where the bound-to-continuum threshold is not an outstanding value of the energy, so it must be a smooth function of energy near threshold. Hence we can write

$$F_{\text{sr}}(E) \overset{\kappa \to 0}{\sim} \gamma_{\text{sr}} E + O\left(E^2\right), \tag{4.19}$$

where γ_{sr} is a constant with the dimension of an inverse energy.

As will be seen in the following, the leading near-threshold behaviour of $F_{\text{tail}}(E)$ is of lower order than E, so this is also the leading near-threshold behaviour of the full quantization function $F(E)$. The short-range contribution $F_{\text{sr}}(E)$ is of higher order, namely $O(E)$, and its magnitude depends on how accurately the reference potential $V_{\text{tail}}(r)$ describes the full interaction at finite distances. Its influence is small if $V_{\text{tail}}(r)$ is a good approximation of the full interaction down to distances where the WKB representation, on which the definition of $F_{\text{tail}}(E)$ is based, accurately describes the solutions of Eq. (4.11). Since the WKB approximation breaks down at the outer classical turning point $r_{\text{out}}(E)$, this implies that the reference potential be a good approximation of the full interaction down to distances somewhat smaller than $r_{\text{out}}(E)$.

If the quantization function is known accurately for a reasonable range of near-threshold energies, then a small number of energy eigenvalues in this range can be used to complement the spectrum and extrapolate to the dissociation threshold. This can, for example, make it possible to reliably predict the energy of the dissociation threshold from the relative separations of a few observed energy levels some distance away from threshold.

With the quantization function decomposed into a tail contribution and a short-range part as in (4.18), and with the ansatz (4.19) for the short-range part, the quantization rule (4.7) can be rewritten as

$$\upsilon + F_{\text{tail}}(E_\upsilon) = \upsilon_{\text{D}} - F_{\text{sr}}(E) \overset{E \to 0}{\sim} \upsilon_{\text{D}} - \gamma_{\text{sr}} E_\upsilon. \tag{4.20}$$

As expressed on the far right of (4.20), the effects of the short-range deviation of the full interaction from the reference potential $V_{\text{tail}}(r)$ are contained in two parameters, the threshold quantum number υ_{D} and the short-range correction coefficient γ_{sr}; the next term is of order E^2. According to (4.20), a plot of $\upsilon + F_{\text{tail}}(E_\upsilon)$ against E_υ should approach a straight-line behaviour towards threshold; υ_{D} and γ_{sr} can be deduced from the interception of this line with the ordinate and the gradient of the line, respectively.

The decomposition (4.18) of the full quantization function into a tail contribution and a short-range part and the representation (4.20) of the quantization rule are always valid. There is *no* semiclassical approximation involved, even though the tail contribution $F_{\rm tail}(E)$ to the quantization function is expressed in tems of WKB wave functions. For the short-range correction term to be small, however, the deviation of the full interaction from the reference potential $V_{\rm tail}(r)$ should be restricted to sufficiently small distances, at which the WKB representations of the solutions of Eq. (4.11) are accurate.

The near-threshold behaviour of $F_{\rm tail}(E)$ is crucially determined by the near-threshold energy dependence of the outer reflection phase. This can be derived under very general conditions, as described in detail in [76] and summarized below.

The solution of (4.11) obeying bound state boundary conditions,

$$u^{(\kappa)}(r) \overset{r\to\infty}{\sim} \mathrm{e}^{-\kappa r}, \tag{4.21}$$

is accurately the represented for $r \to 0$ by the WKB expression

$$u^{(\kappa)}(r) \overset{r\to 0}{\sim} \frac{\mathscr{D}(\kappa)}{\sqrt{p_{\rm tail}(E;r)}} \cos\left(\frac{1}{\hbar}\int_r^{r_{\rm out}(E)} p_{\rm tail}\big(E;r'\big)\mathrm{d}r' - \frac{\phi_{\rm out}(E)}{2}\right). \tag{4.22}$$

Guided by the derivation of the effective-range expansion in Sect. 2.3.8, we introduce two wave functions $u^{(\kappa)}(r)$ and $u^{(0)}(r)$ which solve Eq. (4.11) at the energies $E = -\hbar^2\kappa^2/(2\mu)$ and $E = 0$, respectively. We also introduce two solutions $w^{(\kappa)}$ and $w^{(0)}$, which have the same large-r boundary conditions, but are solutions of the free equation, without $V_{\rm tail}(r)$,

$$\begin{aligned} &w^{(\kappa)}(r) = \mathrm{e}^{-\kappa r}, \qquad w^{(0)}(r) \equiv 1, \\ &u^{(\kappa)}(r) \overset{r\to\infty}{\sim} w^{(\kappa)}(r), \qquad u^{(0)}(r) \overset{r\to\infty}{\sim} w^{(0)}(r). \end{aligned} \tag{4.23}$$

From the radial Schrödinger equation we obtain

$$\int_{r_l}^{r_u} \big(u^{(\kappa)}u^{(0)\prime\prime} - u^{(\kappa)\prime\prime}u^{(0)}\big)\mathrm{d}r = \big[u^{(\kappa)}u^{(0)\prime} - u^{(\kappa)\prime}u^{(0)}\big]_{r_l}^{r_u} = -\kappa^2 \int_{r_l}^{r_u} u^{(\kappa)}u^{(0)}\mathrm{d}r \tag{4.24}$$

for arbitrary lower and upper integration limits r_l and r_u. The contribution of the upper integration limit r_u to the square bracket in the middle part of (4.24) vanishes in the limit $r_u \to \infty$, because of the exponential decay of $u^{(\kappa)}(r)$ at large r. The contribution from the lower integration limit r_l follows from the WKB representation of the wave function (4.22) and its derivative,

$$\begin{aligned} u^{(\kappa)\prime}(r) = \frac{\mathscr{D}(\kappa)}{\sqrt{p_{\rm tail}(E;r)}}\Bigg[&-\frac{1}{2}\frac{p'_{\rm tail}(E;r)}{p_{\rm tail}(E;r)} \cos\left(\frac{1}{\hbar}\int_r^{r_{\rm out}(E)} p_{\rm tail}\big(E;r'\big)\mathrm{d}r' - \frac{\phi_{\rm out}(E)}{2}\right) \\ &+ \frac{p_{\rm tail}(E;r)}{\hbar} \sin\left(\frac{1}{\hbar}\int_r^{r_{\rm out}(E)} p_{\rm tail}\big(E;r'\big)\mathrm{d}r' - \frac{\phi_{\rm out}(E}{2}\right)\Bigg]. \end{aligned} \tag{4.25}$$

Equations (4.22) and (4.25) also apply for $u^{(0)}$ if we insert $E = 0$. Since $V_{\text{tail}}(r)$ is more singular than $-1/r^2$ at the origin, $1/p_{\text{tail}}(E;r)$ vanishes faster than r, and the contributions from the cosine in (4.25) to the products $u^{(\kappa)}u^{(0)\prime}$ and $u^{(\kappa)\prime}u^{(0)}$ in (4.24) vanish for $r_l \to 0$. With the abbreviations

$$S_{\text{tail}}(E) = \int_{r_l}^{r_{\text{out}}(E)} p_{\text{tail}}(E;r)\mathrm{d}r, \qquad I_\kappa = \frac{S_{\text{tail}}(E)}{\hbar} - \frac{\phi_{\text{out}}(E)}{2} \tag{4.26}$$

we obtain from (4.22) and (4.25)

$$\left[u^{(\kappa)}u^{(0)\prime} - u^{(\kappa)\prime}u^{(0)}\right]_{r_l\to 0} = \frac{\mathscr{D}(\kappa)\mathscr{D}(0)}{\hbar}\sin(I_0 - I_\kappa)\Big|_{r_l\to 0} = -\kappa^2\int_0^\infty u^{(\kappa)}u^{(0)}\mathrm{d}r. \tag{4.27}$$

For the free-particle solutions we obtain

$$\left[w^{(\kappa)}w^{(0)\prime} - w^{(\kappa)\prime}w^{(0)}\right]_{r_l}^{r_u} = -\kappa^2\int_{r_l}^{r_u} w^{(\kappa)}w^{(0)}\mathrm{d}r. \tag{4.28}$$

Again, the contributions from r_u vanish for $r_u \to \infty$ while the contribution from r_l is

$$\left[w^{(\kappa)}w^{(0)\prime} - w^{(\kappa)\prime}w^{(0)}\right]_{r_l\to 0} = \kappa = -\kappa^2\int_0^\infty w^{(\kappa)}w^{(0)}\mathrm{d}r. \tag{4.29}$$

Combining (4.27) and (4.29) gives

$$\begin{aligned}
&\frac{\mathscr{D}(\kappa)\mathscr{D}(0)}{\hbar}\sin(I_0 - I_\kappa)\\
&= \frac{\mathscr{D}(\kappa)\mathscr{D}(0)}{\hbar}\sin\left(\frac{S_{\text{tail}}(0) - S_{\text{tail}}(E)}{\hbar} - \frac{\phi_{\text{out}}(0) - \phi_{\text{out}}(E)}{2}\right)\\
&= \kappa + \kappa^2\int_0^\infty \left[u^{(\kappa)}(r)u^{(0)}(r) - w^{(\kappa)}(r)w^{(0)}(r)\right]\mathrm{d}r.
\end{aligned} \tag{4.30}$$

Resolving for $\phi_{\text{out}}(E)$ gives

$$\frac{\phi_{\text{out}}(E)}{2} = \frac{\phi_{\text{out}}(0)}{2} - \frac{S_{\text{tail}}(0) - S_{\text{tail}}(E)}{\hbar} + \arcsin\left[\frac{\kappa - \rho(E)\kappa^2}{\mathscr{D}(0)\mathscr{D}(\kappa)/\hbar}\right], \tag{4.31}$$

with the length $\rho(E)$ defined by

$$\rho(E) = \int_0^\infty \left[w^{(\kappa)}(r)w^{(0)}(r) - u^{(\kappa)}(r)u^{(0)}(r)\right]\mathrm{d}r. \tag{4.32}$$

The action integrals $S_{\text{tail}}(0)$ and $S_{\text{tail}}(E)$ diverge as the lower integration limit tends to zero, but the difference $S_{\text{tail}}(0) - S_{\text{tail}}(E)$ tends to a well defined value in this limit.

In order to account correctly for the contributions of order κ^2 in the arcsin term in (4.31), it is necessary to know the zero-energy limit of $\rho(E)$,

$$\rho(0) = \int_0^\infty \left[\left(w^{(0)}(r)\right)^2 - \left(u^{(0)}(r)\right)^2\right] \mathrm{d}r \stackrel{\text{def}}{=} \rho_{\text{eff}}, \tag{4.33}$$

as well as the behaviour of $\mathscr{D}(\kappa)$ up to first order in κ. This can be obtained, as described in [35], on the basis of the two linearly independent threshold ($E = 0$) solutions $u_0^{(0)}(r)$ and $u_1^{(0)}(r)$ of the Schrödinger equation (4.11) which are defined by the following large-r boundary conditions,

$$u_0^{(0)}(r) \overset{r\to\infty}{\sim} 1, \qquad u_1^{(0)}(r) \overset{r\to\infty}{\sim} r. \tag{4.34}$$

For $r \to 0$, these wave functions can be written as WKB waves,

$$u_{0,1}^{(0)}(r) \overset{r\to 0}{\sim} \frac{D_{0,1}}{\sqrt{p_{\text{tail}}(0;r)}} \cos\left(\frac{1}{\hbar}\int_r^\infty p_{\text{tail}}(0;r')\mathrm{d}r' - \frac{\phi_{0,1}}{2}\right), \tag{4.35}$$

which exactly defines the amplitudes $D_{0,1}$ and the phases $\phi_{0,1}$. The amplitude D_0 is the threshold value $\mathscr{D}(0)$ of the amplitude defined in (4.22), and ϕ_0 is the threshold value of the outer reflection phase $\phi_{\text{out}}(E)$. For small but nonvanishing values of κ, the solution $u^{(\kappa)}(r)$ obeying the bound-state boundary condition (4.21) is given, up to and including the first order in κ, by

$$u^{(\kappa)}(r) \overset{\kappa r\to 0}{\sim} u_0^{(0)}(r) - \kappa u_1^{(0)}(r) \overset{r\to\infty}{\sim} 1 - \kappa r. \tag{4.36}$$

The WKB representation of the wave function (4.36), which is valid for small r and exact in the limit $r \to 0$, follows via (4.35),

$$\begin{aligned} u^{(\kappa)}(r) &\overset{r\to 0}{\sim} \frac{D_0}{\sqrt{p_{\text{tail}}(0;r)}}\left[\cos\left(\frac{S_{\text{tail}}(0)}{\hbar} - \frac{\phi_0}{2}\right) - \frac{D_1}{D_0}\kappa\cos\left(\frac{S_{\text{tail}}(0)}{\hbar} - \frac{\phi_1}{2}\right)\right] \\ &= \frac{D_0}{\sqrt{p_{\text{tail}}(0;r)}}\left[1 - \frac{D_1}{D_0}\kappa\cos\left(\frac{\phi_0-\phi_1}{2}\right)\right] \\ &\quad \times \cos\left(\frac{S_{\text{tail}}(0)}{\hbar} - \frac{\phi_1}{2} - \frac{D_1}{D_0}\kappa\sin\left(\frac{\phi_0-\phi_1}{2}\right)\right) + O\left(\kappa^2\right). \end{aligned} \tag{4.37}$$

Comparing amplitude and phase of the right-hand sides of (4.22) and (4.37) gives

$$\mathscr{D}(\kappa) = D_0\left[1 - \frac{D_1}{D_0}\kappa\cos\left(\frac{\phi_0-\phi_1}{2}\right)\right] + O\left(\kappa^2\right), \tag{4.38}$$

$$\frac{\phi_{\text{out}}(E)}{2} = \frac{\phi_0}{2} - \frac{S_{\text{tail}}(0) - S_{\text{tail}}(E)}{\hbar} + b\kappa + O\left(\kappa^2\right), \tag{4.39}$$

with the length b in (4.39) defined as

$$b = \frac{D_1}{D_0}\sin\left(\frac{\phi_0-\phi_1}{2}\right). \tag{4.40}$$

Expanding the arcsin term on the right-hand side of (4.31) gives the near-threshold expansion of the outer reflection phase up to and including second order in κ as

$$\frac{\phi_{\text{out}}(E)}{2} \overset{\kappa\to 0}{\sim} \frac{\phi_{\text{out}}(0)}{2} - \frac{S_{\text{tail}}(0) - S_{\text{tail}}(E)}{\hbar} + b\kappa - \frac{(d\kappa)^2}{2}; \tag{4.41}$$

the length d is defined by

$$\frac{d^2}{2} = b(\rho_{\text{eff}} - \bar{a}) \quad \text{with} \quad \bar{a} = \frac{D_1}{D_0}\cos\left(\frac{\phi_0 - \phi_1}{2}\right) = b\cot\left(\frac{\phi_0 - \phi_1}{2}\right). \tag{4.42}$$

In deriving (4.41) we compared the linear terms in (4.31) and (4.39) to deduce $\hbar/\mathscr{D}(0)^2 = b$.

Away from threshold, $\kappa \to \infty$, the outer reflection phase approaches its semiclassical limit $\frac{\pi}{2}$. A measure for the proximity to the semiclassical limit is given by the reduced classical turning point $\kappa r_{\text{out}}(E)$, see discussion involving Eqs. (4.12) to (4.15) above, so it is reasonable to assume that the leading high-κ behaviour of the outer reflection phase is given by

$$\phi_{\text{out}}(E) \overset{\kappa\to\infty}{\sim} \frac{\pi}{2} + \frac{D}{\kappa r_{\text{out}}(E)}, \tag{4.43}$$

with some dimensionless constant D characteristic for the reference potential $V_{\text{tail}}(r)$.

A remarkable feature of the near-threshold expansion (4.41) of the outer reflection phase is, that the term containing the difference of the action integrals exactly cancels the corresponding contribution to the quantization function, as represented by the big square bracket in the expression (4.16). The near-threshold behaviour of $F_{\text{tail}}(E)$ is thus given by

$$F_{\text{tail}}(E) \overset{\kappa\to 0}{\sim} \frac{b\kappa}{\pi} - \frac{(d\kappa)^2}{2\pi}. \tag{4.44}$$

The leading term on the right-hand side of (4.44), linear in κ, is reminiscent of Wigner's threshold law for s-waves. Since the short-range correction $F_{\text{sr}}(E)$ is of order E at threshold, this term also represents the leading energy dependence of the full quantization function $F(E)$:

$$F(E) \overset{\kappa\to 0}{\sim} \frac{b\kappa}{\pi}, \tag{4.45}$$

which is universally valid for all potentials falling off faster than $1/r^2$ at large distances. The second term on the right-hand side of (4.44), quadratic in κ, is only well defined for reference potentials falling off faster than $1/r^3$, see the paragraph after Eq. (4.53) below.

For a potential $V(r)$ falling off faster than $1/r^3$ at large distances, the s-wave scattering length a diverges when the threshold quantum number υ_{D} is an integer, i.e. when there is an s-wave bound state exactly at threshold, see Eq. (2.88) in

Sect. 2.3.8. The derivation above enables us to formulate an explicit relation connecting the scattering length a with the threshold quantum number υ_{D}.

The asymptotic behaviour of the regular solution $u(r)$ of the Schrödinger equation with the full potential $V(r)$ is, according to Eqs. (2.83) and (4.34),

$$u(r) \overset{r\to\infty}{\propto} 1 - \frac{r}{a} \quad \Longrightarrow \quad u(r) \overset{r \text{ large}}{\propto} u_0^{(0)}(r) - \frac{1}{a} u_1^{(0)}(r). \tag{4.46}$$

The phrase "r large" refers to distances which are large enough for the full potential to be well approximated by $V_{\mathrm{tail}}(r)$ and at the same time small enough for the WKB representations (4.35) to be accurate representations of $u_0^{(0)}(r)$ and $u_1^{(0)}(r)$. For such values of r,

$$\begin{aligned} u(r) &\propto \frac{D_1}{\sqrt{p(0;r)}} \cos\left(\frac{1}{\hbar}\int_r^\infty p\big(0;r'\big)\mathrm{d}r' - \frac{\phi_1}{2}\right) \\ &\quad - \frac{aD_0}{\sqrt{p(0;r)}} \cos\left(\frac{1}{\hbar}\int_r^\infty p\big(0;r'\big)\mathrm{d}r' - \frac{\phi_0}{2}\right) \\ &\propto \frac{1}{\sqrt{p(0;r)}} \cos\left(\frac{1}{\hbar}\int_r^\infty p\big(0;r'\big)\mathrm{d}r' - \frac{\phi_+}{4} - \eta\right), \end{aligned} \tag{4.47}$$

with the angles $\phi_\pm$ and η given by

$$\phi_\pm = \phi_0 \pm \phi_1, \qquad \tan\eta = \frac{a + D_1/D_0}{a - D_1/D_0} \tan\left(\frac{\phi_-}{4}\right). \tag{4.48}$$

Taking the inner classical turning point as reference gives

$$u(r) \propto \frac{1}{\sqrt{p(0;r)}} \cos\left(\frac{1}{\hbar}\int_{r_{\mathrm{in}}(0)}^r p\big(0;r'\big)\mathrm{d}r' - \frac{\phi_{\mathrm{in}}(0)}{2}\right), \tag{4.49}$$

and compatibility of (4.47) and (4.49) implies

$$\frac{1}{\hbar}\int_{r_{\mathrm{in}}(0)}^\infty p(0;r)\mathrm{d}r = \frac{\phi_{\mathrm{in}}(0)}{2} + \eta + \frac{\phi_+}{4} \pmod{\pi}. \tag{4.50}$$

Comparison with (4.6) gives

$$\eta = \upsilon_{\mathrm{D}}\pi + \frac{\phi_-}{4} \pmod{\pi}. \tag{4.51}$$

Resolving the second equation (4.48) for a and inserting (4.51) for η yields

$$\begin{aligned} a &= \frac{D_1}{D_0} \frac{\tan(\upsilon_{\mathrm{D}}\pi + \frac{\phi_-}{4}) + \tan(\frac{\phi_-}{4})}{\tan(\upsilon_{\mathrm{D}}\pi + \frac{\phi_-}{4}) - \tan(\frac{\phi_-}{4})} \\ &= \frac{D_1}{D_0} \sin\left(\frac{\phi_-}{2}\right)\left[\frac{1}{\tan(\frac{\phi_-}{2})} + \frac{1}{\tan(\upsilon_{\mathrm{D}}\pi)}\right]. \end{aligned} \tag{4.52}$$

In terms of the parameters b and $\bar{a}$ as defined in Eqs. (4.40) and (4.42), this relation simplifies to

$$a = \bar{a} + \frac{b}{\tan(\upsilon_D \pi)} = \bar{a} + \frac{b}{\tan(\Delta_D \pi)}, \quad \Delta_D = \upsilon_D - \lfloor \upsilon_D \rfloor. \tag{4.53}$$

Equation (4.53) is very fundamental, giving an explicit relation between the s-wave scattering length a and the threshold quantum number υ_D. Because of the periodicity of the tangent, it is actually only the *remainder* Δ_D that counts. The remainder can assume values between zero and unity and quantifies the proximity of the most weakly bound state to threshold. A value of Δ_D very close to zero indicates a bound state very close to threshold, while a value very close to unity indicates that the potential just fails to support a further bound state.

Equation (4.53) enables a physical interpretation of the parameters entering the derivation of the expression (4.44) for the near-threshold behaviour of the tail contribution $F_{\text{tail}}(E)$ of the quantization function. In an ensemble of potentials characterized by evenly distributed values of the remainder Δ_D, the values of the scattering length will be evenly distributed around the mean value $\bar{a}$, hence $\bar{a}$ is called the *mean scattering length*, a term first introduced by Gribakin and Flambaum in [36]. We call the length b, which determines the leading term in the near-threshold behaviour (4.44) of the quantization function and the second term on the right-hand side of (4.53), the *threshold length*. The definition (4.33) of ρ_{eff} resembles, except for a factor two, the definition (2.103) of the effective range r_{eff} in Sect. 2.3.8, and we call it the *subthreshold effective range*. Note however, that the wave functions $u^{(0)}$ and $w^{(0)}$ that enter in the definition of ρ_{eff} remain bounded for $r \to \infty$, according to (4.23), so the expression (4.33) gives a well defined value for ρ_{eff} for any reference potential falling off faster than $1/r^3$ at large distances. The length d, which defines the next-to-leading term in the near-threshold behaviour (4.44) of the quantization function, is related to the mean scattering length $\bar{a}$, the threshold length b and the subthreshold effective range ρ_{eff} via the first equation (4.42). We use the term *effective length* for the parameter d.

The relation (4.53) makes it possible to extend Eq. (2.88), which relates the asymptotic inverse penetration depth κ_b of a bound state very near threshold to the scattering length, to the next order in $1/\kappa_b$. With the quantization rule (4.7) we can rewrite (4.53) as

$$a = \bar{a} + \frac{b}{\tan[\pi F(E_b)]} = \bar{a} + \frac{b}{\tan[\pi (F_{\text{tail}}(E_b) + F_{\text{sr}}(E_b))]}, \tag{4.54}$$

where $E_b = -\hbar^2 \kappa_b^2/(2\mu)$ is the energy of the very weakly bound state. Replacing $F_{\text{sr}}(E_b)$ by its leading term $\gamma_{\text{sr}} E_b$ according to (4.19) and using the leading two terms of the Taylor expansion of the tangent yields [76]

$$a = \frac{1}{\kappa_b} + \rho_{\text{eff}} + \pi \frac{\hbar^2 \gamma_{\text{sr}}}{2\mu b} + O(\kappa_b). \tag{4.55}$$

It is interesting to observe, that the next-to-leading term in the expansion (4.55), i.e. the term of order κ_b^0, is *not* the mean scattering length $\bar{a}$, as one might guess from Eq. (4.53) [36], but the subthreshold effective range ρ_{eff}, *plus* a contribution which comes from short-range effects and is proportional to the constant γ_{sr}. In this light, one might ask what sense it makes to extend the near-threshold expansion (4.44) of $F_{\text{tail}}(E)$ up to second order in κ, when short-range effects bring in a term of the same order. The answer lies in the observation, that the length scales associated with the potential tail are generally very large, so that both ρ_{eff} and b are much larger than typical length scales associated with γ_{sr}. The dimensionless ratio $\pi\gamma_{\text{sr}}\hbar^2/(2\mu b\rho_{\text{eff}})$ of the third term on the right-hand side of (4.55) to the second term is thus usually very small, see also Example 1 below. Furthermore, a clean identification of the tail function $F_{\text{tail}}(E)$ over the whole range of energies from threshold to $-\infty$ is a prerequisite for the identification of the short-range correction $F_{\text{sr}}(E)$ due to the deviation of the full interaction from the reference potential at small distances.

At energies far from threshold, $\kappa \to \infty$, the outer reflection phase approaches its semiclassical limit according to (4.43), so the leading high-κ behaviour of $F_{\text{tail}}(E)$ is,

$$F_{\text{tail}}(E) \overset{\kappa\to\infty}{\sim} \frac{S_{\text{tail}}(0) - S_{\text{tail}}(E)}{\pi\hbar} - \left(\frac{\phi_0}{2\pi} - \frac{1}{4}\right) + \frac{D/(2\pi)}{\kappa r_{\text{out}}(E)}. \tag{4.56}$$

The zero-energy value ϕ_0 of the outer reflection phase, the lengths defining its low-κ expansion (4.41), i.e. b, $\bar{a}$, ρ_{eff} and d, and the parameter D in (4.43), (4.56) are *tail parameters*; they are properties of the reference potential $V_{\text{tail}}(r)$ alone. For a reference potential V_{tail} for which the Schrödinger equation (4.11) has analytically known solutions at threshold, $E = 0$, the tail parameters can be derived analytically. The exact behaviour of $F_{\text{tail}}(E)$ in between the near-threshold regime and the high-κ, semiclassical regime is generally not known analytically, but it can be calculated numerically by a straightforward evaluation of Eq. (4.16).

The application of the theory described in this section is particularly elegant for potentials with a large-distance behaviour that is well described by a single-power tail,

$$V_{\text{tail}}(r) \equiv V_\alpha^{\text{att}}(r) = -\frac{C_\alpha}{r^\alpha} = -\frac{\hbar^2}{2\mu}\frac{(\beta_\alpha)^{\alpha-2}}{r^\alpha}, \quad C_\alpha > 0,\ \alpha > 2. \tag{4.57}$$

As for the repulsive inverse-power potentials (2.160) discussed in Sect. 2.4.2, the potential strength coefficient C_α in (4.57) is expressed in terms of the characteristic quantum length

$$\beta_\alpha = \left(\frac{2\mu C_\alpha}{\hbar^2}\right)^{1/(\alpha-2)}, \tag{4.58}$$

which does not exist in classical mechanics. The beauty of single-power reference potentials (4.57) is that the properties of the solution of the Schrödinger equation (4.11) depend only on the dimensionless product $\kappa\beta_\alpha$ and not on energy and potential strength independently, see Appendix A.2. For example, the reduced classical

Table 4.1 Numerical values of tail parameters for single-power reference potentials (4.57), as given analytically in (4.61). The last row contains the values of the dimensionless parameter B_o governing the exponential fall-off of the modulus of the amplitude for quantum reflection according to (4.93) in Sect. 4.1.2

α	3	4	5	6	7	$\alpha \to \infty$
ϕ_0	$\frac{3}{2}\pi$	π	$\frac{5}{6}\pi$	$\frac{6}{8}\pi$	$\frac{7}{10}\pi$	$(\frac{1}{2}+\frac{1}{\alpha-2})\pi$
b/β_α	$\frac{3}{2}$	1	0.6313422	0.4779888	0.3915136	$\frac{1}{\alpha-2}\pi$
$\bar{a}/\beta_\alpha$	–	0	0.3645056	0.4779888	0.5388722	1
$\rho_{\rm eff}/\beta_\alpha$	–	$\frac{\pi}{3}$	0.7584176	0.6973664	0.6826794	1
d/β_α	–	$\sqrt{\frac{2\pi}{3}}$	0.7052564	0.4579521	0.3355665	$\frac{6.43}{(\alpha-2)^{3/2}}$
D	0.8095502	0.5462620	0.4554443	0.4089698	0.3806186	$\frac{1}{12}\pi$
B_o	2.24050	1.69443	1.35149	1.12025	0.95450	$\frac{2}{\alpha}\pi$

turning point is given by

$$\kappa r_{\rm out}(E) = (\kappa\beta_\alpha)^{1-2/\alpha}, \tag{4.59}$$

and the difference of the action integrals appearing in (4.16), (4.56) is

$$\begin{aligned}\lim_{r_{\rm in}\to 0}\frac{1}{\pi\hbar}\left[\int_{r_{\rm in}}^{\infty} p_{\rm tail}(0;r)\mathrm{d}r - \int_{r_{\rm in}}^{r_{\rm out}(E)} p_{\rm tail}(E;r)\mathrm{d}r\right]\\ = \frac{(\kappa\beta_\alpha)^{1-2/\alpha}}{(\alpha-2)\sqrt{\pi}}\frac{\Gamma(\frac{1}{2}+\frac{1}{\alpha})}{\Gamma(1+\frac{1}{\alpha})}.\end{aligned} \tag{4.60}$$

The tail parameters $\phi_{\rm out}(0) \equiv \phi_0$, b, $\bar{a}$, $\rho_{\rm eff}$ and d defining the low-κ expansion (4.41) of the outer reflection phase, and the parameter D in (4.43) are explicitly given for inverse-power tails (4.57) by [35, 76],

$$\begin{aligned}&\phi_0 = \left(\nu+\frac{1}{2}\right)\pi, \qquad \frac{b}{\beta_\alpha} = \nu^{2\nu}\frac{\Gamma(1-\nu)}{\Gamma(1+\nu)}\sin(\pi\nu),\\ &\frac{\bar{a}}{\beta_\alpha} = \nu^{2\nu}\frac{\Gamma(1-\nu)}{\Gamma(1+\nu)}\cos(\pi\nu),\\ &\frac{\rho_{\rm eff}}{\beta_\alpha} = \frac{\pi(2\nu)^{2\nu}\nu\Gamma(\frac{1}{2}+2\nu)}{\sin(\pi\nu)\Gamma(\frac{1}{2}+\nu)\Gamma(1+3\nu)}, \qquad D = \frac{\sqrt{\pi}}{12}\frac{\alpha+1}{\alpha}\frac{\Gamma(\frac{1}{2}-\frac{1}{\alpha})}{\Gamma(1-\frac{1}{\alpha})},\end{aligned} \tag{4.61}$$

with the abbreviation $\nu = 1/(\alpha-2)$. The expression for d follows from those for b, $\bar{a}$ and $\rho_{\rm eff}$ via (4.42). Numerical values are given in Table 4.1.

The behaviour of the outer reflection phase $\phi_{\rm out}(E)$ is illustrated in Fig. 4.2 for powers $\alpha = 3, \ldots, 7$. The abscissa is linear in $\kappa r_{\rm out} = (\kappa\beta_\alpha)^{1-2/\alpha}$, so the initial decrease is linear in the plot, compare (4.39) and (4.60). In contrast to the reflection phases for repulsive inverse-power potentials shown in Fig. 2.16 in Sect. 2.4.2, the threshold values ϕ_0 depend on the power α as given in the first equation (4.61).

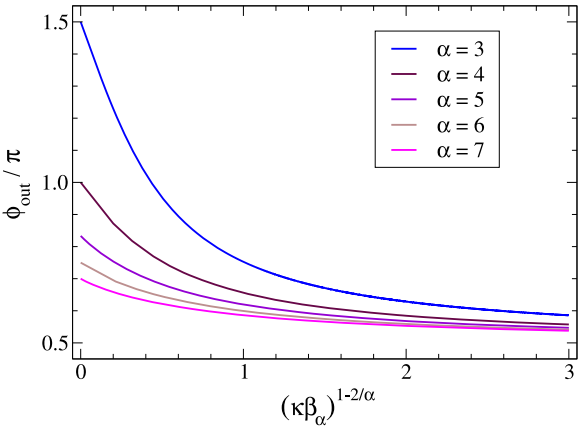

Fig. 4.2 Outer reflection phase ϕ_{out} for attractive inverse-power potentials (4.57) as function of the reduced classical turning point $\kappa r_{\text{out}} = (\kappa\beta_\alpha)^{1-2/\alpha}$. (Adapted from [85])

For a given power $\alpha > 2$, one quantization function $F_{\text{tail}}(E) \equiv F_\alpha(\kappa\beta_\alpha)$ applies for all potential strengths. An expression for $F_\alpha(\kappa\beta_\alpha)$ which is accurate all the way from threshold to the semiclassical limit of large κ, can be obtained by interpolating between the near-threshold expression (4.44) and the high-κ limit (4.56). With (4.59) and (4.60), the high-κ limit of $F_\alpha(\kappa\beta_\alpha)$ is,

$$F_\alpha(E) \overset{\kappa\to\infty}{\sim} \frac{(\kappa\beta_\alpha)^{1-2/\alpha}}{(\alpha-2)\sqrt{\pi}} \frac{\Gamma(\frac{1}{2}+\frac{1}{\alpha})}{\Gamma(1+\frac{1}{\alpha})} - \frac{1}{2(\alpha-2)} + \frac{D/(2\pi)}{(\kappa\beta_\alpha)^{1-2/\alpha}}. \tag{4.62}$$

For $\alpha = 6$, an analytical expression involving one dimensionless fitting parameter B was derived in [76],

$$F_{\alpha=6}(E) = \frac{2b\kappa - (d\kappa)^2}{2\pi[1+(\kappa B)^4]} + \frac{(\kappa B)^4}{1+(\kappa B)^4}\left[-\frac{1}{8} + \frac{D}{2\pi(\kappa\beta_6)^{2/3}} + \frac{\Gamma(\frac{2}{3})(\kappa\beta_6)^{2/3}}{4\sqrt{\pi}\,\Gamma(\frac{7}{6})}\right]. \tag{4.63}$$

All other parameters appearing in (4.63) are as given in Eq. (4.61) and Table 4.1 for $\alpha = 6$. With the value $B = 0.9363\beta_6$, the expression (4.63) reproduces the exact values, calculated by evaluating Eq. (4.16) numerically, to within an accuracy near 10^{-4} or better in the whole range from threshold to the high-κ limit [76].

For $\alpha = 4$, a more sophisticated treatment of the semiclassical, high-κ limit is needed to achieve a comparable accuracy on the basis of a small number of fitting parameters. An extension of the high-κ expansion (4.43) of the outer reflection phase to higher inverse powers of the reduced classical turning point $(\kappa\beta_4)^{1/2}$,

$$\phi_{\text{out}}(E) \overset{\kappa\beta_4\to\infty}{\sim} \frac{\pi}{2} + \sum_{j=1,3,5,7} \frac{D^{(j)}}{(\kappa\beta_4)^{j/2}}, \tag{4.64}$$

Table 4.2 Coefficients $D^{(j)}$ in the high-κ expansion (4.64) of the outer reflection phase for a $-1/r^4$ reference potential

$D^{(1)}$	$D^{(3)}$	$D^{(5)}$	$D^{(7)}$
$\frac{5\sqrt{\pi}}{48}\Gamma(\frac{1}{4})/\Gamma(\frac{3}{4})$	$-\frac{35\sqrt{\pi}}{384}\Gamma(\frac{3}{4})/\Gamma(\frac{1}{4})$	$\frac{475\sqrt{\pi}}{3584}\Gamma(\frac{5}{4})/\Gamma(-\frac{1}{4})$	$-\frac{63305\sqrt{\pi}}{221184}\Gamma(\frac{7}{4})/\Gamma(-\frac{3}{4})$
0.5462620	−0.0546027	−0.0434388	0.0964461

Table 4.3 Coefficients c_i, d_i in the expression (4.66) for $F_{\alpha=3}(E)$

i	c_i	d_i	i	c_i	d_i
1	8.198894514574	7.367727350550	5	185.465618264420	242.028021052411
2	38.229531850326	32.492317936470	6	141.484936909078	250.115055730896
3	85.724646494548	85.380005002970	7	60.927524697423	63.749260455229
4	147.081920247084	169.428485967491	8	56.372265754601	112.744531509202

leads to the following analytical expression based on two fitting parameters, the lengths B_6 and B_7,

$$F_{\alpha=4}(E) = \frac{[2b\kappa - (d\kappa)^2]/(2\pi)}{1+(\kappa B_6)^6+(\kappa B_7)^7} + \frac{(\kappa B_6)^6+(\kappa B_7)^7}{1+(\kappa B_6)^6+(\kappa B_7)^7} \times \left[-\frac{1}{4} + \frac{\Gamma(\frac{3}{4})}{\Gamma(\frac{5}{4})}\frac{(\kappa\beta_4)^{1/2}}{2\sqrt{\pi}} + \frac{D^{(1)}/(2\pi)}{(\kappa\beta_4)^{1/2}} + \frac{D^{(3)}/(2\pi)}{(\kappa\beta_4)^{3/2}} + \frac{D^{(5)}/(2\pi)}{(\kappa\beta_4)^{5/2}} + \frac{D^{(7)}/(2\pi)}{(\kappa\beta_4)^{7/2}}\right]. \tag{4.65}$$

The coefficients $D^{(j)}$, which determine the expansion (4.64), are given analytically and numerically in Table 4.2. With $B_6 = 1.622576\beta_4$ and $B_7 = 1.338059\beta_4$ for the fitted lengths, the expression (4.65) reproduces the exact values, calculated by evaluating Eq. (4.16) numerically, to within an accuracy near 10^{-4} or better in the whole range from threshold to the high-κ limit [77].

For $\alpha = 3$, it turned out to be more practical [62] to approximate $F_{\alpha=3}(E)$ by a rational function of the reduced classical turning point $(\kappa\beta_3)^{1/3}$,

$$F_{\alpha=3}(E) = \frac{\Gamma(\frac{5}{6})}{\sqrt{\pi}\,\Gamma(\frac{4}{3})}(\kappa\beta_3)^{1/3} + \frac{3+\sum_{i=1}^{i_{\max}} c_i(\kappa\beta_3)^{i/3}}{4+\sum_{i=1}^{i_{\max}} d_i(\kappa\beta_3)^{i/3}} - \frac{3}{4}. \tag{4.66}$$

With expansions up to $i_{\max} = 8$ in the numerator and the denominator of the second term on the right-hand side of (4.66), the formula is able to reproduce the exact quantization function, calculated by evaluating Eq. (4.16) numerically, to within an accuracy near $5\cdot 10^{-8}$ or better in the whole range from threshold to the high-κ limit [62]. The coefficients c_i and d_i with which this is achieved are listed in Table 4.3.

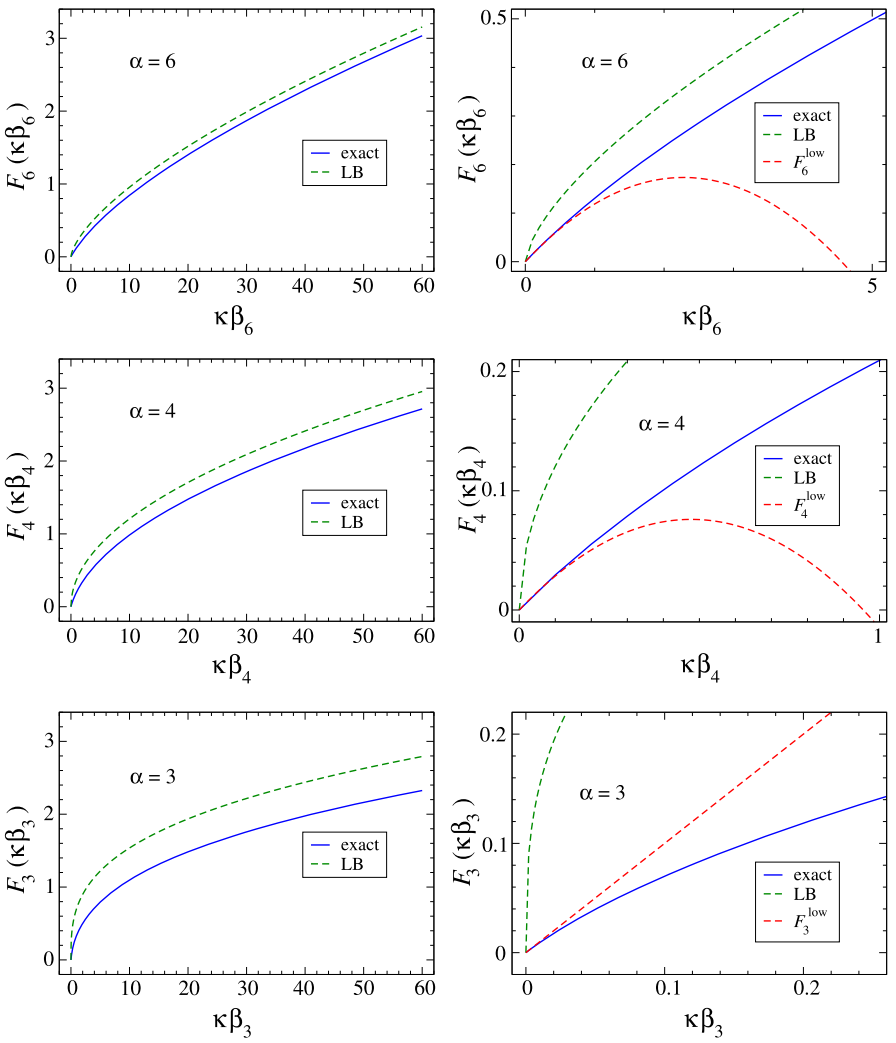

Fig. 4.3 Tail contribution $F_{\rm tail}(E) \equiv F_\alpha(\kappa\beta_\alpha)$ to the quantization function for single-power reference potentials (4.57). The *solid blue lines* are the exact results, which are accurately given by the expressions (4.63), (4.65) and (4.66) for $\alpha = 6, 4$ and 3, respectively. The *dashed green lines* show the LeRoy–Bernstein functions [52, 84], and the *dashed red lines* in the three panels on the right-hand side show the low-energy expansion (4.44) including both terms, linear and quadratic in $\kappa\beta_\alpha$ for $\alpha = 6$ and $\alpha = 4$ and only the leading linear term for $\alpha = 3$

The quantization functions (4.16) for the single-power tails (4.57) are shown for the cases $\alpha = 6, 4$ and 3 in Fig. 4.3 as functions of $\kappa\beta_\alpha$. The solid blue lines show exact functions, which are accurately approximated by the expressions (4.63), (4.65) and (4.66) all the way from threshold to the high-κ limit. The dashed green lines show the LeRoy–Bernstein functions $F_\alpha^{\rm LB}(E)$ [52, 84], which are obtained

by ignoring the contribution from the outer reflection phase in (4.16). The LeRoy–Bernstein function is given explicitly by the first term on the right-hand side of (4.62). It is wrong at threshold, because it misses the energy-dependence (4.41) cancelling the contribution from the action integrals, and it is also wrong in the high-κ, semiclassical limit, because it misses the contribution

$$\frac{\phi_{\rm out}(0)}{2\pi} - \frac{\pi/2}{2\pi} = \frac{1}{2(\alpha-2)}. \tag{4.67}$$

This leads to significant errors when extrapolating from bound-state energies to threshold, e.g. in order to determine the value of the dissociation threshold or of the scattering length from spectroscopic energies [62, 76, 77].

The dashed red lines in the three right-hand panels in Fig. 4.3 show the low-energy expansion (4.44) of $F_\alpha(E)$, including both terms, linear and quadratic in $\kappa\beta_\alpha$ for $\alpha = 6$ and $\alpha = 4$ and only the leading linear term for $\alpha = 3$. They allow us to estimate the extent of the near-threshold quantum regime. From the quantization rule (4.7) it is clear, that the value of $F(E_\upsilon)$ lies between zero and unity for the highest bound state with quantum number $\upsilon_{\rm max} = \lfloor \upsilon_{\rm D} \rfloor$, between one and two for the second-highest bound state with quantum number $\upsilon_{\rm max} - 1$, etc. The range covered in the left-hand panels of Fig. 4.3 thus only accommodates the highest three bound states of a potential with the respective single-power tail. The enlargements in the right-hand part of the figure show that the near-threshold linear behaviour of the quantization function is restricted to a very small energy range indeed; in the majority of cases, it does not even contain the highest bound state, and the second-highest bound state is definitely beyond the range of validity of the near-threshold expansion (4.44), even when the second term, quadratic in κ, is included in the examples $\alpha = 6$ and $\alpha = 4$. The range of validity of near-threshold, effective-range type expansions is *tiny*. Nevertheless, an accurate description of this near-threshold quantum regime and a reliable interpolation to the large-κ semiclassical regime are paramount to a practicable application of the quantization-function concept in realistic situations.

4.1.1.1 Example 1. The Lennard–Jones Potential

We consider again the Lennard–Jones potential,

$$V_{\rm LJ}(r) = \mathscr{E}\left[\left(\frac{r_{\rm min}}{r}\right)^{12} - 2\left(\frac{r_{\rm min}}{r}\right)^{6}\right], \tag{4.68}$$

which was already discussed in Sect. 2.6.5. The quantum mechanical properties of this potential are determined by the parameter $B_{\rm LJ} = \mathscr{E} 2\mu r_{\rm min}^2/\hbar^2$, see (2.299). The natural definition of the reference potential $V_{\rm tail}(r)$ in this case is

$$V_{\rm tail}(r) \equiv V_6^{\rm att}(r) = -2\mathscr{E}\frac{(r_{\rm min})^6}{r^6} = -\frac{\hbar^2}{2\mu}\frac{(\beta_6)^4}{r^6} \quad \text{with } \beta_6 = r_{\rm min}(2B_{\rm LJ})^{1/4}. \tag{4.69}$$

Table 4.4 Energies in units of $\mathscr{E}$ of the highest twelve bound states in the Lennard–Jones potential (4.68) with $B_{\rm LJ} = 10^4$ [72]

υ	E_υ	υ	E_υ	υ	E_υ
12	−0.115225890999	16	−0.031813309316	20	−0.003047136244
13	−0.087766914229	17	−0.020586161356	21	−0.001052747695
14	−0.064982730497	18	−0.012350373216	22	−0.000198340301
15	−0.046469911358	19	−0.006657024344	23	−0.000002696883

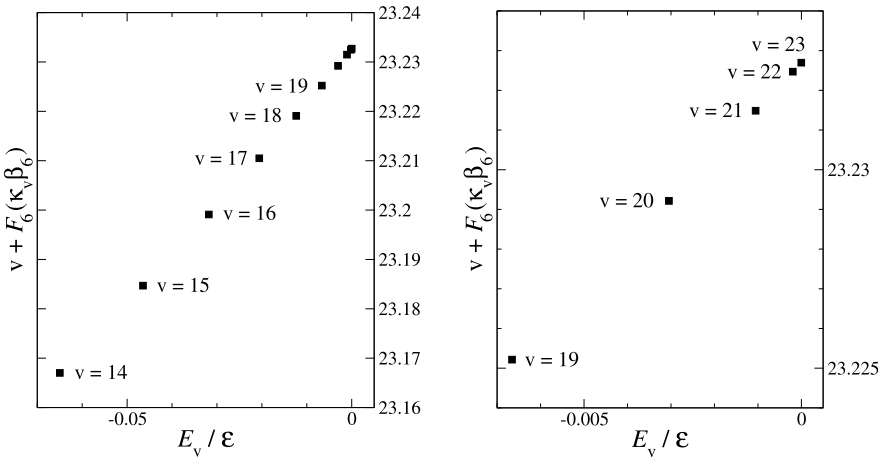

Fig. 4.4 Plot of $\upsilon + F_6(\kappa_\upsilon \beta_6)$ against energy for the highest ten bound states in the Lennard–Jones potential (4.68) with $B_{\rm LJ} = 10^4$. The energies are as listed in Table 4.4 and the quantization function $F_6(\kappa\beta_6)$ is as given by Eq. (4.63)

For $B_{\rm LJ} = 10^4$ we have $\beta_6 = 10 \times 2^{1/4} r_{\rm min}$, and the potential supports 24 bound states, $\upsilon = 0, 1, \ldots, 23$. This is actually the potential illustrated in Fig. 4.1. It was used by Paulsson et al. [72] to discuss the accuracy of higher-order WKB approximations. The energies of the highest twelve bound states are listed in Table 4.4.

According to (4.20), a plot of $\upsilon + F_6(\kappa_\upsilon \beta_6)$ against E_υ should approach a straight-line behaviour towards threshold, κ_υ being the asymptotic inverse penetration depth at the energy E_υ. This is illustrated impressively in Fig. 4.4. The solid squares represent the highest ten bound states in the left-hand part and the highest five bound states in the right-hand part. The x-coordinate of each square is its energy eigenvalue E_υ (in units of $\mathscr{E}$), and the y-coordinate is $\upsilon + F_6(\kappa_\upsilon \beta_6)$, where $F_6(\kappa\beta_6)$ is the quantization function (4.63), and β_6 is as given in (4.69).

The fact that the linear behaviour in Fig. 4.4 reaches from threshold down to several states below threshold shows that the quantization rule based on Eq. (4.63) is reliable over this large energy range. To demonstrate this more quantitatively, Table 4.5 lists the values of the threshold quantum number $\upsilon_{\rm D}$ and the short-range correction parameter $\gamma_{\rm sr}$ as obtained by fitting a straight line through two succes-

Table 4.5 Values of the threshold quantum number υ_D and the short-range correction parameter γ_{sr} [in units of $\mathscr{E}^{-1}$] as obtained by fitting a straight line through two successive bound states, υ and $\upsilon + 1$, according to (4.20), see Fig. 4.4. Also listed are the values of the scattering length a [in units of r_{min}] as obtained via (4.53) with the respective values of υ_D

υ	υ_D	$\gamma_{sr}\mathscr{E}$	a/r_{min}	υ	υ_D	$\gamma_{sr}\mathscr{E}$	a/r_{min}
13	23.227230	−0.926599	12.2461	18	23.232378	−1.075980	12.0355
14	23.229053	−0.954646	12.1706	19	23.232591	−1.107941	12.0270
15	23.230401	−0.983664	12.1155	20	23.232685	−1.138876	12.0232
16	23.231354	−1.013615	12.0768	21	23.232699	−1.151726	12.0227
17	23.231988	−1.044432	12.0512	22	23.232700	−1.159540	12.0226

sive points, υ and $\upsilon + 1$. The values both of υ_D and of γ_{sr} converge rapidly and smoothly with increasing quantum number υ. The value of the threshold quantum number obtained by extrapolating from the sixth- and fifth-highest states ($\upsilon = 18$ and $\upsilon = 19$) already lies within 0.0004 of the value extrapolated via the highest two states, $\upsilon_D = 23.23270$. This is also reflected in the similarly rapid and smooth convergence of the values of the scattering length a, as derived from the respective values of the threshold quantum number υ_D and the tail parameters $\bar{a}$ and b according to (4.53). In the present case of a $1/r^6$ reference potential, $\bar{a}$ and b are identical and both approximately equal to $0.478\beta_6$, see Table 4.1. With β_6 as given in (4.69), we have $\bar{a} = b \approx 5.684 r_{min}$ in the present case. The well converged value of the scattering length, as obtained with the highest two states, is already predicted to within 0.1% when extrapolating from the sixth- and fifth-highest states ($\upsilon = 18$ and $\upsilon = 19$).

Note that the magnitude of the short-range correction coefficient γ_{sr} is of the order of $1/\mathscr{E}$, where $\mathscr{E}$ is the depth of the potential. Characteristic energies associated with the potential tail are typically of the order

$$E_{\beta_6} = \frac{\hbar^2}{2\mu(\beta_6)^2}. \tag{4.70}$$

In the present example, $E_{\beta_6} \approx 0.7 \times 10^{-6}\mathscr{E}$, so the short-range correction coefficient γ_{sr} is near to six powers of ten smaller than typical inverse energies associated with the scale set by the reference potential $V_6(r)$. This justifies carrying the near-threshold expansions of the outer reflection phase (4.41) and the quantization function (4.44) to second order in κ, even though the short-range corrections come in at the same order.

The results above show, that the quantization function (4.63) for a $1/r^6$ reference potential accurately accounts for the level progression of the high-lying bound states in the deep Lennard–Jones potential (4.68), with the large value of B_{LJ} allowing the full potential to support 24 bound states. With only two parameters, υ_D and γ_{sr}, to account for all short-range effects, an accurate extrapolation to threshold, e.g. to deduce the value of the scattering length, is possible from several states below threshold. Such a clean separation of short-range effects from the influence of the

Table 4.6 Energy eigenvalues (in atomic units) relative to the dissociation threshold of the highest ten bound states in the $L = 0$, $1s\sigma_g$ series of the H_2^+ molecular ion according to Hilico et al. [45]

υ	E_υ	υ	E_υ	υ	E_υ	υ	E_υ
10	−0.021970529704	13	−0.009458409007	16	−0.001967933877	18	−0.000109592359
11	−0.017272525961	14	−0.006373841570	17	−0.000709200873	19	$-3.39093933 \cdot 10^{-6}$
12	−0.013097363811	15	−0.003867245551				

potential tail is possible, when the distances at which the full interaction deviates significantly from the reference potential $V_{\text{tail}}(r)$ are small compared to characteristic length scales of $V_{\text{tail}}(r)$. In the present example, it was sufficient to take the leading single-power term of the potential as reference potential, because the deviation of $V(r)$ from $V_{\text{tail}}(r)$ is only given by the repulsive $1/r^{12}$ contribution, which is of very short range. In more realistic cases, a more sophisticated choice of reference potential may be needed to describe a range of near-threshold energies containing more than one or two bound states. This is demonstrated as Example 2 for the H_2^+ molecular ion below.

4.1.1.2 Example 2. The H_2^+ Molecular Ion

The H_2^+ ion, consisting of a proton and a neutral hydrogen atom, is one of the most fundamental molecular systems. Since its properties have been thoroughly examined in experiments and *ab initio* calculations, the system is ideally suited for testing and demonstrating the strengths and possible weaknesses of a theory focussing on the role of the potential tail, as done recently in Ref. [50].

Highly accurate energy eigenvalues of bound states of H_2^+ have been calculated by Hilico et al. [45]; the energies of the highest ten $L = 0$, $1s\sigma_g$ bound states are listed in Table 4.6.

The p-H potential at large distances can be decomposed into a polarisation term $V_{\text{pol}}(r)$, and an exchange term $V_{\text{ex}}(r)$ which is responsible for the energy splitting of the states with gerade and with ungerade parity [55]. The present example focusses on the $1s\sigma_g$ configuration, where the polarisation term is attractive,

$$V_{1s\sigma_g}(r) = V_{\text{pol}}(r) - V_{\text{ex}}(r). \tag{4.71}$$

The expansion of $V_{\text{pol}}(r)$ and $V_{\text{ex}}(r)$ for large internuclear separations r was given to a large number of terms in 1968 by Damburg and Propin [27]. Leading terms, in atomic units, are

$$V_{\text{pol}}^{\text{DP}}(r) = -\frac{9}{4r^4} - \frac{15}{2r^6} - \frac{213}{4r^7}, \qquad V_{\text{ex}}^{\text{DP}}(r) = 2re^{-r-1}\left(1 + \frac{1}{2r} - \frac{25}{8r^2}\right). \tag{4.72}$$

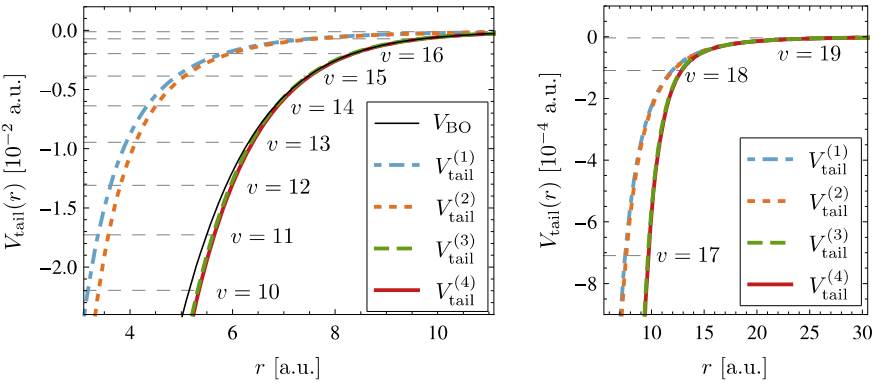

Fig. 4.5 Reference potentials $V_{\rm tail}^{(1)}(r)$ [Eq. (4.73)], $V_{\rm tail}^{(2)}(r)$ [Eq. (4.74)], $V_{\rm tail}^{(3)}(r)$ [Eq. (4.75)] and $V_{\rm tail}^{(4)}(r)$ [Eq. (4.76)] in an energy range encompassing the highest ten bound states in the $L = 0$, $1s\sigma_g$ configuration, see Table 4.6. The corresponding energy levels are shown as *horizontal dashed lines*. The potential $V_{\rm BO}(r)$ corresponds to the minimal electronic energy at internuclear separation r; this should be a good approximation to the full interaction for the range of r-values in the figure. (From [50])

Including only the leading asymptotic term of the polarisation potential to define the reference potential gives a single-power tail (4.57) with $\alpha = 4$,

$$V_{\rm tail}^{(1)}(r) = -\frac{9}{4r^4} \equiv -\frac{\hbar^2}{2\mu}\frac{(\beta_4)^2}{r^4}. \tag{4.73}$$

With the reduced mass $\mu = 918.32627$ a.u. this translates into a quantum length $\beta_4 = 64.2843$ a.u.

The reference potential (4.73) is shown in Fig. 4.5 (dot-dashed blue line) together with the potential $V_{\rm BO}(r)$ (solid black line), which represents the electronic ground-state energy at each internuclear separation r [71] and should be a good approximation to the full interaction in the range of distances in the figure. The energies of the highest ten bound states, as listed in Table 4.6, are shown as horizontal dashed lines in the figure. The single-power reference potential (4.73) is clearly far too weak for distances less than about 12 a.u., while the outer classical turning point lies in this range at the energies E_υ of all states with $\upsilon \leq 17$. Since the dominance of $F_{\rm tail}(E)$ over short-range corrections requires the reference potential to be an accurate approximation of the full interaction down to distances somewhat smaller than the outer classical turning point, the usefulness of the single-power tail (4.73) is expected to be limited to a very narrow range of near-threshold energies, encompassing at most the highest one or two levels.

In order to understand how the choice of reference potential affects the separation of short-range and tail effects, the authors of Ref. [50] investigated three further versions for $V_{\rm tail}(r)$:

$$V_{\rm tail}^{(2)}(r) = -\frac{9}{4r^4} - \frac{15}{2r^6}, \tag{4.74}$$

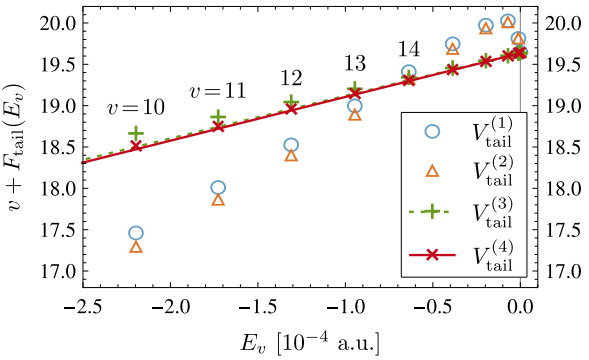

Fig. 4.6 Plots of $\upsilon + F_{\rm tail}(E_\upsilon)$ against E_υ with the quantization function $F_{\rm tail}(E)$ defined via (4.16), (4.17) on the basis of the definitions (4.73)–(4.76) of $V_{\rm tail}$. The *straight dashed green* and *solid red lines* are fitted according to (4.20) through the highest two states, $\upsilon = 18$ and $\upsilon = 19$, with $F_{\rm tail}(E)$ based on $V_{\rm tail}^{(3)}$ and $V_{\rm tail}^{(4)}$, respectively. (Adapted from [50])

Table 4.7 Values $\upsilon + F_{\rm tail}(E_\upsilon)$ at the energies given in Table 4.6 for the quantization functions based on the definitions (4.73), (4.74), (4.75) and (4.76) of $V_{\rm tail}(r)$

υ	$V_{\rm tail}^{(1)}$	$V_{\rm tail}^{(2)}$	$V_{\rm tail}^{(3)}$	$V_{\rm tail}^{(4)}$	υ	$V_{\rm tail}^{(1)}$	$V_{\rm tail}^{(2)}$	$V_{\rm tail}^{(3)}$	$V_{\rm tail}^{(4)}$
10	17.4612	17.2870	18.6570	18.5089	15	19.7486	19.6804	19.4491	19.4310
11	18.0115	17.8571	18.8562	18.7444	16	19.9740	19.9285	19.5374	19.5304
12	18.5268	18.3929	19.0367	18.9557	17	20.0268	20.0028	19.5976	19.5968
13	18.9980	18.8853	19.1968	19.1416	18	19.8143	19.8073	19.6291	19.6287
14	19.4120	19.3213	19.3349	19.3007	19	19.6468	19.6467	19.6346	19.6343

$$V_{\rm tail}^{(3)}(r) = -\frac{9}{4r^4} - 2r\mathrm{e}^{-r-1}, \tag{4.75}$$

$$V_{\rm tail}^{(4)}(r) = -\frac{9}{4r^4} - \frac{15}{2r^6} - \frac{213}{4r^7} - 2r\mathrm{e}^{-r-1}\left(1 + \frac{1}{2r} - \frac{25}{8r^2}\right). \tag{4.76}$$

These further reference potentials are shown as dotted orange $[V_{\rm tail}^{(2)}(r)]$, dashed green $[V_{\rm tail}^{(3)}(r)]$ and solid red lines $[V_{\rm tail}^{(4)}(r)]$ in Fig. 4.5. The addition of the next-order dispersion term $-15/(2r^6)$, which defines $V_{\rm tail}^{(2)}(r)$, is not a significant improvement over $V_{\rm tail}^{(1)}(r)$, but $V_{\rm tail}^{(3)}(r)$ and $V_{\rm tail}^{(4)}(r)$, which include a contribution from the polarization potential, offer a far better representation of the full potential in the whole range $r > 5$ a.u.

The quality with which the reference potentials $V_{\rm tail}^{(i)}(r)$ approximate the full potential is reflected in the accuracy with which a plot of $\upsilon + F_{\rm tail}(E_\upsilon)$ against E_υ yields a straight line with a small gradient according to (4.20). The plots are shown in Fig. 4.6, and the numerical values on which they are based are listed in Table 4.7.

Table 4.8 For the definitions (4.73)–(4.76) of the reference potential, the table lists the values of the threshold quantum number υ_D and the short-range correction coefficient γ_{sr} as obtained by fitting a straight line through the highest two states $\upsilon = 18$ and $\upsilon = 19$ according to (4.20), together with the tail parameters $\bar{a}$, b and ϕ_0. The last column shows the value obtained for the scattering length according to (4.53)

V_{tail}	υ_D	γ_{sr} [a.u.]	$\bar{a}$ [a.u.]	b [a.u.]	ϕ_0	a [a.u.]
$V_{tail}^{(1)}$	19.6414	1577.3	0	64.28	π	−30.60
$V_{tail}^{(2)}$	19.6410	1517.4	$O(10^{-15})$	64.27	3.14396	−30.49
$V_{tail}^{(3)}$	19.6348	−51.57	−2.49	63.09	3.07548	−30.93
$V_{tail}^{(4)}$	19.6345	−52.91	−2.38	63.12	3.06881	−30.77

As already seen in Fig. 4.5, the potential tails $V_{tail}^{(1)}(r)$ and $V_{tail}^{(2)}(r)$ are only a fair approximation of the full potential for distances larger than about 12 a.u. The energy levels for which the outer classical turning point lies in this range are the highest state $\upsilon = 19$ and the second-highest state $\upsilon = 18$, only. Correspondingly, the behaviour of $\upsilon + F_{tail}(E_\upsilon)$ for $\upsilon \leq 17$ and for $\upsilon \geq 18$ cannot, not even approximately, be reconciled to one straight line, see blue circles and red triangles in Fig. 4.6. In contrast the points based on $V_{tail}^{(3)}(r)$ show a much smoother energy dependence, while for $V_{tail}^{(4)}(r)$ the behaviour of $\upsilon + F_{tail}(E_\upsilon)$ is quite close to linear down to $\upsilon = 10$.

Table 4.8 lists the values of the threshold quantum number υ_D and the short-range correction coefficient γ_{sr} as obtained by fitting a straight line through the last two states $\upsilon = 18$ and $\upsilon = 19$ according to (4.20) for the various choices of reference potential. Also listed are the tail parameters $\bar{a}$ (mean scattering length), b (threshold length) and ϕ_0 (threshold value of the outer reflection phase). The last column shows the respective values of the scattering length a that follow via (4.53). Although the choice of reference potential strongly influences the energy range over which the tail contribution to the quantization function governs the energy progression of the near-threshold bound states, the extrapolation to $E = 0$ yields a very stable value of the threshold quantum number υ_D, which turns out to be quite insensitive to the choice of $V_{tail}(r)$. This puts rather tight bounds on the value of the scattering length, which follows via (4.53) and is seen to lie in the range between −31 and −30.5 a.u. Interestingly, this range does not include the value $a = -29.3$ a.u., which was derived in [16] by solving the appropriate Faddeev equations for the three-body *ppe* system. Two of the authors of Ref. [45], who obtained the energy eigenvalues in Table 4.6, were also coauthors of Ref. [16]. It seems that the scattering length given there is not quite consistent with the progression of near-threshold energy levels given in [45]. The same applies to the value $a = -28.8$ a.u., which was obtained in Ref. [13] by calculating p-H scattering cross sections down to very low energies.

Figure 4.7 shows the scattering length derived via (4.53), with the threshold quantum number υ_D obtained by fitting a straight line through two bound states υ and $\upsilon + 1$ according to (4.20), as function of the quantum number υ. For the reference potentials (4.73) and (4.74), the predictions are outside the range of the figure

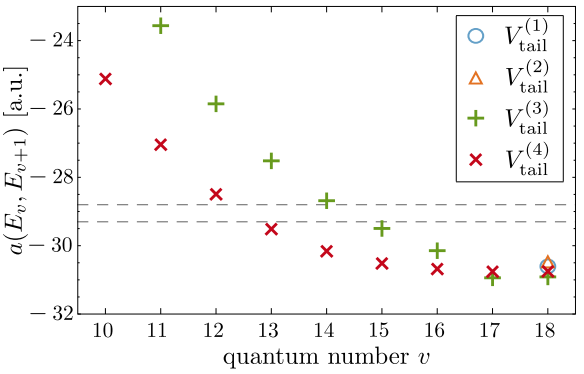

Fig. 4.7 Scattering length a according to (4.53) with $\upsilon_{\rm D}$ obtained by fitting a straight line through the points υ and $\upsilon+1$ in Fig. 4.6 according to (4.20). The *blue circle* and the *red triangle* at $\upsilon = 18$ are based on $V_{\rm tail}^{(1)}(r)$ and $V_{\rm tail}^{(2)}(r)$. The *upright green* and *diagonal red crosses* are based on $V_{\rm tail}^{(3)}(r)$ and $V_{\rm tail}^{(4)}(r)$, respectively. The *dashed horizontal lines* show the values $a = -29.3$ a.u. and $a = -28.8$ a.u. given in [16] and [13]. (Adapted from[50])

for $\upsilon \leq 17$. With the more sophisticated choices (4.75) and (4.76) of reference potential, a rapid and smooth convergence with υ is observed, similar to the case of the Lennard–Jones potential, see Table 4.5. With the reference potential $V_{\rm tail}^{(4)}(r)$, the scattering length obtained from the fifth and fourth highest state ($\upsilon = 15$ and $\upsilon = 16$) already lies within 0.3 a.u. of the value obtained with the highest two states.

This example shows, how a sufficiently sophisticated choice of reference potential can substantially increase the energy range over which the progression of near-threshold energy levels can be understood as a property of $V_{\rm tail}(r)$. The "bad news" is, that any choice of $V_{\rm tail}(r)$ beyond the single-power form (4.57) destroys the universality of the quantization function. Whereas the quantization function $F_\alpha(\kappa\beta_\alpha)$ for a single-power tail caters for all values of the potential strength, expressed through the quantum length β_α, adding any further term to the definition of $V_{\rm tail}(r)$ only makes sense in an application to a specific system. For any reference potential containing two or more terms, however, the quantization function will depend on the ratios of the strengths of the various terms. These ratios are most likely to be unique to a particular system, so the quantization function derived for a given system will be applicable to this special case only.

4.1.2 Quantum Reflection

Above threshold, the radial Schrödinger equation with a reference potential $V_{\rm tail}(r)$ is still of the form (4.11), but the energy is now positive,

$$E = \frac{\hbar^2 k^2}{2\mu}, \tag{4.77}$$

and its spectrum continuous. We assume again, that the reference potential $V_{\text{tail}}(r)$ is attractive, falls off faster than $1/r^2$ at large distances and is more singular than $-1/r^2$ at small distances. Proximity to the semiclassical or anticlassical limits can, as for energies below threshold, be estimated by the value of a typical classical action in units of $\hbar$, see discussion involving Eqs. (4.12) to (4.15) above. At positive energies, there is no outer classical turning point, but a classically defined characteristic distance can be identified as the distance r_E at which the value of the potential is equal to minus the absolute value of the energy E:

$$V_{\text{tail}}(r_E) = -|E|. \tag{4.78}$$

The distance r_E is the classical turning point in the potential $-V_{\text{tail}}(r)$ at energy $|E|$. A typical classical action is now provided the product of r_E and the asymptotic momentum $\hbar k$, corresponding in units of $\hbar$ to kr_E. Thus kr_E is a generalization of the concept of the reduced classical turning point introduced in Sect. 4.1.1. For the singular attractive potential $V_{\text{tail}}(r)$, the high-energy limit $k \to \infty$ implies $kr_E \to \infty$ and corresponds to the semiclassical limit of the Schrödinger equation (4.11), while the threshold limit $k \to 0$ implies $kr_E \to 0$ and corresponds to the anticlassical limit.

The local classical momentum $p_{\text{tail}}(E; r) = \sqrt{2\mu[E - V_{\text{tail}}(r)]}$ is real and positive for all distances $0 < r < \infty$. At distances noticeably smaller than r_E, as defined in (4.78), $p_{\text{tail}}(E; r)$ is dominated by the contribution from $V_{\text{tail}}(r)$ and becomes independent of energy. The quantality function (2.139) becomes insensitive to the energy and vanishes for $r \to 0$, so the WKB representations of the solutions of (4.11) become exact in the limit $r \to 0$. This implies that the solutions of (4.11) can, for any energy E, be unambiguously decomposed into incoming and outgoing radial waves at small distances. At distances much larger than r_E, the potential $V_{\text{tail}}(r)$ is only a small correction to the dominant, constant part $\hbar k$ of $p_{\text{tail}}(E; r)$, and the Schrödinger equation (4.11) becomes that for free-particle motion. For $r \gg r_E$, the wave function essentially describes free-particle motion and can also be decomposed into incoming and outgoing waves. In between the near-origin regime $r \to 0$ and the large-distance regime $r \gg r_E$, there is a *nonclassical region* of the reference potential $V_{\text{tail}}(r)$, with distances of the order of the generalized reduced classical turning point r_E, where the condition (2.141) is not well fulfilled—at least at low energies. Even though there is no potential barrier and no classical turning point, incoming waves can be partially reflected in this nonclassical region of coordinate space, so that only a fraction of the incoming radial wave penetrates through to the near-origin regime. Such classically forbidden reflection is a purely quantum mechanical phenomenon and is called *quantum reflection*; it is the counterpart of classically forbidden transmission through a potential barrier—called tunnelling.

For each energy E, i.e. for each wave number k, there are two linearly independent solutions of Eq. (4.11), and the physically relevant linear combination of these two solutions is chosen by defining appropriate boundary conditions at small distances. For ordinary scattering problems, this boundary condition is chosen to ensure that the regular solution of the radial Schrödinger equation with the full interaction matches to the solution of (4.11) at large distances. Other choices are,

however, possible. Choosing incoming boundary conditions at $r \to 0$,

$$u(r) \overset{r\to 0}{\sim} \frac{T}{\sqrt{p_{\text{tail}}(E;r)}} \exp\left(-\frac{\mathrm{i}}{\hbar}\int_{r_0}^{r} p_{\text{tail}}\big(E;r'\big)\mathrm{d}r'\right), \tag{4.79}$$

corresponds to assuming that all incoming flux which is transmitted through the nonclassical region of the potential tail to small distances is absorbed. Note that, for sufficiently small r, the upper integration limit r is smaller than the lower integration limit r_0 in the integral in (4.79), so the integral itself is negative. Writing the argument of the WKB wave function as upper limit in the action integral has the advantage, that wave functions containing $\exp(-\frac{\mathrm{i}}{\hbar}\int^r \cdots)$ are easily identified as inward-travelling waves, whereas wave functions containing $\exp(+\frac{\mathrm{i}}{\hbar}\int^r \cdots)$ are outward-travelling waves.

Starting with the incoming boundary conditions (4.79), the Schrödinger equation (4.11) can be integrated outwards, which yields a well defined solution that can be decomposed into incoming and outgoing radial waves at large distances,

$$u(r) \overset{r\to\infty}{\sim} \frac{1}{\sqrt{\hbar k}}\big(\mathrm{e}^{-\mathrm{i}kr} + R\mathrm{e}^{+\mathrm{i}kr}\big). \tag{4.80}$$

Since the potential $V_{\text{tail}}(r)$ is strongly r-dependent for $r \to 0$, the right-hand side of (4.79) necessarily contains the prefactor $1/\sqrt{p_{\text{tail}}(E;r)}$. The factor $1/\sqrt{\hbar k}$ on the right-hand side of (4.80) is included for consistency. The transmission coefficient T in (4.79) can be chosen such that there is no further proportionality constant in front of the incoming wave in (4.80). The phase of T also depends on the choice of the lower integration limit r_0 in the action integral. Equation (4.80) defines the *quantum reflection amplitude* R. Comparing Eq. (4.80) with Eqs. (2.68) and (2.69) in Sect. 2.3.6 shows that the reflection amplitude R can be interpreted as minus the s-wave S-matrix,

$$R \equiv -S_{l=0} = -\mathrm{e}^{2\mathrm{i}\delta_0}, \tag{4.81}$$

with an s-wave scattering phase shift δ_0. Incoming boundary conditions imply absorption, so the S-matrix is no longer unitary, which is expressed through a complex phase shift δ_0.

The immediate near-threshold behaviour of the quantum reflection amplitude can be easily derived [35] on the basis of the two threshold ($E = 0$) solutions $u_0^{(0)}(r)$ and $u_1^{(0)}(r)$ of the radial Schrödinger equation (4.11), which are defined by their asymptotic behaviour (4.34). From their small-r behaviour (4.35), it follows that the linear combination

$$\begin{aligned} u(r) \;&=\; \frac{\mathrm{e}^{\mathrm{i}\phi_0/2}}{D_1}u_1^{(0)}(r) - \frac{\mathrm{e}^{\mathrm{i}\phi_1/2}}{D_0}u_0^{(0)}(r) \\ &\overset{r\to 0}{\propto} \frac{1}{\sqrt{p_{\text{tail}}(0;r)}} \exp\left(-\frac{\mathrm{i}}{\hbar}\int_{\infty}^{r} p_{\text{tail}}\big(0;r'\big)\mathrm{d}r'\right) \end{aligned} \tag{4.82}$$

obeys incoming boundary conditions for $r \to 0$. At large distances, the superposition (4.82) behaves as

$$u(r) \overset{r\to\infty}{\sim} -\frac{\mathrm{e}^{\mathrm{i}\phi_1/2}}{D_0} + \frac{\mathrm{e}^{\mathrm{i}\phi_0/2}}{D_1} r, \tag{4.83}$$

which is to be compared with

$$\frac{1}{\sqrt{\hbar k}}\left(\mathrm{e}^{-\mathrm{i}kr} + R\mathrm{e}^{+\mathrm{i}kr}\right) \overset{kr\to 0}{\propto} 1 + R - \mathrm{i}k(1-R)r. \tag{4.84}$$

Since the ratio of the constant term and the coefficient of r must be the same in (4.83) and (4.84), we obtain

$$\frac{D_0}{D_1}\mathrm{e}^{\mathrm{i}(\phi_0-\phi_1)/2} = \frac{\mathrm{i}k(1-R)}{1+R} \quad \Longrightarrow \quad R \overset{k\to 0}{\sim} -\frac{1-\mathrm{i}k\mathrm{e}^{-\mathrm{i}(\phi_0-\phi_1)/2}D_1/D_0}{1+\mathrm{i}k\mathrm{e}^{-\mathrm{i}(\phi_0-\phi_1)/2}D_1/D_0}, \tag{4.85}$$

and, with the threshold length b and mean scattering length $\bar{a}$ as defined in (4.40), (4.42),

$$R \overset{k\to 0}{\sim} -\left[1 - 2k\frac{D_1}{D_0}\left[\sin\left(\frac{\phi_0-\phi_1}{2}\right) + \mathrm{i}\cos\left(\frac{\phi_0-\phi_1}{2}\right)\right]\right] = -\big[1 - 2\mathrm{i}(\bar{a} - \mathrm{i}b)k\big]. \tag{4.86}$$

Expressing R in terms of the complex phase shift $\boldsymbol{\delta}_0$ according to (4.81) reveals the following near-threshold behaviour of $\boldsymbol{\delta}_0$,

$$\boldsymbol{\delta}_0 \overset{k\to 0}{\sim} -(\bar{a} - \mathrm{i}b)k = -\mathscr{A}k. \tag{4.87}$$

Thus the mean scattering length $\bar{a}$ and the threshold length b, introduced in Sect. 4.1.1 as tail parameters of a singular reference potential $V_{\mathrm{tail}}(r)$, appear as the real part and minus the imaginary part of the *complex scattering length* [3, 88, 89],

$$\mathscr{A} = \bar{a} - \mathrm{i}b, \tag{4.88}$$

which describes the leading near-threshold behaviour of the quantum reflection amplitude. The mean scattering length is well defined only for potentials falling off faster than $1/r^3$ at large distances, but the threshold length b is well defined for potentials falling off faster than $1/r^2$. The leading near-threshold behaviour of the modulus of the quantum reflection amplitude is determined by the threshold length b,

$$|R| \overset{k\to 0}{\sim} 1 - 2bk + O\big(k^2\big) = \mathrm{e}^{-2bk} + O\big(k^2\big). \tag{4.89}$$

Note that the probability $|R|^2$ for quantum reflection approaches unity at threshold, so quantum reflection always becomes dominant at sufficiently low energies.

The effective-range expansion, described for the phase shifts of ordinary scattering in Sect. 2.3.8, can be adapted for the complex phase shifts of quantum reflection,

as described in Ref. [3]. Equation (2.103) becomes

$$k\cot\delta_0 \overset{k\to 0}{\sim} -\frac{1}{\bar{a}-\mathrm{i}b}+\frac{1}{2}\mathscr{R}_{\mathrm{eff}}k^2, \quad \mathscr{R}_{\mathrm{eff}}=2\int_0^\infty \left(\left[w^{(0)}(r)\right]^2-\left[u^{(0)}(r)\right]^2\right)\mathrm{d}r, \tag{4.90}$$

but the radial wave function $u^{(0)}(r)$ is now defined as the solution of (4.11) which obeys incoming boundary conditions for $r\to 0$ and the following boundary conditions for large r:

$$u^{(0)}(r) \overset{r\to\infty}{\sim} 1-\frac{r}{\bar{a}-\mathrm{i}b}. \tag{4.91}$$

The wave function $w^{(0)}(r)$ in (4.90) assumes the form (4.91) in the whole range of r-values, from the origin to infinity,

$$w^{(0)}(r)=1-\frac{r}{\bar{a}-\mathrm{i}b}. \tag{4.92}$$

The parameter $\mathscr{R}_{\mathrm{eff}}$ in (4.90) is the complex effective range. As for the real effective range in ordinary scattering, it is well defined for potentials $V_{\mathrm{tail}}(r)$ falling off faster than $1/r^5$ at large distances.

At high energies corresponding to the semiclassical limit of the Schrödinger equation (4.11), the probability for the classically forbidden process of quantum reflection vanishes. For an infinitely differentiable potential $V_{\mathrm{tail}}(r)$, the probability generally decreases exponentially with an exponent proportional to a typical classical action in units of $\hbar$, e.g. to the generalized reduced classical turning point kr_E introduced above,

$$|R| \overset{k\to\infty}{\propto} \mathrm{e}^{-B_{\mathrm{o}}kr_E}, \tag{4.93}$$

with some dimensionless constant B_{o}.

For an attractive single-power tail (4.57), the generalized reduced classical turning point is given by

$$kr_E=(k\beta_\alpha)^{1-2/\alpha}, \tag{4.94}$$

and the quantum reflection amplitude depends only on $k\beta_\alpha$. The exponent on the right-hand side of (4.93) describing the high-energy behaviour of $|R|$ is $B_{\mathrm{o}}kr_E=B_{\mathrm{o}}(k\beta_\alpha)^{1-2/\alpha}$ in this case; the coefficients B_{o} were derived in [33] and are given in the last row of Table 4.1 in Sect. 4.1.1. Plots of $\ln|R|$, as function both of $k\beta_\alpha$ and of $(k\beta_\alpha)^{1-2/\alpha}$, are shown in Fig. 4.8. The linear initial fall-off of the various curves in the left-hand part of the figure is in agreement with (4.89), and the gradients $-2b/\beta_\alpha$ reflect the respective threshold lengths b as already given in Eq. (4.61) and Table 4.1. In the right-hand part of the figure, the fall-off at large values of $(k\beta_\alpha)^{1-2/\alpha}$ is in agreement with (4.93); the straight dashed lines show $-B_{\mathrm{o}}(k\beta_\alpha)^{1-2/\alpha}$ with the values B_{o} as given in the bottom row of Table 4.1. With increasing power α, the exponent $B_{\mathrm{o}}(k\beta_\alpha)^{1-2/\alpha}$ describing the high-energy behaviour of $|R|$ approaches the exponent $-2bk$ describing its low-energy behaviour, see the corresponding entries in

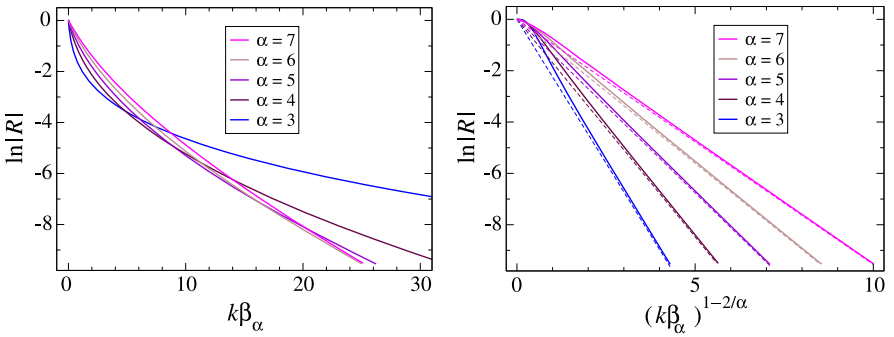

Fig. 4.8 Logarithmic plot of the modulus $|R|$ of the quantum reflection amplitude for attractive inverse-power potentials (4.57) for $\alpha = 3, \ldots, 7$ as functions of $k\beta_\alpha$ (*left-hand part*) and of $(k\beta_\alpha)^{1-2/\alpha}$ (*right-hand part*). The *straight dashed lines* in the right-hand part show the functions $-B_o(k\beta_\alpha)^{1-2/\alpha}$ with the coefficients B_o given in the bottom row of Table 4.1. (Adapted from [33])

the last column of Table 4.1. Thus the low- and high-energy behaviour of $|R|$ merges into a single exponential form for single-power tails (4.57) with large power α,

$$|R| \overset{\alpha\to\infty}{\sim} \mathrm{e}^{-2\pi k\beta_\alpha/\alpha} \tag{4.95}$$

for all energies.

The tail parameters of attractive single-power tails (4.57) can be related in a very elegant way to corresponding parameters of the repulsive inverse-power potentials (2.160) discussed in Sect. 2.4. To see this, observe that the repulsive inverse-power potential (2.160) becomes the attractive inverse-power potential (4.57) by an appropriate transformation of the quantum length β_α. With $\nu = 1/(\alpha - 2)$:

$$\beta_\alpha \to \beta_\alpha^{-\mathrm{i}\pi\nu} \quad \Longrightarrow \quad \frac{(\beta_\alpha)^{\alpha-2}}{r^\alpha} \to -\frac{(\beta_\alpha)^{\alpha-2}}{r^\alpha}. \tag{4.96}$$

The same transformation, $\beta_\alpha \to \beta_\alpha^{-\mathrm{i}\pi\nu}$, transforms the purely imaginary local classical momentum under the repulsive inverse-power potential to a real local classical momentum in the attractive inverse-power potential. The radial wave function which is exactly equal to its WKB representation in the limit $r \to 0$ for inverse-power tails with $\alpha > 2$, is transformed from the regular solution which vanishes monotonically for $r \to 0$ in the repulsive case to the oscillating solution obeying incoming boundary conditions in the attractive case. All properties which depend on the quantum length β_α carry over from the repulsive to the attractive case via the transformation (4.96). The scattering length, which is given by (2.181) for the repulsive inverse-power potential (2.160), transforms according to

$$a = \nu^{2\nu}\frac{\Gamma(1-\nu)}{\Gamma(1+\nu)}\beta_\alpha \quad \longrightarrow \quad \nu^{2\nu}\frac{\Gamma(1-\nu)}{\Gamma(1+\nu)}\beta_\alpha\big[\cos(\pi\nu) - \mathrm{i}\sin(\pi\nu)\big] = \bar{a} - \mathrm{i}b \tag{4.97}$$

to the complex scattering length $\mathscr{A} = \bar{a} - \mathrm{i}b$; the expressions following for the mean scattering length $\bar{a}$ and the threshold length b according to (4.97) are those already given in (4.61) . Similarly, the complex effective range $\mathscr{R}_{\mathrm{eff}}$ appearing in (4.90) is, for attractive single-power potentials (4.57) with $\alpha > 5$, just $\mathrm{e}^{-\mathrm{i}\pi\nu}$ times the real effective range r_{eff} of the corresponding repulsive inverse-power potential (4.57) with the same quantum length β_α [3]. The straightforward relationship between repulsive and attractive inverse-power potentials makes it possible to adapt the extensive results on the near-threshold behaviour of phase shifts which were derived in [22] for repulsive inverse-power potentials to the description of quantum reflection by attractive inverse-power potentials.

4.1.2.1 Observation of Quantum Reflection

Quantum reflection is observable in collisions of ultracold atoms with surfaces. At *large* distances, the projectile interacts with a plane surface via electrostatic van der Waals forces, which are modified at *very large* distances due to retardation [19]. Such "Casimir-Polder potentials" have all the properties assumed for the reference potential $V_{\mathrm{tail}}(r)$ in this section. Due to translational invariance parallel to the surface, the motion normal to the surface is decoupled from the parallel motion, and it is governed by a one-dimensional Schrödinger equation equivalent to the s-wave radial equation of scattering in three-dimensional space. Very low normal velocities can be achieved with grazing incidence of very slow projectiles. Atoms which are transmitted through the nonclassical region of the potential are accelerated towards the surface and are likely to transfer at least some small fraction of their kinetic energy to the surface, which leads to trapping of the atom at the surface if its total energy falls below zero. Such "sticking" is classically expected to become dominant at very low velocities, but early experiments with liquid helium surfaces indicated a suppression of sticking probabilities towards threshold, which was confirmed in quantum mechanical calculations [10, 12]. The quenched sticking probabilities are due to quantum reflection in the potential tail, whereby only a fraction of the incident atoms actually penetrates through to the deep attractive part of the atom-surface potential [18, 90]. Quantitative measurements of quantum reflection probabilities for ultracold atoms scattering off solid surfaces have since been performed by several groups, e.g. [21, 74, 78], and the growing activity in the field of ultracold atoms and molecules has drawn particular attention to this phenomenon [15, 20, 26, 32, 60, 61, 70, 91].

The van der Waals interaction between a neutral atom and a plane conducting or dielectric surface is $-C_3/r^3$, but at very large distances it becomes equal to $-C_4/r^4$ due to retardation effects [19]. The quotient of the strength coefficients in the limiting cases has the dimension of a length,

$$L = \frac{C_4}{C_3}; \tag{4.98}$$

it roughly defines a transition range separating the nonretarded van der Waals regime $r \ll L$ from the highly retarded regime $r \gg L$. At very small distances of a few atomic units or so, the atom-surface potential is rather complicated, but this "close region" is not important when considering quantum reflection with incoming boundary conditions. Beyond the close region, the singular, attractive atom-surface potential can be written as

$$V_{\rm tail}(r) = -\frac{C_3}{r^3}\mathrm{v}\left(\frac{r}{L}\right), \qquad \lim_{x\to 0}\mathrm{v}(x) = 1, \qquad \lim_{x\to\infty}\mathrm{v}(x) = \frac{1}{x}. \tag{4.99}$$

The *shape function* $\mathrm{v}(x)$ interpolates between the $-C_3/r^3$ behaviour for $r \ll L$ and the $-C_4/r^4$ behaviour for $r \gg L$.

In order to explain the quantum reflection probabilities that he observed in his pioneering experiments involving metastable neon atoms and solid surfaces, Shimizu [78] modelled the atom-surface potential with a very simple shape function,

$$\mathrm{v}_1(x) = \frac{1}{1+x} \quad \Longrightarrow \quad V_{\rm tail}(r) = -\frac{\hbar^2}{2\mu}\left[\frac{r^3}{\beta_3} + \frac{r^4}{(\beta_4)^2}\right]^{-1}. \tag{4.100}$$

The lengths β_3 and β_4 are the quantum lengths for the single-power forms (4.57), which the potential (4.99) approaches in the limits $r \to 0$ and $r \to \infty$, respectively. An alternative interpolation is guided by the exact potential for a hydrogen atom interacting with a perfectly conducting surface, which was calculated numerically in [57]. For this we define the shape function

$$\mathrm{v}_{\rm H}(r) = \frac{1+\xi x}{1+x+\xi x^2}, \quad \xi = 0.31608. \tag{4.101}$$

With the shape function (4.101) and the coefficients C_3, C_4 appropriate for the case of a hydrogen atom in front of a conducting surface,

$$C_3 = \frac{1}{12}\langle\psi_0|r^2|\psi_0\rangle = \frac{1}{4}\ \text{a.u.}, \qquad C_4 = \frac{3}{8\pi}\frac{\alpha_{\rm d}(0)}{\alpha_{\rm fs}} \approx 73.61\ \text{a.u.} \tag{4.102}$$

the potential (4.99) reproduces the values of the hydrogen-surface potential tabulated in [57] to within 0.6 % in the whole range of r-values. In (4.102), ψ_0 stands for the hydrogen atom's ground-state wave function, $\alpha_{\rm d}(0) = \frac{9}{2}$ a.u. is its static dipole polarizability and $\alpha_{\rm fs}$ is the dimensionless fine structure constant. The parameter ξ in (4.101) is not a fit parameter, but is determined by the condition that the universal next-to-leading term in the small-distance expansion of the potential of a Z-electron atom in front of a conducting wall [9],

$$V_Z(r) \overset{r\to 0}{\sim} \frac{C_3}{r^3} + \frac{Z\alpha_{\rm fs}}{4\pi r^2}, \tag{4.103}$$

is given correctly by the formula (4.101) for the hydrogen case $Z = 1$. This leads to $\xi = 1 - \alpha_{\rm fs}C_4/[4\pi(C_3)^2]$.

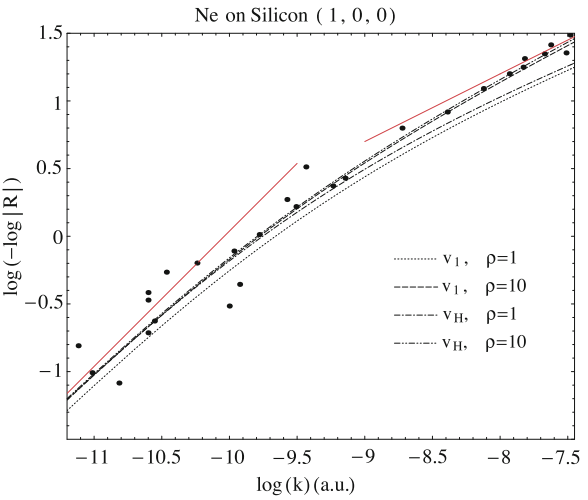

Fig. 4.9 Modulus of the quantum reflection amplitude, as observed in the scattering of metastable neon atoms off a silicon surface [78]. The figure shows $\ln(-\ln|R|)$ as function of $\ln(k)$ (natural logarithms) with k measured in atomic units, i.e. in units of the inverse Bohr radius. The curves show the results obtained by numerically solving the Schrödinger equation (4.11) with potentials (4.99) constructed with the shape functions v_1 and v_H. The quantum length β_4 associated with the strength C_4 of the potential in the highly retarded limit is $\beta_4 = 11400$ a.u. in all cases. For the $-C_3/r^3$ van der Waals limit of the potential, the quantum length is $\beta_3 = 11400$ a.u. for $\rho = 1$ and $\beta_3 = 114000$ a.u. for $\rho = 10$. The *straight red line* in the *bottom left* corner shows the behaviour $\ln|R| \sim -2\beta_4 k$ expected in the low-k regime. The *straight red line* in the *top right* corner shows the behaviour $\ln|R| \propto -\sqrt{\beta_4 k}$ expected in the high-k regime for a single-power $1/r^4$ potential. (From [33])

As shown in [33], which part of the atom-wall potential dominantly influences quantum reflection depends on the ratio $\rho = \beta_3/\beta_4$ of the quantum lengths characterizing the single-power limits at small and large distances. For $\rho < 1$, the energy dependence of $|R|$ is largely determined by the nonretarded van der Waals part of the potential; for $\rho > 1$, the retarded $-C_4/r^4$ part is dominant. Thus the smaller of the two quantum lengths is the one belonging to the dominant term. This observation may be counter-intuitive, but it is understandable when looking at the expression for the atom-wall potential that is given on the far right of (4.100).

The transition from the leading linear behaviour (4.89) of $|R|$ near threshold to the high-k behaviour (4.93) can be exposed by studying $\ln(-\ln|R|)$ as a function of $\ln k$,

$$|R| = \mathrm{e}^{-Bk^C} \quad \Longrightarrow \quad \ln\bigl(-\ln|R|\bigr) = \ln(B) + C\ln(k). \tag{4.104}$$

A plot of $\ln(-\ln|R|)$ against $\ln(k)$ is shown in Fig. 4.9 for the quantum reflection of metastable neon atoms by a silicon surface, as studied by Shimizu in [78]. The dots are the experimental data and the curves are the results obtained by numerically solving the Schrödinger equation (4.11) with potentials (4.99) constructed with the

shape functions v_l and v_H. The quantum length corresponding to the highly retarded $-C_4/r^4$ part of the potential was $\beta_4 = 11400$ a.u. in all four cases. The value of β_3 was chosen to be equal to β_4, corresponding to $\rho = 1$, or to be ten times larger, corresponding to $\rho = 10$. The straight red line in the bottom left of the figure has unit gradient, corresponding to the universal near-threshold behaviour (4.89). The results obtained with all potentials in Fig. 4.9 approach such behaviour in the low-k limit, and the data are consistent, albeit with a very large scatter. Towards large k, the gradients of the curves in Fig. 4.9 decrease gradually. The experimental points are well fitted by the two curves with $\rho = 10$, i.e. with $\beta_3 = 114000$ a.u. They are essentially the same for both shape functions, (4.100) and (4.101), and they are also independent of β_3 as long as β_3 is significantly larger than β_4. Essentially the same result is obtained with a single-power $-1/r^4$ potential with the appropriate quantum length $\beta_4 = 11400$ a.u. The straight red line in the top right corner of the figure shows the large-k behaviour expected in this case according to (4.93), with $B_o k r_E = B_o(k\beta_4)^{1/2}$; its gradient is $\frac{1}{2}$. In contrast, the large-k behaviour of the two curves with $\rho = 1$ is closer to the expectation of a $-1/r^3$ potential, where the asymptotic gradient is $\frac{1}{3}$. One expects the nonretarded $-1/r^3$ part of the potential at moderate distances to have increasing influence at higher energies, but at the energies where this happens, the quantum reflection yields are very small.

As already pointed out by Shimizu in [78], the highly retarded part of the neon-surface interaction is essentially responsible for quantum reflection observed in the experiment. Also for other atom-wall systems, involving e.g. bosonic alkali atoms, hydrogen or metastable helium, the crucial parameter β_3/β_4 is generally significantly larger than unity [33, 35]. Quantum reflection is well described on the basis of the highly retarded, single-power $-1/r^4$ potential in all these cases.

It is also worth noting, that all characteristic lengths, including the transition length (4.98) are very large, typically several hundreds or thousands of atomic units (Bohr radii) [33, 35]. Quantum reflection is generated at really large atom-surface distances. The same applies for the quantum reflection of ultracold molecules, as was impressively demonstrated in a recent experiment by Zhao et al. who scattered helium dimers off a solid diffraction grating at very low energies corresponding to normal incident velocities near 10 cm/s, translating to a kinetic energy near 0.6 neV ($\approx 2 \times 10^{-11}$ a.u.) in the normal direction. The very fragile helium dimer, with a binding energy of only 4×10^{-8} a.u. and a bond length of almost 100 a.u. (Bohr radii), is expected to fragment while being accelerated under the influence of the attractive molecule-surface potential with a well depth near 2×10^{-4} a.u. However, a noticeable fraction of the incident dimers is spared this fate due to quantum reflection, which occurs "tens of nanometers above the actual surface where the $\cdots$ forces are still too feeble to break up even the fragile He_2 bond" [91].

4.1.2.2 Nonplanar Surfaces

For atoms scattering off an absorbing sphere, the radius of the sphere enters as a further length in the problem. As shown in [4], the nonclassical region of the

potential tail moves to smaller r-values when the radius of the sphere is decreased, but the transition region between nonretarded van der Waals regime and the highly retarded regime is essentially independent of this radius and roughly the same as for an atom in front of a plane surface. The sensitivity of quantum reflection to the nonretarded part of the atom-surface potential thus becomes increasingly noticeable for smaller spheres.

It is interesting to consider the threshold limits of the cross sections for elastic scattering and for absorption of atoms interacting with an absorbing sphere. The electrostatic van der Waals potential is proportional to $1/r^6$, but at very large distances the atom-sphere potential is proportional to $1/r^7$ due to retardation effects [19]. Towards threshold, the scattering amplitude is dominated by the s-wave ($l = 0$), and the complex scattering phase shift is determined by the complex scattering length. With Eq. (2.47) in Sect. 2.3.3 and Eqs. (4.87), (4.88) above,

$$f(\theta) \overset{k\to 0}{\sim} \frac{1}{k}\boldsymbol{\delta}_0 \overset{k\to 0}{\sim} -\bar{a} + \mathrm{i}b. \tag{4.105}$$

The elastic scattering cross section $|f(\theta)|^2$ remains finite, the square of the real scattering length in the nonabsorbing case is simply replaced by the absolute square of the complex scattering length in the presence of absorption,

$$\frac{\mathrm{d}\sigma_{\mathrm{el}}}{\mathrm{d}\Omega} \overset{k\to 0}{\sim} |\mathscr{A}|^2 = \bar{a}^2 + b^2, \quad \sigma_{\mathrm{el}} \overset{k\to 0}{\sim} 4\pi\left(\bar{a}^2 + b^2\right). \tag{4.106}$$

In contrast, the absorption cross section, as given by Eq. (3.53) in Sect. 3.4, behaves as follows towards threshold:

$$\sigma_{\mathrm{abs}} \overset{k\to 0}{\sim} \frac{\pi}{k^2}\left(1 - \left|\mathrm{e}^{2\mathrm{i}\boldsymbol{\delta}_0}\right|^2\right) \overset{k\to 0}{\sim} \frac{\pi}{k^2}\left(1 - |1 - 2kb - 2\mathrm{i}\bar{a}k|^2\right) \overset{k\to 0}{\sim} \frac{4\pi b}{k}. \tag{4.107}$$

This is consistent with the optical theorem (3.17), according to which

$$\sigma_{\mathrm{tot}} = \frac{4\pi}{k}\Im\left[f(\theta = 0)\right] \overset{k\to 0}{\sim} \frac{4\pi}{k}\Im[-\bar{a} + \mathrm{i}b]; \tag{4.108}$$

the total cross section $\sigma_{\mathrm{tot}} = \sigma_{\mathrm{el}} + \sigma_{\mathrm{abs}}$ is dominated towards threshold by the diverging contribution of the absorption cross section (4.107).

The absorption cross section, which is related to the probability for transmission through the nonclassical region of the potential tail, can be used to calculate the rate for a reaction that occurs when projectile and target meet [24]. Since this involves an average over the product of σ_{abs} and the asymptotic relative velocity $\hbar k/\mu$, reaction rates following from absorption cross sections that diverge as in (4.107) tend to finite limits at threshold.

For an atom interacting with a conducting cylinder, the nonclassical region of the potential tail is not so sensitive to the radius of the cylinder. As in the case of the plane wall, the highly retarded part of the atom-cylinder potential is important for

quantum reflection by a conducting cylinder with realistic dimensions. The nonretarded part of the interaction is more likely to play a role for dielectric cylinders [30]. Note that for a cylinder, the atom-surface interaction is much more complicated than for a plane or spherical surface. Furthermore, due to translational invariance along the direction parallel to the cylinder axis, the scattering problem is actually two-dimensional, and quantum mechanical scattering theory in two dimensions is somewhat more subtle than in the one- and three-dimensional cases, in particular near threshold. A detailed description of scattering theory in two spatial dimensions is given later in Sect. 4.3.

4.1.3 Elastic Scattering

Near-threshold quantization, discussed in Sect. 4.1.1, involved matching the regular solution of the radial Schrödinger equation with the full potential to a solution of the radial Schrödinger equation (4.11) obeying bound-state boundary conditions. The potential in (4.11) is the attractive reference potential $V_{\text{tail}}(r)$, which is more singular than $1/r^2$ at small distances, is a good approximation of the full potential at large distances and falls off faster than $1/r^2$ for $r \to \infty$. The influence of the potential tail was contained in one single quantization function (4.16), constructed at each energy E with the help of the small-r behaviour of the asymptotically bound solution of (4.11), which is accurately given by its WKB representation for $r \to 0$.

At positive energies, there are two linearly independent physically meaningful solutions of (4.11) for each energy E, and the small-r behaviour of each solution is determined by an amplitude and a phase, e.g. in the WKB representation of this solution for $r \to 0$. One overall normalization constant is always arbitrary, so the quantum mechanical properties of the reference potential are manifest not in one tail function, as in subthreshold quantization, but in three tail functions at positive energies. In the previous subsection on quantum reflection, the two linearly independent solutions of (4.11) were the incoming and outgoing radial waves $\mathrm{e}^{\pm \mathrm{i}kr}/\sqrt{\hbar k}$, and three appropriate tail functions are the modulus and phase of the quantum reflection amplitude R and the phase of the transmission amplitude T, the modulus of T being already determined by flux conservation, $|R|^2 + |T|^2 = 1$.

An alternative choice of two linearly independent solutions of (4.11) is provided by the wave functions obeying the following large-r boundary conditions [65]:

$$u_{\text{s}}(r) \overset{r\to\infty}{\sim} \sin(kr), \qquad u_{\text{c}}(r) \overset{r\to\infty}{\sim} \cos(kr). \tag{4.109}$$

Beyond the short-range deviations of the full interaction from the reference potential $V_{\text{tail}}(r)$, the regular solution $u_{\text{reg}}(r)$ of the full problem is a superposition of the two solutions of (4.11),

$$u_{\text{reg}}(r) \overset{r \text{ large}}{\propto} \cos\delta_0 u_{\text{s}}(r) + \sin\delta_0 u_{\text{c}}(r). \tag{4.110}$$

The properties of the reference potential $V_{\rm tail}(r)$ are contained in the amplitudes and phases of the WKB representations of $u_{\rm s}(r)$ and $u_{\rm s}(r)$ for $r \to 0$, where these representation become exact. The explicit expressions for the WKB representations contain the lower integration limit in the action integrals as point of reference. In the presence of a classical turning point, this turning point is a natural choice, but for the singular, attractive reference potential $V_{\rm tail}(r)$, there is no classical turning point at positive energy. One conspicuous point is the distance r_E at which the potential $V(r_E)$ is equal to minus the energy E, see Eq. (4.78) in Sect. 4.1.2; it lies in the heart of the nonclassical region of $V_{\rm tail}(r)$. With this choice, the WKB representations of the two solutions of (4.11) defined by the boundary conditions (4.109) can be written as

$$\begin{aligned} u_{\rm s}(r) &\overset{r\to 0}{\sim} \frac{A_{\rm s}}{\sqrt{p_{\rm tail}(E;r)}} \sin\!\left(\frac{1}{\hbar}\int_{r_E}^{r} p_{\rm tail}\big(E;r'\big)\mathrm{d}r' - \phi_{\rm s}\right), \\ u_{\rm c}(r) &\overset{r\to 0}{\sim} \frac{A_{\rm c}}{\sqrt{p_{\rm tail}(E;r)}} \cos\!\left(\frac{1}{\hbar}\int_{r_E}^{r} p_{\rm tail}\big(E;r'\big)\mathrm{d}r' - \phi_{\rm c}\right), \end{aligned} \tag{4.111}$$

with the local classical momentum $p_{\rm tail}(E;r) = \sqrt{2\mu[E - V_{\rm tail}(r)]}$, which is real and positive in the whole range $0 < r < \infty$. Equation (4.111) defines the amplitudes $A_{\rm s,c}$ which are real and taken to be positive, and the phases $\phi_{\rm s,c}$, which are real. These amplitudes and phases are tail functions determined entirely by the reference potential $V_{\rm tail}(r)$. They are functions of energy, but for simplicity in notation this is not explicitly written in the formulae below. Note that the lower limit r_E of the integrals in (4.111) is larger than the upper limit r when $r \to 0$.

At distances r which are small enough for the WKB representations (4.111) of $u_{\rm s}(r)$ and $u_{\rm c}(r)$ to be valid, and at the same time large enough so that the reference potential $V_{\rm tail}(r)$ is a good approximation of the full interaction, the regular solution (4.110) behaves as

$$u_{\rm reg}(r) \propto \frac{1}{\sqrt{p_{\rm tail}(E;r)}} \sin\!\left(\frac{1}{\hbar}\int_{r_E}^{r} p_{\rm tail}\big(E;r'\big)\mathrm{d}r' - \phi_{\rm sr}(E)\right). \tag{4.112}$$

The position r in (4.112) lies beyond the short-range deviations of the full interaction from the reference potential $V_{\rm tail}(r)$, and the inner boundary condition $u_{\rm reg}(0) = 0$ is carried over in terms of the phase $\phi_{\rm sr}(E)$. From (4.110) and (4.111) it follows, that $\phi_{\rm sr}(E)$ is related to the scattering phase shift δ_0 by

$$\tan\delta_0 = \frac{A_{\rm s}}{A_{\rm c}} \frac{\sin(\phi_{\rm s} - \phi_{\rm sr}(E))}{\cos(\phi_{\rm c} - \phi_{\rm sr}(E))}. \tag{4.113}$$

The choice of the reference point r_E in (4.112) may seem unconventional, but it allows the WKB expression to be written in terms of $p_{\rm tail}(E;r')$ rather than $p(E;r')$, which is defined in (4.3) and involves the full interaction. A more conventional WKB representation for $u_{\rm reg}(r)$ is,

$$u_{\rm reg}(r) \propto \frac{1}{\sqrt{p(E;r)}} \cos\!\left(\frac{1}{\hbar}\int_{r_{\rm in}(E)}^{r} p\big(E;r'\big)\mathrm{d}r' - \frac{\phi_{\rm in}(E)}{2}\right), \tag{4.114}$$

which defines the inner reflection phase $\phi_{\rm in}(E)$, compare Eq. (4.2) in Sect. 4.1.1. For distances r beyond the short-range deviations of the full interaction from the reference potential $V_{\rm tail}(r)$, $p_{\rm tail}(E;r)$ and $p(E;r)$ are essentially equal, so the factors in front of the sine in (4.112) and cosine (4.114) are the same. Equating the sine and cosine parts relates $\phi_{\rm in}(E)$ to $\phi_{\rm sr}(E)$:

$$\begin{aligned}\phi_{\rm sr}(E) &= \frac{\phi_{\rm in}(E)}{2} - \frac{\pi}{2} - \frac{1}{\hbar}\int_{r_{\rm in}(E)}^{r} p\big(E;r'\big)\mathrm{d}r' - \frac{1}{\hbar}\int_{r}^{r_E} p_{\rm tail}\big(E;r'\big)\mathrm{d}r' \\ &= \frac{\phi_{\rm in}(E)}{2} - \frac{\pi}{2} - \frac{1}{\hbar}\int_{r_{\rm in}(E)}^{r_E} p\big(E;r'\big)\mathrm{d}r'. \end{aligned} \tag{4.115}$$

Since the range of integration in the second integral in the top line of (4.115) is beyond the short-range deviations, the momentum $p_{\rm tail}(E;r')$ can be replaced by $p(E;r')$ in this integral, which leads to the expression in the bottom line. With the quantization condition at threshold, Eq. (4.6) in Sect. 4.1.1, the phase $\phi_{\rm sr}(E)$ can be related to the threshold quantum number $\upsilon_{\rm D}$,

$$\begin{aligned}\phi_{\rm sr}(E) = -\upsilon_{\rm D}\pi - \frac{\phi_{\rm out}(0)}{2} - \frac{\pi}{2} - \frac{\phi_{\rm in}(0)-\phi_{\rm in}(E)}{2} \\ + \frac{1}{\hbar}\int_{r_E}^{\infty} p(0;r)\mathrm{d}r + \frac{1}{\hbar}\int_{r_{\rm in}(0)}^{r_E} p(0;r)\mathrm{d}r - \frac{1}{\hbar}\int_{r_{\rm in}(E)}^{r_E} p(E;r)\mathrm{d}r.\end{aligned} \tag{4.116}$$

The difference $\phi_{\rm in}(0) - \phi_{\rm in}(E)$ of the inner reflection phases in (4.116) is a smooth function of energy and vanishes at $E = 0$. The leading near-threshold energy dependence of the right-hand side of (4.116) comes from the difference of action integrals in the lower line. Replacing the momenta $p(0;r)$ and $p(E:r)$ in the second and third integrals, i.e. in those with upper limit r_E, by $p_{\rm tail}(0;r)$ and $p_{\rm tail}(E:r)$ introduces an error of order E at most. This is because the difference between p and $p_{\rm tail}$ is limited to short distances and hence a smooth function of E, while the difference of the two integrals clearly vanishes at $E = 0$. In the first integral, covering the range r_E to infinity, $p(0;r)$ can be replaced by $p_{\rm tail}(0;r)$, because r is always beyond the range of the short-range deviations. With the abbreviation

$$\xi = \frac{1}{\hbar}\int_{r_E}^{\infty} p_{\rm tail}(0;r)\mathrm{d}r + \frac{1}{\hbar}\int_{0}^{r_E}\big[p_{\rm tail}(0;r) - p_{\rm tail}(E;r)\big]\mathrm{d}r - \frac{\phi_{\rm out}(0)}{2} - \frac{\pi}{2}, \tag{4.117}$$

we can rewrite Eq. (4.116) as

$$\phi_{\rm sr}(E) = -\upsilon_{\rm D}\pi + \xi + \pi f_{\rm sr}(E), \tag{4.118}$$

where $f_{\rm sr}(E)$ is a smooth function of energy which vanishes at threshold and accounts for all residual short-range effects. The expression (4.113) thus becomes

$$\tan\delta_0 = \frac{A_{\rm s}}{A_{\rm c}}\frac{\sin([\upsilon_{\rm D} - f_{\rm sr}(E)]\pi - \xi + \phi_{\rm s})}{\cos([\upsilon_{\rm D} - f_{\rm sr}(E)]\pi - \xi + \phi_{\rm c})}. \tag{4.119}$$

The influence of the reference potential $V_{\rm tail}(r)$ on the low-energy behaviour of the scattering phase shift δ_0 is expressed through the three tail functions, $A_{\rm s}/A_{\rm c}$, $\phi_{\rm s}$ and $\phi_{\rm c}$. The auxiliary tail function ξ defined in (4.117) is needed to compensate the effects of choosing the lower integration limit in the action integrals to be r_E rather than some energy independent value. Such a choice would introduce an unnecessary element of arbitrariness in the formulation.

Towards threshold, the solutions $u_{\rm s}(r)$ and $u_{\rm c}(r)$ of (4.11), defined by their asymptotic behaviour (4.109), approach the threshold solutions $u_1^{(0)}(r)$ and $u_0^{(0)}(r)$, which were introduced in Sect. 4.1.1 and are defined by the asymptotic behaviour (4.34),

$$u_{\rm s}(r) \overset{k\to 0}{\sim} k u_1^{(0)}(r), \qquad u_{\rm c}(r) \overset{k\to 0}{\sim} u_0^{(0)}(r). \tag{4.120}$$

Consequently, the threshold limits of the tail functions can be expressed in terms of the amplitudes $D_{0,1}$ and phases $\phi_{0,1}$ defining the WKB representations (4.35) of $u_1^{(0)}(r)$ and $u_0^{(0)}(r)$, and the threshold value of ξ follows from (4.117):

$$\begin{aligned} &\frac{A_{\rm s}}{A_{\rm c}} \overset{k\to 0}{\sim} k\frac{D_1}{D_0}, \qquad \phi_{\rm s} \overset{k\to 0}{\longrightarrow} -\frac{\pi}{2} - \frac{\phi_1}{2}, \qquad \phi_{\rm c} \overset{k\to 0}{\longrightarrow} -\frac{\phi_0}{2}, \\ &\xi \overset{k\to 0}{\longrightarrow} -\frac{\pi}{2} - \frac{\phi_0}{2}. \end{aligned} \tag{4.121}$$

With $f_{\rm sr}(E=0)=0$, the near-threshold limit of Eq. (4.119) is seen to be

$$\tan\delta_0 \overset{k\to 0}{\sim} -k\frac{D_1}{D_0}\left[\cos\left(\frac{\phi_0-\phi_1}{2}\right) + \frac{\sin(\frac{\phi_0-\phi_1}{2})}{\tan(\upsilon_{\rm D}\pi)}\right] = -k\left(\bar{a} + \frac{b}{\tan(\upsilon_{\rm D}\pi)}\right). \tag{4.122}$$

The threshold length b and the mean scattering length $\bar{a}$ are as already defined in (4.40) and (4.42) in Sect. 4.1.1, so Eq. (4.122) is consistent with the expression (4.53) for the scattering length a. Remember that a finite value for the mean scattering length $\bar{a}$ exists only for reference potentials $V_{\rm tail}(r)$ falling off faster than $1/r^3$ at large distances.

As mentioned at the beginning of this subsection, the parameters of quantum reflection by the nonclassical part the reference potential $V_{\rm tail}(r)$ can also serve as appropriate tail functions to describe the influence of $V_{\rm tail}(r)$ on the scattering phase shifts [66]. To see this, consider the solution $u_{\rm inc}(r)$ of (4.11) which obeys incoming boundary conditions for $r\to 0$ and behaves as (4.80) for $r\to\infty$. In terms of the solutions $u_{\rm s}(r)$ and $u_{\rm s}(r)$, with the asymptotic behaviour (4.109) we have

$$u_{\rm inc}(r) = -\frac{\rm i}{\sqrt{\hbar k}}(1-R)u_{\rm s}(r) + \frac{1}{\sqrt{\hbar k}}(1+R)u_{\rm c}(r). \tag{4.123}$$

From (4.111) the small-r behaviour of this wave function is

$$u_{\mathrm{inc}}(r) \overset{r\to 0}{\sim} \frac{\mathrm{e}^{-\mathrm{i}I}}{2\sqrt{\hbar k p_{\mathrm{tail}}(E;r)}}\left[(1-R)A_{\mathrm{s}}\mathrm{e}^{\mathrm{i}\phi_{\mathrm{s}}}+(1+R)A_{\mathrm{c}}\mathrm{e}^{\mathrm{i}\phi_{\mathrm{c}}}\right] + \frac{\mathrm{e}^{+\mathrm{i}I}}{2\sqrt{\hbar k p_{\mathrm{tail}}(E;r)}}\left[(1+R)A_{\mathrm{c}}\mathrm{e}^{-\mathrm{i}\phi_{\mathrm{c}}}-(1-R)A_{\mathrm{s}}\mathrm{e}^{-\mathrm{i}\phi_{\mathrm{s}}}\right], \quad (4.124)$$

with $I=\frac{1}{\hbar}\int_{r_E}^{r} p_{\mathrm{tail}}(E;r')\mathrm{d}r'$. Since $u_{\mathrm{inc}}(r)$ is required to obey incoming boundary conditions for $r\to 0$, the content of the square bracket in the lower line of (4.124) must vanish,

$$(1+R)A_{\mathrm{c}}\mathrm{e}^{-\mathrm{i}\phi_{\mathrm{c}}}=(1-R)A_{\mathrm{s}}\mathrm{e}^{-\mathrm{i}\phi_{\mathrm{s}}}. \quad (4.125)$$

The quotient $A_{\mathrm{s}}/A_{\mathrm{c}}$ of the real and positive amplitudes defined by (4.111) is thus related to the quantum reflection amplitude R by

$$\frac{A_{\mathrm{s}}}{A_{\mathrm{c}}}=\left|\frac{1+R}{1-R}\right|. \quad (4.126)$$

The phase of the square bracket on the right-hand side of the upper line of (4.124) can be deduced by exploiting (4.125) to replace either $(1-R)A_{\mathrm{s}}$ by $(1+R)A_{\mathrm{c}}\mathrm{e}^{\mathrm{i}(\phi_{\mathrm{c}}-\phi_{\mathrm{s}})}$ or $(1+R)A_{\mathrm{c}}$ by $(1-R)A_{\mathrm{s}}\mathrm{e}^{\mathrm{i}(\phi_{\mathrm{s}}-\phi_{\mathrm{c}})}$. This phase represents the argument of the transmission coefficient T as defined by (4.79), provided that the lower limit r_0 in the action integral is taken as r_E. With this definition of T,

$$\arg T=\phi_{\mathrm{s}}+\arg(1+R)=\phi_{\mathrm{c}}+\arg(1-R). \quad (4.127)$$

In terms of the amplitudes for reflection by and transmission through the nonclassical region of the reference potential $V_{\mathrm{tail}}(r)$, Eq. (4.119) reads

$$\tan\delta_0=\left|\frac{1+R}{1-R}\right|\frac{\sin([\upsilon_{\mathrm{D}}-f_{\mathrm{sr}}(E)]\pi-\xi+\arg T-\arg(1+R))}{\cos([\upsilon_{\mathrm{D}}-f_{\mathrm{sr}}(E)]\pi-\xi+\arg T-\arg(1-R))}. \quad (4.128)$$

Equation (4.119) and its rephrased version (4.128) transparently expose how the energy dependence of the scattering phase shift δ_0 is influenced by the reference potential $V_{\mathrm{tail}}(r)$. As for near-threshold quantization discussed in Sect. 4.1.1, the threshold quantum number υ_{D}, more precisely the remainder $\Delta_{\mathrm{D}}=\upsilon_{\mathrm{D}}-\lfloor\upsilon_{\mathrm{D}}\rfloor$, crucially determines the leading energy dependence of δ_0.

For reference potentials $V_{\mathrm{tail}}(r)$ falling off faster than $1/r^3$ at large distances, the leading proportionality of $\tan\delta_0$ to k comes from the prefactor (4.126) in front of the quotient of sine and cosine, and the actual value of the scattering length a depends sensitively on Δ_{D}, as seen in Eq. (4.122) and in Eq. (4.53) in Sect. 4.1.1. The scattering length a and the remainder Δ_{D} are interchangeable parameters; each one characterizes how near the most weakly bound state is to threshold.

For potentials falling off as $-1/r^3$ asymptotically, there is no finite scattering length, and the threshold quantum number's remainder Δ_{D} assumes the role of the critical parameter determining the near-threshold beahaviour of the s-wave phase shift δ_0. In 2013, Müller [67] derived the exact analytical expression for the leading

behaviour of δ_0 up to and including all terms of order k^2,

$$\tan\delta_0 = -\left[\ln(k\beta_3) + \frac{\pi}{\tan(\pi\Delta_D)} + 3\gamma_E + \ln 2 - \frac{3}{2}\right](k\beta_3) + \pi\left[\ln(k\beta_3) + \frac{\pi}{\tan(\pi\Delta_D)} + 3\gamma_E + \ln 2 - \frac{19}{12}\right](k\beta_3)^2 + O\big(k^3\big). \quad (4.129)$$

In (4.129), $\gamma_E = 0.577\cdots$ is Euler's constant (see Appendix B.3) and β_3 is the quantum length corresponding to the leading asymptotic term $-C_3/r^3$ according to (4.58).

At large energies, for which the quantum reflection amplitude is close to zero, the prefactor in (4.119), (4.128) is essentially unity and the arguments of sine and cosine in the quotient are essentially the same and equal to δ_0 itself,

$$\delta_0 \overset{k\to\infty}{\sim} \big[\upsilon_D - f_{sr}(E)\big]\pi - \xi + \phi_s = \big[\upsilon_D - f_{sr}(E)\big]\pi - \xi + \arg T. \quad (4.130)$$

In this semiclassical regime, the threshold quantum number υ_D affects the scattering phase shift only as an additive constant. Further effects due to the short-range deviation of the full interaction from the reference potential $V_{tail}(r)$ enter via the correction term $f_{sr}(E)$, which is a smooth function of energy, in particular at threshold, and vanishes at $E = 0$:

$$f_{sr}(E) = \gamma_{sr}E + O\big(E^2\big). \quad (4.131)$$

Again, the description above is particularly useful for single-power tails (4.57), for which the tail properties depend not on energy and potential strength independently, but only on the dimensionless product $k\beta_\alpha$ of the wave number k and the quantum length β_α. The point of reference in units of β_α is $r_E/\beta_\alpha = (k\beta_\alpha)^{-2/\alpha}$ according to (4.94), and the auxiliary function (4.117) is given by [65]

$$\xi = -\left(\frac{3}{4} + \frac{\nu}{2}\right)\pi + 2\nu\eta_\alpha(k\beta_\alpha)^{1-2/\alpha}, \quad \text{with } \nu = \frac{1}{\alpha-2} \quad \text{and} \quad (4.132)$$

$$\eta_\alpha = \sqrt{2} - \frac{\alpha}{\alpha+2}\,{}_2F_1\left(\frac{1}{2}, \frac{1}{2} + \frac{1}{\alpha}; \frac{3}{2} + \frac{1}{\alpha}; -1\right); \quad (4.133)$$

${}_2F_1$ stands for the hypergeometric function defined by Eq. (B.52) in Appendix B.5. The leading near-threshold behaviour of the tail functions A_s/A_c, ϕ_s and ϕ_c is, for any $\alpha > 3$ [65],

$$\frac{A_s}{A_c} \overset{k\to 0}{\sim} \nu^{2\nu}\frac{\Gamma(1-\nu)}{\Gamma(1+\nu)}k\beta_\alpha = k\sqrt{\bar{a}^2 + b^2}, \quad (4.134)$$

$$\phi_{s/c} \overset{k\to 0}{\sim} \left(-\frac{1}{2} \pm \frac{\nu - \frac{1}{2}}{2}\right)\pi + 2\nu\eta_\alpha(k\beta_\alpha)^{1-2/\alpha}. \quad (4.135)$$

The leading near-threshold behaviour of $\tan\delta_0$ is as given in (4.122), with $\bar{a}$ and b as given in Eq. (4.61) and Table 4.1 in Sect. 4.1.1. In the semiclassical limit of large k, the prefactor (4.126) approaches unity exponentially, compare Eq. (4.93),

Table 4.9 Numerical values of dimensionless parameters η_α and ρ_α as defined in Eqs. (4.133) and (4.136), respectively

α	3	4	5	6	7	$\alpha \to \infty$
η_α	0.908797	0.847213	0.802904	0.769516	0.743463	0.532840
ρ_α	0.769516	0.847213	0.885769	0.908797	0.924102	1

and

$$\phi_{\mathrm{s/c}} \overset{k\to\infty}{\sim} -\rho_\alpha (k\beta_\alpha)^{1-2/\alpha}, \quad \rho_\alpha = \sqrt{2} - \frac{\alpha/2}{\alpha-1} {}_2F_1\left(\frac{1}{2}, 1-\frac{1}{\alpha}; 2-\frac{1}{\alpha}; -1\right), \quad \alpha > 2. \tag{4.136}$$

The high-k behaviour of the phase shift is thus

$$\delta_0 \overset{k\to\infty}{\sim} \left(\upsilon_{\mathrm{D}} - f_{\mathrm{sr}}(E) + \frac{3}{4} + \frac{\nu}{2}\right)\pi - (\rho_\alpha + 2\nu\eta_\alpha)(k\beta_\alpha)^{1-2/\alpha}, \tag{4.137}$$

as already given in [31]. Numerical values of the dimensionless parameters η_α and ρ_α are listed in Table 4.9

For a single power tail (4.57), the quantum length β_α can be related to an energy E_{β_α},

$$E_{\beta_\alpha} = \frac{\hbar^2}{2\mu\beta_\alpha^2}, \tag{4.138}$$

which defines a scale separating the extreme quantum region immediately near threshold from the regime of somewhat larger energies, where the influence of the reference potential can be described semiclassically. (See also Eq. (4.70) in Sect. 4.1.1.) For $E \ll E_{\beta_\alpha}$ corresponding to $k\beta_\alpha \ll 1$, the near-threshold expansions (4.134), (4.135) apply and the phase shift may be expressed via the scattering length according to (4.122); for $\alpha = 3$ the near-threshold expansion of the phase shift is expressed via the remainder Δ_{D} according to (4.129). As the energy increases beyond E_{β_α} corresponding to $k\beta_\alpha$ growing beyond unity, the semiclassical expression (4.137) becomes increasingly accurate.

As specific examples consider single-power reference potentials (4.57) with $\alpha = 6$ and $\alpha = 4$. The auxiliary function (4.117) is given according to (4.132) in these cases by

$$\xi = -\frac{7}{8}\pi + \frac{1}{2}\eta_6 (k\beta_6)^{2/3} \quad \text{for } \alpha = 6 \quad \text{and} \tag{4.139}$$

$$\xi = -\pi + \frac{1}{2}\eta_4 (k\beta_4)^{1/2} \quad \text{for } \alpha = 4. \tag{4.140}$$

The tail functions $A_{\mathrm{s}}/A_{\mathrm{c}}$, ϕ_{s} and ϕ_{c} are shown for both powers in Fig. 4.10.

The scattering phase shifts that follow via (4.119) are shown for various values of the remainder Δ_{D} in Fig. 4.11. The leading linear behaviour near threshold, which is in accordance with Wigner's threshold law, is restricted to the extreme quantum regime $k\beta_\alpha \ll 1$ corresponding to $E \ll E_{\beta_\alpha}$. The scattering length a depends sensi-

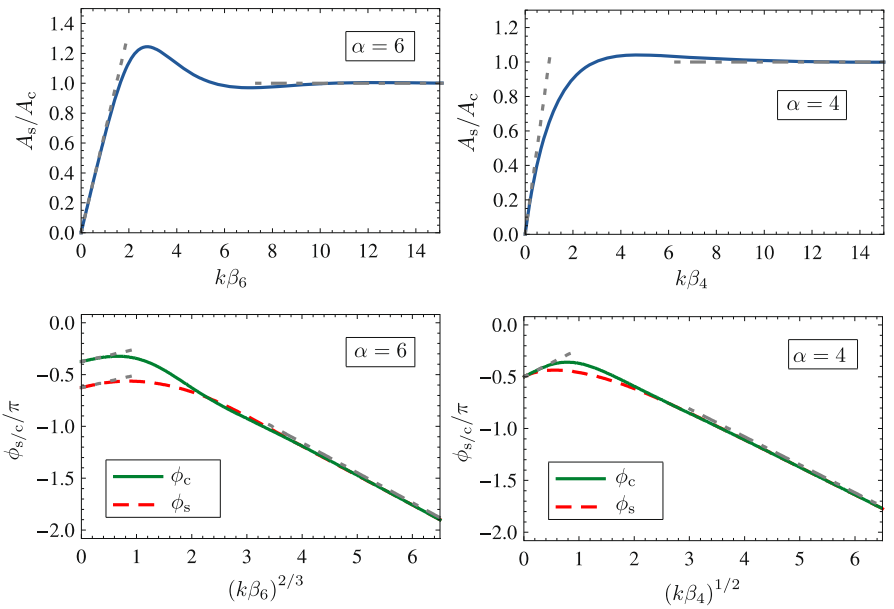

Fig. 4.10 Tail functions for a single-power reference potential (4.57) with $\alpha = 6$ (*left-hand panels*) and $\alpha = 4$ (*right-hand panels*). The *upper panels* show the ratios A_s/A_c of the amplitudes defined by the WKB representations (4.111) of the wave functions $u_s(r)$ and $u_c(r)$ in the limit $r \to 0$, as functions of $k\beta_\alpha$; the *lower panels* show the phases ϕ_s and ϕ_c as functions of $(k\beta_\alpha)^{1-2/\alpha}$. The straight *grey dashed lines* show the low-energy limits (4.134), (4.135). The straight *grey dot-dashed lines* show the high-energy limit: unity for A_s/A_c and Eq. (4.136) for $\phi_{s/c}$. (From [65])

tively on the remainder Δ_D according to (4.53) and for large $|a|$, the linear regime is restricted even further by the condition $k|a| < 1$. The dot-dashed lines in Fig. 4.11 show the cases of vanishing scattering length, which are achieved with $\Delta_D = \frac{3}{4}$ for $\alpha = 6$ and $\Delta_D = \frac{1}{2}$ for $\alpha = 4$. In these cases, the versions (2.103) or (2.286) of the effective-range expansion don't work, but the corresponding expansions for $\tan\delta_0$, e.g. (2.104) for potentials falling off faster than $1/r^5$ at large distances, are applicable. See Sects. 2.3.8 and 2.6.3 in Chap. 2.

Since the quantum lengths β_α are very large in realistic systems, typically hundreds or even many thousands of atomic units (Bohr radii), the truly quantum mechanical near-threshold regime $k\beta_\alpha \ll 1$ is tiny, as already observed for near-threshold quantization in Sect. 4.1.1. In contrast to the bound regime below threshold however, the energy spectrum above threshold is continuous and any ever so small range of energies near threshold accommodates physically meaningful wave functions.

The phase shifts shown in Fig. 4.11 were obtained via (4.119) without considering possible short-range corrections due to the deviation of the full interaction from the reference potential $V_{tail}(r)$ at small distances, i.e. assuming $f_{sr} \equiv 0$. The characteristic length scale for such short-range corrections is typically of the order of a few atomic units (Bohr radii), associated with a characteristic energy much larger

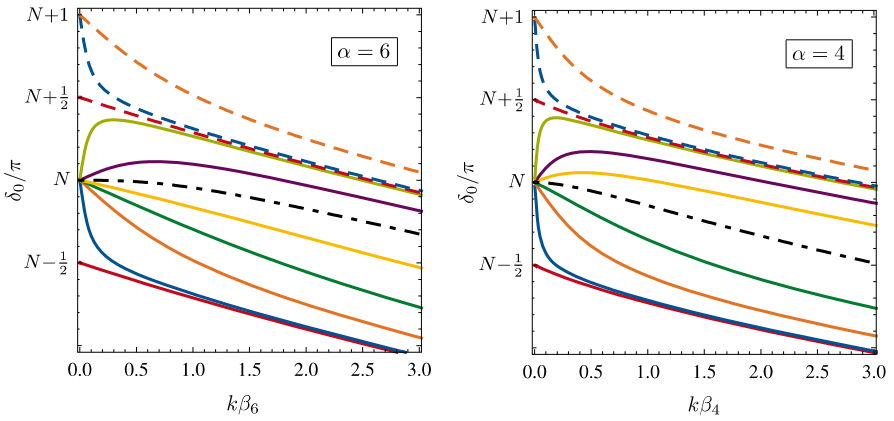

Fig. 4.11 s-wave phase shifts as given by (4.119) for a potential with a single-power tail (4.57) for various values of the remainder Δ_{D}. The additional short-range correction given through $f_{\mathrm{sr}}(E)$ is taken to be zero. The *solid lines* show the results obtained with $\Delta_{\mathrm{D}} = 0, 0.01, 0.1, 0.5, 0.99$ (from bottom to top). For the lowest three values of Δ_{D}, the plots are repeated (as *dashed lines*) with a shift of π, which would correspond to one additional bound state in a potential well. The *dot-dashed lines* show the respective phase shift for the value of Δ_{D} for which the scattering length vanishes, $\Delta_{\mathrm{D}} = \frac{3}{4}$ for $\alpha = 6$ and $\Delta_{\mathrm{D}} = \frac{1}{2}$ for $\alpha = 4$. (Adapted from [65])

than E_{β_α}. In the energy range covered in Fig. 4.11, the effect of the short-range correction term f_{sr} in (4.119) is negligibly small in a sufficiently deep Lennard–Jones type potential where the potential tail is well described by the single-power form (4.57) [65].

Consider again the Lennard–Jones potential (4.68) with $B_{\mathrm{LJ}} = 10^4$, which was studied as Example 1 in Sect. 4.1.1. The short-range correction function $f_{\mathrm{sr}}(E)$ was derived from the exact numerically calculated phase shifts by resolving Eq. (4.119), and $\upsilon_{\mathrm{D}} - f_{\mathrm{sr}}(E)$ is shown as the solid curve in the right-hand part ($E > 0$) of Fig. 4.12. The left-hand part ($E < 0$) of the figure repeats the plot in the right-hand part of Fig. 4.4, where $\upsilon + F_6(\kappa_\upsilon \beta_6)$ is plotted as function of energy for the highest five bound states $\upsilon = 19, \ldots, 23$. Note that the energy is now given in the units of E_{β_6} as defined in (4.70). It is related to the depth $\mathscr{E}$ of the Lennard–Jones potential by $E_{\beta_6}/\mathscr{E} = (B_{\mathrm{LJ}})^{-3/2}/\sqrt{2}$, which in the present case means $E_{\beta_6} \approx 0.7 \times 10^{-6}\mathscr{E}$. According to the quantization rule (4.7) and the decomposition (4.18), the squares in the left-hand part of Fig. 4.12 lie on the curve $\upsilon_{\mathrm{D}} - F_{\mathrm{sr}}(E)$, where $F_{\mathrm{sr}}(E)$ is the short-range correction to the quantization function. This curve clearly merges smoothly into the function $f_{\mathrm{sr}}(E)$ accounting for the analogous short-range correction above threshold. So the short-range correction coefficient γ_{sr}, defined by (4.19) in the subthreshold regime and by (4.131) on the scattering side of the threshold, is seen to be the same in both cases. The dashed horizontal line in Fig. 4.12 indicates the value $\upsilon_{\mathrm{D}} = 23.2327$ of the threshold quantum number and the other dashed line shows the linear function $\upsilon_{\mathrm{D}} - \gamma_{\mathrm{sr}} E$, with $\gamma_{\mathrm{sr}} = -1.16/\mathscr{E} = -8.2 \times 10^{-7}/E_{\beta_6}$, compare Table 4.5 in Sect. 4.1.1.

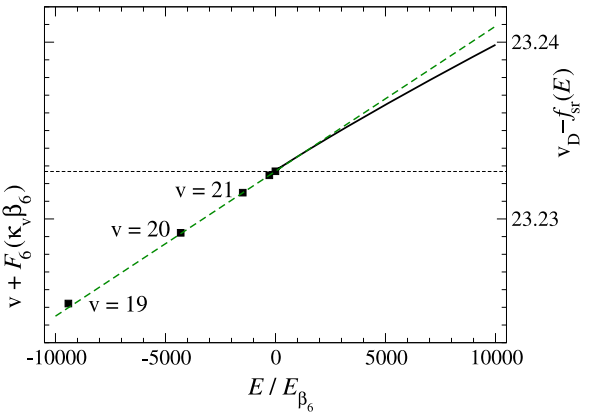

Fig. 4.12 For the Lennard–Jones potential (4.68) with $B_{LJ} = 10^4$, the left-hand part ($E < 0$) shows $\upsilon + F_6(\kappa_\upsilon \beta_6)$ as function of energy for the highest five bound states $\upsilon = 19, \ldots, 23$ (*solid squares*). The right-hand part ($E > 0$) shows $\upsilon_D - f_{sr}(E)$, derived from the exact numerically calculated phase shifts by resolving Eq. (4.119). The *dashed horizontal line* indicates the value $\upsilon_D = 23.2327$ of the threshold quantum number; the other *dashed line* shows the linear function $\upsilon_D - \gamma_{sr} E$, with $\gamma_{sr} = -1.16/\mathscr{E} = -8.2 \times 10^{-7}/E_{\beta_6}$, compare Table 4.5

4.1.4 Nonvanishing Angular Momentum

For nonvanishing angular momentum quantum number l, the radial Schrödinger equation (4.11) with the reference potential $V_{tail}(r)$ becomes

$$-\frac{\hbar^2}{2\mu}\frac{d^2u}{dr^2} + V_{tail}^{(l)}(r)u(r) = Eu(r), \quad V_{tail}^{(l)}(r) = V_{tail}(r) + \frac{l(l+1)\hbar^2}{2\mu r^2}. \tag{4.141}$$

Since $V_{tail}(r)$ is more singular than $1/r^2$ at small distances, its influence becomes increasingly dominant for $r \to 0$, and the influence of the centrifugal potential in (4.141) becomes negligible in this limit. At large distances, however, the centrifugal term dominates over $V_{tail}(r)$, which falls off faster than $1/r^2$, and this gives rise to a centrifugal barrier separating the regime of free-particle motion at large distances from the region of WKB validity for $r \to 0$. For a sufficiently deep full interaction, there still is a region of r-values where r is large enough for the full interaction to be accurately represented by the reference potential $V_{tail}(r)$ and at the same time small enough for the WKB representations of the solutions of (4.141) to be sufficiently accurate.

As example, Fig. 4.13 shows the tail of the potential already featured in Fig. 4.1 together with the effective potential, which includes the centrifugal potential, in this case for angular momentum quantum number $l = 8$. The procedure outlined in the previous three subsections can also be applied in the case of nonvanishing angular momentum. In the bound state regime, the outer classical turning point $r_{out}(E)$ does not go to infinity for $E \to 0$, but assumes a finite value $r_{E=0}$ corresponding to the inner base point of the centrifugal barrier. With this in mind, the tail contribution

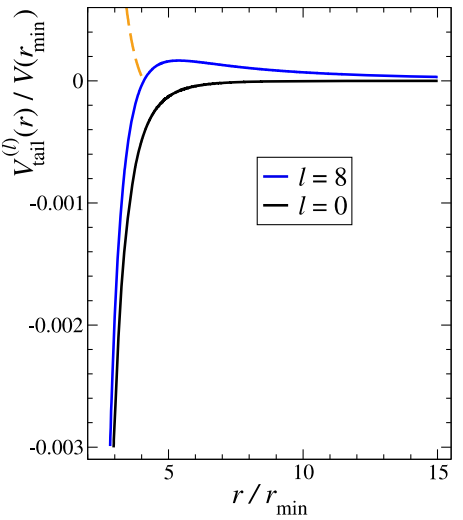

Fig. 4.13 Tail of the deep potential already featured in Fig. 4.1 (*solid black line*), together with the effective potential $V_{\rm tail}^{(l)}(r)$ as defined in (4.141), for angular momentum quantum number $l = 8$ (*solid blue line*). The *dashed orange line* shows the location of the reference point r_E which is defined for positive energies by (4.149)

$F_{\rm tail}(E)$ to the quantization function is still defined by Eq. (4.16) in Sect. 4.1.1, but the local classical momentum $p_{\rm tail}(r')$ in the action integrals is now replaced by

$$p_{\rm tail}^{(l)}(r') = \sqrt{2\mu\big[E - V_{\rm tail}^{(l)}(r')\big]}. \tag{4.142}$$

For small noninteger values of l in the range $-\frac{1}{2} < l < +\frac{1}{2}$, the leading near-threshold behaviour of $F_{\rm tail}(E)$ was derived in [59] for single power tails (4.57),[1]

$$F_\alpha^{(l)}(\kappa\beta_\alpha) \overset{\kappa\to 0}{\sim} \frac{\pi\,\nu(0)^{2\nu(l)}}{\sin[(l+\frac{1}{2})\pi](l+\frac{1}{2})\nu(l)[\Gamma(l+\frac{1}{2})\Gamma(\nu(l))]^2}\left(\frac{\kappa\beta_\alpha}{2}\right)^{2l+1} + O\big((\kappa\beta_\alpha)^{4l+2}\big) + O(E), \quad -\frac{1}{2} < l < +\frac{1}{2}; \tag{4.143}$$

here $\nu(l)$ is a generalization of $\nu \equiv \nu(0)$ as defined in (4.132),

$$\nu(l) = \frac{2l+1}{\alpha - 2}. \tag{4.144}$$

At the upper end of the interval given in (4.143), i.e., $l = \frac{1}{2}$, the energy dependence $(\kappa\beta_\alpha)^{2l+1}$ is already of order E. For all higher l-values, in particular for all positive integers, the leading energy dependence of the tail contribution to the quantization function $F_{\rm tail}^{(l)}(E)$ is of order E. A separation of tail effects from the influence of

[1] Noninteger values of l are not merely of academic interest. They can describe the effects of inverse-square potentials of other origin than the centrifugal term. In two-dimensional scattering described in Sect. 4.3, the radial Schrödinger equation with integer angular momentum quantum number m resembles that of the 3D case when $l = |m| - \frac{1}{2}$.

short-range deviations of the full interaction from the reference potential $V_{\text{tail}}(r)$ is still possible for $l > 0$. As in Figs. 4.4 and 4.6 in Sect. 4.1.1, a plot of $\upsilon + F_{\text{tail}}^{(l)}(E_\upsilon)$ against E_υ approaches a straight-line behaviour towards threshold, from which the parameters $\upsilon_{\text{D}}(l)$ and γ_{sr} can be extracted. For inverse-power tails (4.57), the threshold quantum number $\upsilon_{\text{D}}(l)$ for nonvanishing l is related to the threshold quantum number $\upsilon_{\text{D}}(0)$ by [35, 59],

$$\upsilon_{\text{D}}(l) = \upsilon_{\text{D}}(0) - \frac{l}{\alpha - 2}. \tag{4.145}$$

This relation has been used by Lemeshko and Friedrich [53, 54] to estimate the number of ro-vibrational bound states in diatomic molecules and molecular ions.

Turning to "quantum reflection", the imposition of incoming boundary conditions on the solutions of (4.141) remains meaningful for $l > 0$; it describes the absorption of all inward travelling flux which manages to penetrate the nonclassical region of the effective reference potential $V_{\text{tail}}^{(l)}(r)$. For energies below the maximum of the centrifugal barrier, the term "quantum reflection" is inappropriate, because reflection is classically allowed whereas transmission is classically forbidden. The leading near-threshold behaviour of the transmission (tunnelling) probabilities P_{T} was calculated in [58] for centrifugal barriers consisting of a single-power tail (4.57) plus the centrifugal potential, i.e., for the potential $V_{\text{tail}}^{(l)}(r)$ in (4.141),

$$P_{\text{T}} \overset{k\to 0}{\sim} \frac{4\pi^2 \nu(0)^{2\nu(l)} (k\beta_\alpha/2)^{2l+1}}{(l+\frac{1}{2})\nu(l)[\Gamma(l+\frac{1}{2})\Gamma(\nu(l))]^2}, \tag{4.146}$$

wherefrom the behaviour of the modulus of the reflection amplitude follows via

$$|R| = \sqrt{1 - P_{\text{T}}} \overset{P_{\text{T}}\to 0}{\sim} 1 - \frac{1}{2} P_{\text{T}}. \tag{4.147}$$

Note that the penetrability of the centrifugal barrier is always proportional to k^{2l+1} near threshold, and only the proportionality constant depends on the power in the reference potential $V_{\text{tail}}(r)$. In contrast to similar formulas for the near-threshold behaviour of the phases of the transmission and reflection amplitudes, the proportionality of P_{T} and of $1 - |R|$ to k^{2l+1} is not restricted by a relation like $2l + 3 < \alpha$, compare Sect. 2.6 in Chap. 2. All quantities based on the tunnelling probability through a centrifugal barrier obey Wigner's threshold law.

For ordinary scattering, the procedure described in Sect. 4.1.3 can easily be extended to the case of nonvanishing angular momentum quantum number l. For $l \neq 0$, the two linearly independent solutions of (4.141) are chosen to be those behaving asymptotically as

$$\begin{aligned} u_{\text{s}}^{(l)}(r) &\overset{r\to\infty}{\sim} kr j_l(kr) \overset{r\to\infty}{\sim} \sin\left(kr - l\frac{\pi}{2}\right), \\ u_{\text{c}}^{(l)}(r) &\overset{r\to\infty}{\sim} -kr y_l(kr) \overset{r\to\infty}{\sim} \cos\left(kr - l\frac{\pi}{2}\right). \end{aligned} \tag{4.148}$$

The amplitudes $A_{\mathrm{s,c}}$ and phases $\phi_{\mathrm{s,c}}$ are defined via the WKB representations of these wave functions for $r \to 0$, as in (4.111) for the case $l = 0$, but the local classical momentum p_{tail} is replaced by $p_{\mathrm{tail}}^{(l)}$ given by (4.142). The point of reference r_E is now chosen as the classical turning point of $-V_{\mathrm{tail}}^{(l)}(r)$,

$$V_{\mathrm{tail}}^{(l)}(r_E) = V_{\mathrm{tail}}(r_E) + \frac{l(l+1)\hbar^2}{2\mu(r_E)^2} = -E < 0. \tag{4.149}$$

The dashed orange line in Fig. 4.13 shows the location of reference point r_E for each positive energy E. At threshold, $r_E \equiv r_0$ coincides with the inner base point of the centrifugal barrier, which is also the limit of the outer classical turning point $r_{\mathrm{out}}(E)$ when the threshold is approached from below. The auxiliary tail function (4.117) is, for $l > 0$, defined by

$$\xi^{(l)} = \frac{1}{\hbar}\int_{r_E}^{r_0} p_{\mathrm{tail}}^{(l)}(0;r)\mathrm{d}r + \frac{1}{\hbar}\int_0^{r_E}\left[p_{\mathrm{tail}}^{(l)}(0;r) - p_{\mathrm{tail}}^{(l)}(E;r)\right]\mathrm{d}r - \frac{\phi_{\mathrm{out}}(0)}{2} - \frac{\pi}{2}. \tag{4.150}$$

The theory described above, including nonvanishing angular momenta, has been shown to work well in a realistic application to near-threshold bound and continuum states of the $^{88}Sr_2$ molecule in Ref. [49].

4.1.5 Summary

For a deep potential with an attractive tail falling off faster than $1/r^2$ at large distances, tail effects and short-range effects are most effectively identified by defining a reference potential $V_{\mathrm{tail}}(r)$, which describes the full interaction accurately at large distances and tends to $-\infty$ more rapidly than $-1/r^2$ at small distances. The influence of the reference potential is contained in a few tail functions, which are functions of energy that are determined solely by $V_{\mathrm{tail}}(r)$. They are related to the amplitudes and phases in the WKB representation of exact solutions of the Schrödinger equation, with $V_{\mathrm{tail}}(r)$, in the limit $r \to 0$. Since the WKB approximation is exact for $r \to 0$ in this case, referring to the WKB representation does *not* imply a semiclassical approximation.

The near-threshold bound state energies and scattering phase shifts are significantly influenced by the threshold quantum number υ_{D}, or rather by its remainder $\Delta_{\mathrm{D}} = \upsilon_{\mathrm{D}} - \lfloor \upsilon_{\mathrm{D}} \rfloor$, which is a property of the full interaction and tells us how close this is to supporting a bound state exactly at threshold. Further effects of the short-range deviation of the full interaction from $V_{\mathrm{tail}}(r)$ enter via a smooth function of energy which vanishes at threshold. We called it $F_{\mathrm{sr}}(E)$ below threshold and $f_{\mathrm{sr}}(E)$ above threshold, but both functions merge smoothly with a common gradient at $E = 0$:

$$F_{\mathrm{sr}}(E) = \gamma_{\mathrm{sr}}E + O\left(E^2\right) \quad \text{for } E < 0, \qquad f_{\mathrm{sr}}(E) = \gamma_{\mathrm{sr}}E + O\left(E^2\right) \quad \text{for } E > 0. \tag{4.151}$$

The short-range correction (4.151) vanishes in the limit that the range of the deviations of the full interaction from the reference potential $V_{\mathrm{tail}}(r)$ is small compared to the characteristic length scales of $V_{\mathrm{tail}}(r)$.

The positions of the near-threshold energy levels are determined by the quantization rule (4.7), which can be written as (4.20) when the quantization function is written as a sum of $F_{\mathrm{tail}}(E)$ and the short-range correction $F_{\mathrm{sr}}(E)$. The contribution $F_{\mathrm{tail}}(E)$ is a tail function depending only on the properties of the reference potential $V_{\mathrm{tail}}(r)$. The immediate near-threshold behaviour of the quantization function $F(E)$ and of the quantization rule (4.7) is universal for all potentials falling off faster than $1/r^2$ at large distances,

$$F(E) \overset{\kappa\to 0}{\sim} \frac{b\kappa}{\pi} + O(E), \qquad \upsilon_{\mathrm{D}} - \upsilon \overset{\kappa_\upsilon\to 0}{\sim} \frac{b\kappa_\upsilon}{\pi} + O(E), \tag{4.152}$$

where b is the threshold length. It is a property of $V_{\mathrm{tail}}(r)$ alone and is defined by Eq. (4.40).

At above-threshold energies, the s-wave scattering phase shift is given by (4.119) or, alternatively, by (4.128). In Eq. (4.119) the ratio $A_{\mathrm{s}}/A_{\mathrm{c}}$, the angles ϕ_{s}, and ϕ_{c}, as well as the auxiliary function ξ are tail functions depending only on the reference potential $V_{\mathrm{tail}}(r)$. The same holds for the quantum reflection amplitude R, the phase of the transmission amplitude T and the same auxiliary function ξ in the alternative formulation (4.128).

The immediate near-threshold behaviour of the phase shift depends sensitively on the remainder $\Delta_{\mathrm{D}} = \upsilon_{\mathrm{D}} - \lfloor \upsilon_{\mathrm{D}} \rfloor$. For potentials falling off faster than $1/r^3$ at large distances, we have $\tan\delta_0 \overset{k\to 0}{\sim} -ka$ and the scattering length a is related to the remainder Δ_{D} by (4.53), i.e.

$$a = \bar{a} + \frac{b}{\tan(\Delta_{\mathrm{D}}\pi)}, \tag{4.153}$$

where $\bar{a}$ is the mean scattering length defined in Eq. (4.42). The relation (4.153) follows from the immediate near-threshold behavior (4.121) of the tail functions occurring in (4.119). For potentials falling off as $-1/r^3$ asymptotically, the near-threshold behaviour of the tail functions yields the behaviour (4.129).

The mean scattering length $\bar{a}$ and the threshold length b together make up the complex scattering length $\mathscr{A}$ which determines the leading near-threshold behaviour of the amplitude R for quantum reflection by the reference potential $V_{\mathrm{tail}}(r)$,

$$R = -\mathrm{e}^{2\mathrm{i}\delta_0}, \quad \delta_0 \overset{k\to 0}{\sim} -k\mathscr{A}, \quad \mathscr{A} = \bar{a} - \mathrm{i}b. \tag{4.154}$$

Note that the leading near-threshold behaviour of the modulus $|R|$ of the quantum reflection amplitude is determined according to (4.89) by the threshold length b alone

$$|R| \overset{k\to 0}{\sim} 1 - 2bk + O\big(k^2\big) = \mathrm{e}^{-2bk} + O\big(k^2\big). \tag{4.155}$$

The semiclassical limit is approached away from threshold, both for positive and negative energies, i.e. for large $|E|$. The behaviour of the scattering phase shift is given in the high-k limit by Eq. (4.130), and the influence of the threshold quantum number reduces to a simple additive constant in this limit.

The theory described in this section is particularly elegant for potential tails that are well described by a single-power reference potential (4.57). In this case, all tail functions depend only on $\kappa\beta_\alpha$ (below threshold) or $k\beta_\alpha$ (above threshold). The transition between the immediate near-threshold quantum regime and the semiclassical regime away from threshold occurs when $\kappa\beta_\alpha$ or $k\beta_\alpha$ is of the order of unity. The range of the quantum regime is tiny when compared with typical potential depths, because the length scale of the reference potential is very large (in atomic units) for typical atomic or molecular interactions, see e.g. Table 1 in Ref. [17].

4.1.6 Relation to Other Approaches

Deep potentials typically occurring in atomic and molecular physics have been studied by many researchers over the years. Inspired by the success of quantum-defect theory for Coulombic potentials, i.e. modified Coulomb potentials with short-range deviations from the pure $1/r$ behaviour, Greene et al. [41, 43] and Giusti [42] formulated an adaptation of quantum-defect theory to more general situations, in particular to potentials falling off faster than $1/r^2$ at large distances. This approach was applied to elastic and inelastic scattering by several authors [37, 39, 40, 44, 63, 64]. The description of scattering in these references is essentially equivalent to the theory described in the previous five subsections in that it attempts to separate the effects due to the singular reference potential from the short-range effects due to the deviation of the full interaction from the reference potential at small distances. For a compact review of this line of work see the description beginning on p. 4962 of Ref. [75]. Although the applications of this "generalized quantum-defect theory" have been very successful, the use of the language of quantum-defect theory in connection with potentials falling off faster than $1/r^2$ at large distances has been and remains unfortunate.

The term "quantum defect" was introduced for systems described by modified Coulomb potentials to account for the shift of energy levels relative to the levels in a pure Coulomb potential, which serves as reference potential. Above the ionization threshold, the quantum-defect function describes the additional phase shift, relative to the phase of the regular wave functions in the reference potential, the pure Coulomb potential, see Sect. 2.5.4 in Chap. 2 and Sect. 3.7 in Chap. 3.

For potentials falling off faster than $1/r^2$ at large distances, the reference potentials generally in use are too singular to supply a reference spectrum of bound states or a definite phase of scattering states, relative to which a "defect" or additional phase shift could be defined. Other marked differences are the number of bound states, which is infinite for Coulombic potentials and finite for potentials falling off faster than $1/r^2$ at large distances, and the semiclassical limit, which is at $E \to 0$ for Coulombic potentials and $|E| \to \infty$ for potentials falling off faster than $1/r^2$.

Samuel Johnson once wrote: "Language is the dress of thought" [47]. For the treatment of potentials which fall off faster than $1/r^2$ at large distances, the language of quantum-defect theory is more of a disguise. Interpreting potentials that fall off faster than $1/r^2$ as a generalization of Coulombic potentials tends to obscure the fundamental differences between these two types of interaction. This is potentially confusing and can promote misconceptions. One example is provided by the observation made by Gao in 1999, that for single-power potential tails proportional to $-1/r^6$ or to $-1/r^3$ conventional WKB quantization leads to poorer results towards the dissociation threshold [38]. Although the failure of conventional WKB quantization at threshold was long well known [72], the observation in Ref. [38] was celebrated as sensational evidence for the "breakdown" of Bohr's correspondence principle, according to which the behaviour of a quantized system is expected to become increasingly (semi-)classical as the quantum number tends to infinity. This alledged breakdown of Bohr's correspondence principle was spotlighted in two key media, *Physical Review Focus* [73] and *Nature*'s "News" [6]. Apart from the fact that the limit of infinite quantum number cannot be reached in a system with a finite number of bound states, it was textbook knowledge at the time, that for homogeneous potential tails proportional to $1/r^\alpha$, the semiclassical limit is for $|E| \to \infty$ when $\alpha > 2$, and this means $E \to -\infty$ in the bound-state regime, see e.g. discussion involving Eqs. (5.153)–(5.156) in [34]. "Large quantum numbers" means not large υ, but large $\upsilon_\mathrm{D} - \upsilon$, and the semiclassical limit is approached not towards threshold but towards increasing binding energy, at least as far as the finite depth of any realistic potential well permits. Deep potentials falling off faster than $1/r^2$ at large distances thus show conformity with Bohr's correspondence principle and not its breakdown. Appropriate refutations of Ref. [38] were published in 2001 [8, 29]. In order to avoid accidents such as the one documented by Refs. [6, 38, 73], it is important to have a proper appreciation of the differences between potentials with a Coulombic tail and those falling off faster than $1/r^2$ at large distances.

A further difference to Coulombic potentials is, that realistic atomic potentials falling off faster than $1/r^2$ are often not so well represented at large distance by the leading asymptotic inverse-power term alone, at least not in an energy range encompassing more than one or two of the most weakly bound states. The universality of the theory for single-power reference potentials (4.57), where the universal tail functions depending on $\kappa\beta_\alpha$ below and on $k\beta_\alpha$ above threshold apply to all potentials with a given power α, regardless of strength, is lost when a more sophisticated reference potential is used. The tail functions must then be calculated independently for each specific system, and the question arises, whether it may not be worthwhile to simply solve the radial Schrödinger equation directly to obtain bound-state energies and scattering phase shifts.

A pragmatic approach to describe near-threshold states of deep potentials is based on defining a (analytical) model potential $V_\mathrm{mod}(r)$, which is a good approximation of the potential tail at large distances, where it is well known, and is non-singular at small distances, where the exact interaction is often not so well known. Being regular at the origin, the model potential supports a finite number of bound states below threshold and well defined scattering states above threshold. The lesser

known short-range part of the potential can be equipped with a small number of model parameters to be fitted in order to reproduce known benchmarks of problem under investigation, e.g. bound-state energy levels and the scattering length. For the bound and continuum states in a relatively narrow energy range around threshold, the behaviour of the wave functions at short distances is essentially independent of energy, and their behaviour at large distances can be obtained by solving the radial Schrödinger equation. Near-threshold effects depending on the potential tail can be described accurately in this way, because the model potential accurately represents the exact interaction at large distances. This approach is very flexible and easily extended to multi-channel scattering situations. It has been followed successfully in recent years, in particular by Tiemann and collaborators [28, 56, 79, 80, 82, 83].

4.2 Near-Threshold Feshbach Resonances

4.2.1 Motivation

The successful preparation of Bose–Einstein condensates of dilute atomic gases in 1995 [2, 25] gave a tremendous boost to the field of ultracold atoms and molecules. A new book series of annual reviews on the subject was launched in 2013 [69].

In a first approximation, a condensate of N indistinguishable bosonic particles is described by a completely symmetric many-body wave function, in which each individual boson occupies the same single-particle quantum state, $\psi_N(\mathbf{r})$. In a mean-field treatment of the interparticle interactions, this single-particle wave function is determined via the Gross–Pitaevskii equation, also called the "nonlinear Schrödinger equation". With the assumption that the mutual two-body interaction of the bosons is of short range [46], this equation can be approximately written as [23]

$$\left(-\frac{\hbar^2}{2M}\Delta + W(\mathbf{r}) + \frac{4\pi\hbar^2}{M}a\left|\psi_N(\mathbf{r})\right|^2\right)\psi_N(\mathbf{r}) = \mu_{\mathrm{cp}}\psi_N(\mathbf{r}), \tag{4.156}$$

where M is the mass of each boson, $W(\mathbf{r})$ is an external confining potential and μ_{cp} is the chemical potential which corresponds to the energy of the single-particle ground state. In this approximate version of the Gross–Pitaevskii equation, the two-particle interaction between the bosons (e.g. bosonic alkali atoms) is accounted for by the scattering length a in the term which contains $|\psi_N(\mathbf{r})|^2$ and makes the equation nonlinear. Clearly, the magnitude and the sign of the scattering length have a dominating influence of the solution of (4.156) and on whether or not a Bose–Einstein condensate can form at all.

As discussed on several occasions in this book, the scattering length depends sensitively on how close the highest bound state in a potential well is to the continuum threshold, which in an atom-atom system is the dissociation threshold, see e.g. Eq. (2.88) in Sect. 2.3.8 and Eq. (4.55) in Sect. 4.1.1; it acquires large positive values for bound states very close to threshold and large negative values if the potential

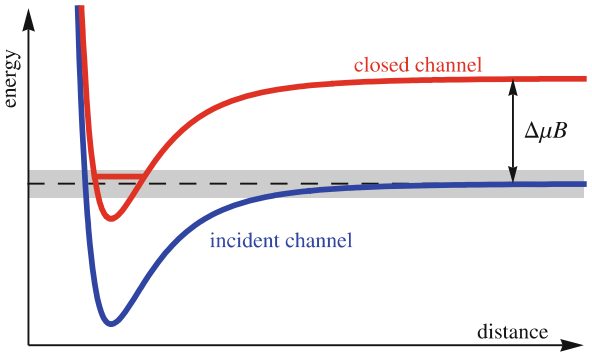

Fig. 4.14 Schematic illustration of atom–atom potentials in a two-channel situation. The closed channel (*red curve*) acquires a shift $\Delta\mu B$ relative to the lower, the "incident" channel (*blue curve*) due to different effect of a magnetic field of strength B. The closed channel supports a bound state close to the threshold of the incident channel

just fails to support a further bound state, see e.g. Fig. 2.5 in Sect. 2.3.8. As shown below, this general behaviour of the scattering length also holds when the weakly or almost bound state involved originates from an inelastic channel, i.e., when there is a Feshbach resonance at an energy very near to the threshold of the elastic channel. In diatomic systems, elastic and inelastic channels can have different magnetic properties (e.g. magnetic moments of the individual atoms), so the bound and continuum states in the elastic and in inelastic channels can acquire different shifts in the presence of an external magnetic field. This makes it possible to tune the position of a Feshbach resonance relative to the threshold of the elastic channel by varying the strength of the external field, and thus offers a practical way of manipulating and controlling Bose–Einstein condensates through the corresponding variations of the scattering length. A comprehensive review on Feshbach resonances as a tool to control the interaction in gases of ultracold atoms was published in 2010 by Chin et al. [14].

Consider the two-channel situation illustrated schematically in Fig. 4.14. In the presence of an external magnetic field of strength B, the channel thresholds are shifted by $\Delta\mu B$ due to the difference $\Delta\mu$ in the relevant magnetic moments. The upper channel is closed for energies near the threshold of the lower channel, which we call "incident channel" for want of a better word. In the absence of channel coupling, the closed channel supports a bound state at an energy E_0 near the threshold of the incident channel, and the coupling of this state to the incident-channel wave functions appears as a Feshbach resonance in the incident channel.

Close to the threshold of the incident channel, which we take to be at $E = 0$, the behaviour of the incident-channel phase shift δ is determined by the scattering length a: $\delta \overset{k\to 0}{\sim} -ak$. As the position of the Feshbach resonance is tuned to pass the threshold of the incident channel, a pole singularity of the scattering length is observed at a given strength B_0 of the magnetic field. This is generally empirically parametrized as [14, 68]

$$a = a_{\mathrm{bg}}\left(1 + \frac{\Delta B}{B - B_0}\right), \tag{4.157}$$

where a_{bg} is the background scattering length for the incident channel in the absence of channel coupling. It has become customary in the cold-atoms community to use

the term "magnetic Feshbach resonance" to describe such a pole in the scattering length. This can be confusing to anyone with a broader education in scattering theory, because Feshbach resonances are a much more general phenomenon and not restricted to energies near a threshold.

The empirical formula (4.157) satisfactorily describes the pole of the scattering length that occurs when a Feshbach resonance crosses the threshold of the incident channel, but it does not reveal the physical origin of the parameters involved nor their interdependencies. The theory described in the next two subsections aims to provide a physically motivated parametrization of a Feshbach resonance near threshold which transparently reveals its influence on scattering properties and on the bound-state spectrum.

4.2.2 Threshold-Insensitive Parametrization of a Feshbach Resonance

The influence of a single isolated Feshbach resonance on the scattering phase shift of the incident channel was given in Sect. 3.5.1 in Chap. 3,

$$\delta = \delta_{\mathrm{bg}} + \delta_{\mathrm{res}}, \qquad \tan\delta_{\mathrm{res}} = -\frac{\Gamma/2}{E - E_{\mathrm{R}}}, \tag{4.158}$$

where δ_{bg} is the background phase shift due to the potential in the uncoupled incident channel and δ_{res} is the resonant phase shift due to coupling to the bound state in the closed channel. The parameters E_{R} and Γ are given by

$$E_{\mathrm{R}} = E_0 + \langle u_{\mathrm{c}}|V_{\mathrm{c,i}}\hat{G}V_{\mathrm{i,c}}|u_{\mathrm{c}}\rangle, \qquad \Gamma = 2\pi\left|\langle u_{\mathrm{c}}|V_{\mathrm{c,i}}|\bar{\mathrm{u}}_{\mathrm{i}}^{(\mathrm{reg})}\rangle\right|^2, \tag{4.159}$$

where u_{c} is the wave function of the bound state in the uncoupled closed channel, $V_{\mathrm{c,i}}$ and $V_{\mathrm{i,c}}$ are the channel-coupling potentials, $\bar{\mathrm{u}}_{\mathrm{i}}^{(\mathrm{reg})}(r)$ is the energy-normalized regular wave function in the uncoupled incident channel and the operator $\hat{G}$ is the propagator (Green's operator) in the uncoupled incident channel; its kernel is the Green's function

$$\mathscr{G}(r, r') = -\pi\,\bar{\mathrm{u}}_{\mathrm{i}}^{(\mathrm{reg})}(r_<)\bar{\mathrm{u}}_{\mathrm{i}}^{(\mathrm{irr})}(r_>). \tag{4.160}$$

The pole of $\tan\delta_{\mathrm{res}}$ defines the resonance energy, i.e. the position E_{R} of the resonance, which differs from the bound-state energy E_0 in the uncoupled closed channel by a shift given by the matrix element containing the incident-channel propagator. When E_{R} is far from the incident-channel threshold and the channel coupling is not too strong, the energy dependence of Γ is weak and its value at $E = E_{\mathrm{R}}$ defines the width of the resonance. This straightforward interpretation breaks down towards the incident-channel threshold. The matrix element describing the shift between E_0 and E_{R} goes smoothly through a constant value at threshold, but the energy dependence of the parameter Γ poses a more serious problem.

The behaviour of $\bar{u}_i^{(\mathrm{reg})}(r)$ is, beyond the range of the incident-channel potential, given by

$$\bar{u}_i^{(\mathrm{reg})}(r) = \sqrt{\frac{2\mu}{\pi\hbar^2 k}}\sin\bigl[k(r+\delta_{\mathrm{bg}}/k)\bigr] \overset{k\to 0}{\sim} \sqrt{\frac{2\mu k}{\pi\hbar^2}}(r-a_{\mathrm{bg}}), \tag{4.161}$$

compare (3.64) in Sect. 3.5.1. Remember that the near-threshold behaviour of the phase shift δ_{bg} in the uncoupled incident channel is $\delta_{\mathrm{bg}} \overset{k\to 0}{\sim} -a_{\mathrm{bg}}k$. From (4.161) it follows, that $\bar{u}_i^{(\mathrm{reg})}(r)$ can be written as

$$\bar{u}_i^{(\mathrm{reg})}(r) = \sqrt{\frac{2\mu k}{\pi\hbar^2}}\tilde{u}_i^{(\mathrm{reg})}(r) \quad \text{with} \quad \tilde{u}_i^{(\mathrm{reg})}(r) \overset{r\to\infty,k\to 0}{\sim} (r-a_{\mathrm{bg}}). \tag{4.162}$$

The irregular radial wave $\bar{u}_i^{(\mathrm{irr})}(r)$ behaves, beyond the range of the incident-channel potential, as

$$\bar{u}_i^{(\mathrm{irr})}(r) = \sqrt{\frac{2\mu}{\pi\hbar^2 k}}\cos\bigl[k(r+\delta_{\mathrm{bg}}/k)\bigr] \overset{k\to 0}{\sim} \sqrt{\frac{2\mu}{\pi\hbar^2 k}}\cos\bigl[k(r-a_{\mathrm{bg}})\bigr], \tag{4.163}$$

and can thus be written as

$$\bar{u}_i^{(\mathrm{irr})}(r) = \sqrt{\frac{2\mu}{\pi\hbar^2 k}}\tilde{u}_i^{(\mathrm{irr})}(r) \quad \text{with} \quad \tilde{u}_i^{(\mathrm{irr})}(r) \overset{r\to\infty,k\to 0}{\longrightarrow} 1; \tag{4.164}$$

the wave function $\tilde{u}_i^{(\mathrm{irr})}(r)$ converges to a k-independent function of r at threshold. In a product of $\bar{u}_i^{(\mathrm{reg})}(r)$ and $\bar{u}_i^{(\mathrm{irr})}(r)$, the near-threshold dependencies on k cancel, so the Green's function (4.160) and the matrix element defining the energy shift in the first equation (4.159) tend to finite limits at threshold. On the other hand, the parameter Γ as defined in (4.159) vanishes proportional to k, which makes Eq. (4.158) less easy to interpret near threshold.

This problem can be solved by formulating a threshold-insensitive description of the Feshbach resonance, which is possible when the incident-channel is deep in the spirit of Sect. 4.1 and well described at large distances by a singular reference potential $V_{\mathrm{tail}}(r)$ [81]. If channel-coupling effects are of sufficiently short range, then the regular wave function in the incident channel can be written in the form (4.112) in a range of r-values, which are large enough so that the wave function already contains the effects due to the deviation of the full interaction, including channel coupling, from the uncoupled reference potential $V_{\mathrm{tail}}(r)$, and at the same time small enough for the WKB representation of the wave in the reference potential $V_{\mathrm{tail}}(r)$ to be sufficiently accurate. As elaborated in Ref. [81], the effect of the Feshbach resonance on the phase of the regular wave under the influence of $V_{\mathrm{tail}}(r)$ can be obtained in a way similar to the derivation of (4.158) and (4.159) above, except that the (energy-normalized) continuum wave functions of the incident channel are replaced by incident-channel wave functions $u_i^{(\mathrm{reg})}(r)$ which, in the range

of r-values referred to above, have the form (4.112) with the phase $\phi_{\rm sr}$ given by (4.118),

$$u_{\rm i}^{\rm (reg)}(r) = \sqrt{\frac{2\mu}{\pi\hbar}} \frac{1}{\sqrt{p_{\rm tail}(E;r)}} \sin\left(\frac{1}{\hbar}\int_{r_E}^{r} p_{\rm tail}\big(E;r'\big){\rm d}r' - \phi_{\rm sr}(E)\right). \tag{4.165}$$

[Remember that, in the range of r-values considered here, the upper limit r of the integral in (4.165) is smaller than the lower limit r_E.] The effect of channel coupling on the incident-channel wave is the same as in the standard treatment leading to Eqs. (4.158) and (4.159). The regular solution acquires an additional resonant phase

$$\phi_{\rm sr}(E) \longrightarrow \phi_{\rm sr}(E) + \arctan\left(\frac{\bar{\Gamma}/2}{E - E_{\rm R}}\right), \tag{4.166}$$

and the width $\bar{\Gamma}$ is given by

$$\bar{\Gamma} = 2\pi \left|\langle u_{\rm c}|V_{\rm c,i}|u_{\rm i}^{\rm (reg)}\rangle\right|^2, \tag{4.167}$$

where the wave function $u_{\rm i}^{\rm (reg)}(r)$ is as defined in connection with Eq. (4.165). As long as the range of r-values, where both the bound-state wave function $u_{\rm c}(r)$ in the uncoupled closed channel and the coupling potential $V_{\rm c,i}$ are significantly non-vanishing, is small, the matrix element in (4.167) is essentially independent of energy in the near-threshold regime, because the regular wave function, which behaves as (4.165) at small distances, only becomes sensitive to the threshold at large distances. The width $\bar{\Gamma}$ defined by (4.167) is thus threshold-insensitive. At energies far above the incident-channel threshold, the wave function (4.165) becomes equal to the energy-normalized regular wave function $\bar{\rm u}_{\rm i}^{\rm (reg)}(r)$ for all moderate and large distances, so

$$\Gamma \overset{E\ \text{large}}{\longrightarrow} \bar{\Gamma}. \tag{4.168}$$

With the appropriate choice of the irregular radial wave function $u_{\rm i}^{\rm (irr)}(r)$, to replace $\bar{\rm u}_{\rm i}^{\rm (irr)}(r)$ in (4.160), the product of $u_{\rm i}^{\rm (reg)}$ and $u_{\rm i}^{\rm (irr)}$ converges to a well-defined function at $E = 0$. The matrix element defining the small shift between the position $E_{\rm R}$ of the Feshbach resonance and the energy E_0 of the bound state in the uncoupled closed channel is threshold-insensitive.

The determination of the scattering phase shift in the incident channel follows as already described in Sect. 4.1.3 after Eq. (4.112). The result is

$$\tan\delta = \frac{A_{\rm s}}{A_{\rm c}} \frac{\sin([\Delta_{\rm D} - f_{\rm sr}(E)]\pi + \bar{\delta}_{\rm res} - \xi + \phi_{\rm s})}{\cos([\Delta_{\rm D} - f_{\rm sr}(E)]\pi + \bar{\delta}_{\rm res} - \xi + \phi_{\rm c})}, \tag{4.169}$$

with the threshold-insensitive resonant phase shift,

$$\bar{\delta}_{\rm res} = -\arctan\left(\frac{\bar{\Gamma}/2}{E - E_{\rm R}}\right). \tag{4.170}$$

In (4.169), $\Delta_\mathrm{D} = \upsilon_\mathrm{D} - \lfloor \upsilon_\mathrm{D} \rfloor$ is the noninteger remainder of the threshold quantum number υ_D, and the functions $A_\mathrm{s}/A_\mathrm{c}$, ϕ_s and ϕ_c as well as the auxiliary function ξ are tail functions depending only on the reference potential $V_\mathrm{tail}(r)$ in the incident channel, as defined through Eqs. (4.109), (4.111) and (4.117) in Sect. 4.1.3; $f_\mathrm{sr}(E)$ is a smooth function of E which vanishes at threshold and accounts for residual corrections due to the deviation of the full interaction in the uncoupled incident channel from the reference potential at small distances.

Since the resonance is a short-range effect, it makes sense to amalgamate the threshold-insensitive resonant phase and the uncoupled, single-channel remainder Δ_D to an "extended remainder",

$$\bar{\Delta}_\mathrm{D}(E) = \Delta_\mathrm{D} - \frac{1}{\pi} \arctan\left(\frac{\bar{\Gamma}/2}{E - E_\mathrm{R}} \right). \tag{4.171}$$

With the definition (4.171) of the extended remainder the formula (4.169) becomes,

$$\tan\delta = \frac{A_\mathrm{s}}{A_\mathrm{c}} \frac{\sin([\bar{\Delta}_\mathrm{D}(E) - f_\mathrm{sr}(E)]\pi - \xi + \phi_\mathrm{s})}{\cos([\bar{\Delta}_\mathrm{D}(E) - f_\mathrm{sr}(E)]\pi - \xi + \phi_\mathrm{c})}. \tag{4.172}$$

At energies sufficiently far above the incident-channel threshold, the ratio $A_\mathrm{s}/A_\mathrm{c}$ tends to unity and the phases ϕ_s and ϕ_c become equal. Hence the arguments of sine and cosine in the quotient on the right-hand side of (4.172) become the same and equal to the phase δ on the left-hand side, but instead of Eq. (4.130) in Sect. 4.1.3 we now have

$$\delta \overset{E \text{ large}}{\approx} \left[\bar{\Delta}_\mathrm{D}(E) - f_\mathrm{sr}(E)\right]\pi - \xi + \phi_\mathrm{s} = \delta_\mathrm{bg} + \delta_\mathrm{res} \quad \text{with}$$
$$\delta_\mathrm{bg} = \left[\Delta_\mathrm{D} - f_\mathrm{sr}(E)\right]\pi - \xi + \phi_\mathrm{s} \quad \text{and} \quad \delta_\mathrm{res} = -\arctan\left(\frac{\bar{\Gamma}/2}{E - E_\mathrm{R}} \right); \tag{4.173}$$

this is consistent with Eqs. (4.158), (4.168) above.

4.2.3 *Influence on the Scattering Length*

We now assume, that the potential falls off faster than $1/r^3$ asymptotically, so that a well defined scattering length exists. Towards threshold, an additive decomposition of the scattering phase shift δ into a background contribution and a resonant term, as in (4.173), is no longer possible. The behaviour $A_\mathrm{s}/A_\mathrm{c} \overset{k\to 0}{\propto} k$, as given in the first equation (4.121) in Sect. 4.1.3, ensures the behaviour $\delta \overset{k\to 0}{\sim} -ak$ for the scattering phase shift, and the value of the scattering length is obtained by the same steps that led to the far right-hand side of (4.122),

$$\tan\delta \overset{k\to 0}{\sim} -k\left(\bar{a} + \frac{b}{\tan(\bar{\upsilon}_\mathrm{D}(E=0)\pi)} \right) = -k\left(\bar{a} + \frac{b}{\tan(\bar{\Delta}_\mathrm{D}(E=0)\pi)} \right). \tag{4.174}$$

The essential difference between Eqs. (4.174) and (4.122) is that, in place of the threshold quantum number υ_D, Eq. (4.174) contains the threshold value of the "extended threshold quantum number",

$$\bar{\upsilon}_D(E) = \upsilon_D - \frac{1}{\pi}\arctan\left(\frac{\bar{\Gamma}/2}{E - E_R}\right), \tag{4.175}$$

or, equivalently, the extended remainder (4.171). Equation (4.174) shows that, even in the presence of a near-threshold Feshbach resonance, the phase shift $\delta(k)$ is nailed down to be an integer multiple of π at threshold, which precludes the existence of a resonance feature of finite width in the scattering phase shift straddling the threshold, as observed for the additional phase shifts in potentials with an attractive Coulombic tail, see Fig. 3.5 in Sect. 3.7.1.

The scattering length following from (4.174) is the term in the big round brackets on the right-hand sides,

$$a = \bar{a} + \frac{b}{\tan[\bar{\Delta}_D(E=0)\pi]} = \bar{a} + \frac{b}{\tan[\Delta_D\pi + \arctan(\bar{\Gamma}/(2E_R))]}. \tag{4.176}$$

In the absence of channel coupling, the incident-channel phase shift is the background phase shift δ_{bg}, and its leading near-threshold behaviour is $\delta_{bg} \overset{k\to 0}{\sim} -a_{bg}k$, which defines the background scattering length a_{bg}. It is related to the single-channel remainder, i.e. the remainder Δ_D in the uncoupled incident channel by (4.53),

$$a_{bg} = \bar{a} + \frac{b}{\tan(\Delta_D\pi)} \quad \Longrightarrow \quad \Delta_D\pi = \arctan\left(\frac{b}{a_{bg} - \bar{a}}\right). \tag{4.177}$$

Inserting the expression on the far right of (4.177) for $\Delta_D\pi$ in (4.176) gives

$$a = \left[a_{bg} + \frac{\bar{\Gamma}/2}{E_R}\left(\bar{a}\frac{a_{bg} - \bar{a}}{b} - b\right)\right]\left[1 + \frac{\bar{\Gamma}/2}{E_R}\left(\frac{a_{bg} - \bar{a}}{b}\right)\right]^{-1}. \tag{4.178}$$

Equation (4.178) is a universally valid formula for the scattering length a as function of the position E_R of a Feshbach resonance, which may be tuned, e.g. as a function of the strength of an external field, from values above threshold, $E_R > 0$, to values below threshold $E_R < 0$. On the right-hand side of (4.178), a_{bg} is the background scattering length due to the potential in the uncoupled incident channel and $\bar{\Gamma}$ is the threshold-insensitive width (4.167). The lengths $\bar{a}$ and b are the mean scattering length and the threshold length of the singular reference potential $V_{tail}(r)$; they are properties of the $V_{tail}(r)$ only and independent of the position and width of the Feshbach resonance. For a given reference potential describing the large-distance behaviour of the potential in the incident channel, the value of the scattering length depends on two quantities with a clear physical interpretation: the background scattering length a_{bg} and the ratio of the threshold-insensitive width $\bar{\Gamma}$ to the position E_R of the Feshbach resonance relative to the threshold.

If the distance E_R of the Feshbach resonance from threshold is much larger than its width, then the scattering length a is barely affected by the channel coupling,

$$\frac{\bar{\Gamma}}{E_R} \to 0 \quad \Longrightarrow \quad a \to a_{bg}. \tag{4.179}$$

If the uncoupled incident channel supports a bound state exactly at threshold, then $|a_{bg}| \to \infty$. From (4.178) we deduce,

$$|a_{bg}| \to \infty \quad \Longrightarrow \quad a = \bar{a} + b\frac{E_R}{\bar{\Gamma}/2}. \tag{4.180}$$

In this case, the scattering length a is a linear function of E_R and there is no pole.

For $|a_{bg}| < \infty$, the pole of the scattering length, which is customarily called *the* (magnetic) Feshbach resonance in the cold-atoms community, generally occurs for a nonvanishing value of E_R:

$$|a| \to \infty \quad \text{for } E_R = E_{Rpole}, \quad E_{Rpole} = \frac{\bar{\Gamma}}{2}\frac{(\bar{a} - a_{bg})}{b} = -\frac{\bar{\Gamma}/2}{\tan(\Delta_D \pi)}. \tag{4.181}$$

Whether the value of E_{Rpole} is above or below threshold depends on the sign of $\bar{a} - a_{bg}$, which in turn depends on whether the (single-channel) remainder Δ_D is smaller or larger than $\frac{1}{2}$. If the background scattering length a_{bg} is smaller than the mean scattering length of the reference potential $V_{tail}(r)$, then $\tan(\Delta_D \pi)$ is negative, corresponding to $\frac{1}{2} < \Delta_D < 1$, and $E_{Rpole} > 0$; if $a_{bg} > \bar{a}$, then $\tan(\Delta_D \pi)$ is positive, corresponding to $0 < \Delta_D < \frac{1}{2}$, and $E_{Rpole} < 0$.

A plot of the scattering length (4.178) as function of a_{bg} and $E_R/(\bar{\Gamma}/2)$ is shown in Fig. 4.15 for an inverse-power tail (4.57) with $\alpha = 6$. Dark red areas indicate large positive, dark blue areas large negative values. The white diagonal shows the position of the pole of a as given by (4.181). It crosses the vertical axis $a_{bg} = 0$ at $E_R/(\bar{\Gamma}/2) = 1$, because the two tail parameters $\bar{a}$ and b are equal in this case, compare Eq. (4.61) and Table 4.1 in Sect. 4.1.1.

4.2.4 Influence on the Bound-State Spectrum

The derivation of Eq. (4.169) was based on the influence of the Feshbach resonance on the regular incident-channel wave function (4.165), and this influence consists of an additional resonant phase in the argument of the sine on the right-hand side, see (4.166). The distances r where the representation (4.165) of the regular radial wave function is valid lie in the WKB regime where the potential is deep and where the wave functions are insensitive to the position of the threshold. The derivation can thus be continued to the bound-state regime at negative energies, which leads to a simple modification of the quantization rule (4.7)

$$\upsilon_D - \frac{1}{\pi}\arctan\left(\frac{\bar{\Gamma}/2}{E_\upsilon - E_R}\right) - \upsilon = F(E_\upsilon), \tag{4.182}$$

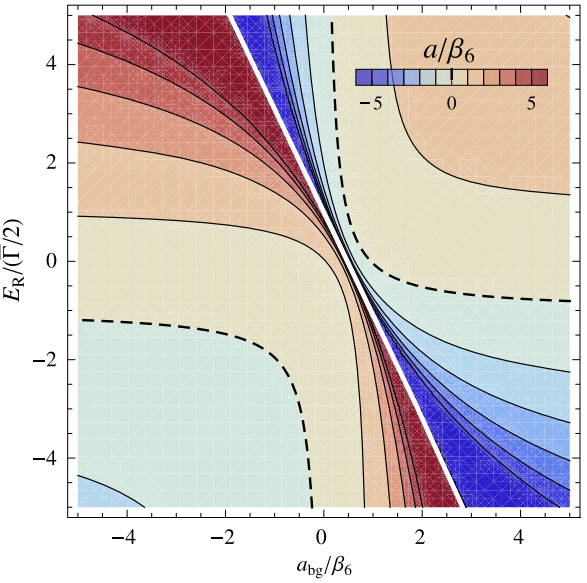

Fig. 4.15 For a single-power reference potential (4.57) with $\alpha = 6$, the figure shows values of the scattering length a given by Eq. (4.178) as function of the background scattering length a_{bg} (in units of β_6) and the position E_R of a Feshbach resonance (in units of half its threshold-insensitive width, i.e. of $\bar{\Gamma}/2$). *Dark red areas* indicate large positive, *dark blue areas* large negative values. The white diagonal shows the pole E_{Rpole} as given by (4.181). Vanishing values of a occur along the *dashed lines*. (From [81])

i.e., the threshold quantum number υ_D is simply replaced by the extended threshold quantum number (4.175),

$$\bar{\upsilon}_D(E_\upsilon) - \upsilon = F(E_\upsilon) = F_{tail}(E_\upsilon) + F_{sr}(E_\upsilon), \tag{4.183}$$

where the expression on the far-right contains the decomposition (4.18) of the quantization function $F(E)$ into the tail contribution $F_{tail}(E)$, as defined by (4.16) in Sect. 4.1.1, and the short-range correction $F_{sr}(E)$, which is a smooth function of energy and vanishes at $E = 0$. Since the quantization functions in (4.183) vanish for $E_\upsilon = 0$, the condition for the existence of a bound state exactly at threshold is now, that the threshold value of the extended threshold quantum number $\bar{\upsilon}_D(E = 0)$ be an integer, i.e. that the threshold value of the extended remainder be zero:

$$\bar{\Delta}_D(E = 0) = \Delta_D + \frac{1}{\pi}\arctan\left(\frac{\bar{\Gamma}/2}{E_R}\right) = 0. \tag{4.184}$$

[Remember that the branch of the arcus-tangent is chosen such that $\arctan(1/x)$ varies smoothly from zero to $-\pi$ as x varies from $-\infty$ to ∞.]

If the position E_R of the Feshbach resonance lies somewhat above threshold, then its influence on the bound-state spectrum is small. If it lies below threshold, $E_R < 0$, then the quantization rule (4.183) produces one additional bound state, an *intruder* or *perturber state* in the vicinity of E_R, compared to the "unperturbed" spectrum of the uncoupled incident channel. [We keep the term "incident" channel at subthreshold energies, even though there can be no genuine incident waves when the channel is closed.]

The exact position of the intruder state, i.e. of the perturber, depends on the position and width of the Feshbach "resonance" and on the unperturbed spectrum.

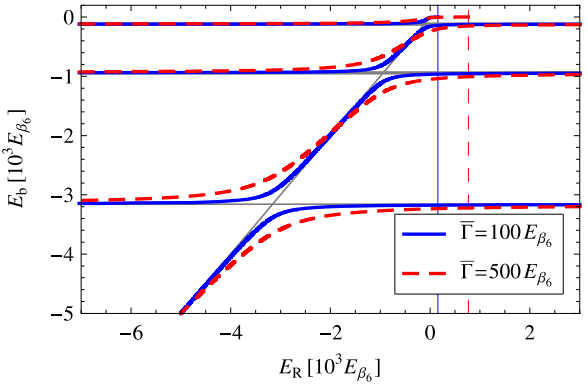

Fig. 4.16 For a deep incident-channel potential with a single-power tail (4.57) with $\alpha = 6$ and a remainder $\Delta_D = 0.9$, the highest three bound-state energies following from (4.182) are shown as functions of the position E_R of a Feshbach resonance. The *solid blue* (*dashed red*) *lines* correspond to a threshold-insensitive width $\bar{\Gamma} = 100E_{\beta_6}$ ($\bar{\Gamma} = 500E_{\beta_6}$). The short-range correction term $F_{sr}(E)$ is neglected. The unit of energy is $E_{\beta_6} = \hbar^2/[2\mu(\beta_6)^2]$. The *straight horizontal lines* show the unperturbed bound-state energies and the *straight diagonal line* corresponds to $E_b = E_R$. The *straight vertical lines* indicate the respective values of E_R at which the scattering length diverges according to (4.181). (Adapted from [81])

Near the threshold of a deep incident-channel potential, the unperturbed spectrum is essentially determined by the singular reference potential $V_{tail}(r)$ and the remainder Δ_D, as discussed in Sect. 4.1.1. Figure 4.16 shows the dependence on E_R of the energies of the highest three states, as given by Eq. (4.182), in a deep potential with an inverse-power tail (4.57) with $\alpha = 6$ for a value $\Delta_D = 0.9$ of the (single-channel) remainder. The straight horizontal lines in Fig. 4.16 show the unperturbed bound-state energies; the solid blue and dashed red lines show the perturbed bound-state energies corresponding, respectively, to the values $\bar{\Gamma} = 100E_{\beta_6}$ and $\bar{\Gamma} = 500E_{\beta_6}$ of the threshold-insensitive width. The short-range correction $F_{sr}(E)$ is neglected here.

Without channel coupling, the spectrum would consist of the unperturbed levels in the incident channel (straight horizontal lines in Fig. 4.16) plus the intruder at $E_b = E_R$ (straight diagonal line in Fig. 4.16). Channel coupling leads to avoided crossings between the unperturbed levels and the intruder state. The value of E_R for which the least bound state is exactly at threshold defines the position E_{Rpole} of the pole of the scattering length as given by (4.181). The straight vertical lines in Fig. 4.16 indicate the values of E_R at which this pole occurs for the respective choice of $\bar{\Gamma}$. According to (4.181), the pole occurs at $E_R = -\bar{\Gamma}/[2\tan(0.9\pi)] \approx 1.54 \times \bar{\Gamma}$ in the present case(s).

The bound state at threshold is a two-component wave function with contributions from the incident channel and the closed channel. Its composition can be understood in a physically appealing way as a consequence of level repulsion between the Feshbach resonance at E_R, which comes from the closed-channel bound state, and a weakly bound incident-channel state just below threshold or a state just

above threshold, which is only marginally unbound. A small value of the single-channel remainder Δ_D implies that the uncoupled incident channel supports a bound state close to threshold, which can be pushed to threshold by level repulsion from a lower-lying Feshbach resonance. A single-channel remainder Δ_D close to unity suggests a marginally unbound state just above threshold, which can be pushed down to threshold from a higher-lying Feshbach resonance; this is the situation depicted in Fig. 4.16. In both cases, the bound state at threshold is close to the uncoupled incident channel wave function with a small contribution due to coupling from the closed channel. If Δ_D is close to $\frac{1}{2}$, then the uncoupled incident channel is as far as possible from supporting a bound state at threshold. The two-channel wave function of the bound state at threshold is then strongly influenced by the Feshbach resonance from the closed-channel and it occurs at a value E_{Rpole} close to zero. If Δ_D is a little below $\frac{1}{2}$, then $E_{\mathrm{Rpole}} < 0$; a Feshbach resonance just below threshold is pushed up to threshold by the highest bound state of the incident channel. When Δ_D is a little above $\frac{1}{2}$, a Feshbach resonance just above threshold is pushed down by coupling to the incident channel; $E_{\mathrm{Rpole}} > 0$ in this case.

A relation connecting the scattering length as given by (4.176) with the asymptotic inverse penetration length κ_b of a bound state very near threshold can be found, as in the derivation of Eq. (4.55) in Sect. 4.1.1, by exploiting Eqs. (4.182)–(4.184). The low-energy expansion of the quantization function (multiplied by π) gives,

$$\pi F(E_b) \overset{\kappa_b \to 0}{\sim} b\kappa_b - \frac{1}{2}(d\kappa_b)^2 + \pi\gamma_{sr}E_b. \tag{4.185}$$

From (4.182) we have

$$\Delta_D\pi = \pi F(E_b) + \arctan\left(\frac{\bar{\Gamma}/2}{E_b - E_R}\right) \pmod{\pi}; \tag{4.186}$$

inserting this expression for $\Delta_D\pi$ in the argument of the tangent on the far right-hand side of (4.176) leads to

$$a \overset{\kappa_b \to 0}{\sim} \frac{1}{\kappa_b} + \rho_{\mathrm{eff}} + \frac{\hbar^2}{2\mu b}\left[\pi\gamma_{sr} - \frac{\bar{\Gamma}/2}{E_R^2 + (\bar{\Gamma}/2)^2}\right] + O(\kappa_b). \tag{4.187}$$

Equation (4.187) shows that the leading universal result already formulated as Eq. (2.88) in Sect. 2.3.8, namely $a \overset{\kappa_b \to 0}{\sim} 1/\kappa_b + O(\kappa_b^0)$, also holds when the near-threshold bound state is generated by the coupling of the incident channel to a near-threshold Feshbach resonance. A different result given at the end of Sect. 4.1.3 in the third edition of Ref. [34] is incorrect.

4.2.5 *Relation to the Empirical Formula (4.157)*

In a typical experiment involving a Feshbach resonance whose position is tuned past an incident channel's threshold, the quintessential observation is the pole of the scat-

tering length, which occurs when the energy E_R of the Feshbach resonance assumes the value E_{Rpole}, as given in (4.181). Expressing E_R as $E_{Rpole} + E_R - E_{Rpole}$ and exploiting (4.177) and (4.181), we can rewrite Eq. (4.176) as

$$a = a_{bg} - \frac{b}{\sin^2(\Delta_D \pi)} \frac{\bar{\Gamma}/2}{E_R - E_{Rpole}}. \tag{4.188}$$

In order to connect to the empirical formula (4.157), let's assume that the energy E_R of the Feshbach resonance depends linearly on the strength B of an external magnetic (or other) field,

$$E_R = E_{Rpole} + \Delta\mu(B - B_0), \tag{4.189}$$

where B_0 is the field strength of the pole and $\Delta\mu$ is a constant with physical dimension energy per field strength. This choice of notation is consistent with the label $\Delta\mu B$ for the variable energy in Fig. 4.14. As function of the field strength B, the scattering length (4.188) is

$$a = a_{bg} - \frac{b}{\sin^2(\Delta_D \pi)} \frac{\bar{\Gamma}/2}{\Delta\mu(B - B_0)} = a_{bg}\left[1 - \frac{b/a_{bg}}{\sin^2(\Delta_D \pi)} \frac{\bar{\Gamma}/2}{\Delta\mu(B - B_0)}\right], \tag{4.190}$$

so the width ΔB, introduced as an empirical parameter in (4.157), is explicitly given as

$$\Delta B = -\frac{b}{a_{bg}} \frac{1}{\sin^2(\Delta_D \pi)} \frac{\bar{\Gamma}}{2\Delta\mu}. \tag{4.191}$$

Expressing $\sin^2(\Delta_D \pi)$ in terms of a_{bg} according to (4.177) gives an expression for ΔB in terms of a_{bg} and the tail parameters $\bar{a}$ and b:

$$\Delta B = -\frac{\bar{\Gamma}}{2\Delta\mu} \frac{1}{b}\left[\frac{\bar{a}^2 + b^2}{a_{bg}} - 2\bar{a} + a_{bg}\right]. \tag{4.192}$$

Equations (4.191), (4.192) show that the width ΔB of a "magnetic Feshbach resonance", as observed in a typical experiment, reflects not only the strength of the coupling between the bound state in the closed channel and the incident-chanel wave functions, which is expressed in the threshold-insensitive width $\bar{\Gamma}$. It also depends sensitively on the properties of the uncoupled incident channel, as expressed in the background phase shift a_{bg}. If the uncoupled incident channel supports a bound state (or if there is a virtual state) very near threshold, a_{bg} becomes very large and the empirical formula (4.157) is no longer applicable, as discussed in connection with Eq. (4.180) above. Another interesting situation is $a_{bg} \to 0$, corresponding to little or no interaction in the absence of channel coupling. In this case, the width ΔB as defined via (4.157) diverges, and a more appropriate empirical formula would be,

$$a = a_{bg} + \frac{\Delta_B}{B - B_0} \quad \text{with} \quad \Delta_B \equiv a_{bg}\Delta B = -\frac{\bar{\Gamma}}{2\Delta\mu} \frac{1}{b}\left(\bar{a}^2 + b^2 - 2a_{bg}\bar{a} + a_{bg}^2\right). \tag{4.193}$$

The width Δ_B defined in this way has the physical dimension of a length times field strength. In the limit of vanishing background phase shift, $a_{\rm bg} \to 0$, it converges to a finite value determined by the threshold-insensitive width $\bar{\Gamma}$ of the Feshbach resonance and the tail parameters $\bar{a}$ and b.

4.3 Quantum Description of Scattering in Two Spatial Dimensions

Two-dimensional scattering problems arise naturally when the motion of projectile and target is restricted to a plane, e.g. a surface separating two bulk media. A scattering problem can also become effectively two-dimensional, if a three-dimensional configuration is translationally invariant in one direction. This is the case for a projectile scattering off a cylindrically symmetric target, e.g., an atom or molecule scattering off a cylindrical wire or nanotube. The motion of the projectile is free in the direction parallel to the cylinder axis, and we are left with a two-dimensional scattering problem in a plane perpendicular to the cylinder axis. Essential features of the two-dimensional scattering problem were illuminated by Lapidus [51], Verhaar et al. [87] and Adhikari [1] some decades ago. The recent intense activity in physics involving ultracold atoms and their interaction with nanostructures such as cylindrical nanotubes has lead to a renewed interest in this subject, in particular in the low-energy, near-threshold regime [5, 30, 48, 86].

As in Sect. 1.4 in Chap. 1 we assume that the 2D scattering process occurs in the y–z plane, where the scattering angle θ varies between $-\pi$ and π, see Fig. 4.17. As in Chap. 2, the quantum mechanical description of the scattering process is based on the Schrödinger equation

$$\left[-\frac{\hbar^2}{2\mu}\Delta + V(\mathbf{r})\right]\psi(\mathbf{r}) = E\psi(\mathbf{r}), \tag{4.194}$$

but $\mathbf{r}$ now stands for the two-component displacement vector in the y–z plane, and Δ is the 2D-Laplacian.

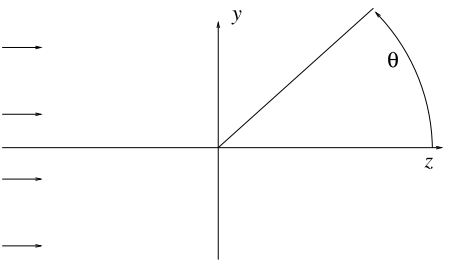

Fig. 4.17 Two-dimensional scattering in the y–z plane. The z-axis shows in the direction of incidence, and the scattering angle θ varies between $-\pi$ and π

4.3.1 Scattering Amplitude and Scattering Cross Section

We look for solutions of (4.194) with the following boundary conditions,

$$\psi(\mathbf{r}) \overset{r\to\infty}{\sim} \mathrm{e}^{\mathrm{i}kz} + f(\theta)\frac{\mathrm{e}^{\mathrm{i}kr}}{\sqrt{r}}. \tag{4.195}$$

Essential differences to the three-dimensional case (2.2) are, that the outgoing spherical wave becomes an outgoing circular wave whose amplitude decreases proportional to $1/\sqrt{r}$ instead of to $1/r$, and that the physical dimension of the scattering amplitude $f(\theta)$ is the square root of a length in the two-dimensional case. The current density $\mathbf{j}_{\mathrm{out}}(\mathbf{r})$ associated with the outgoing circular wave is

$$\mathbf{j}_{\mathrm{out}}(\mathbf{r}) = \frac{\hbar k}{\mu}\left|f(\theta)\right|^2\frac{\hat{\mathbf{e}}_{\mathbf{r}}}{r} + O\left(\frac{1}{r^{3/2}}\right), \tag{4.196}$$

while the incoming current density associated with the "plane wave" $\mathrm{e}^{\mathrm{i}kz}$ in (4.195) can again be written as $\mathbf{j}_{\mathrm{in}} = \hat{\mathbf{e}}_z\hbar k/\mu$. The surface element of a large sphere in the three-dimensional case, $r^2\mathrm{d}\Omega$, is now replaced by the arc-element of a large circle, $r\mathrm{d}\theta$, and the differential scattering cross section is defined by the flux scattered into this arc, $\mathbf{j}_{\mathrm{out}}(\mathbf{r})\cdot\hat{\mathbf{e}}_{\mathbf{r}}r\mathrm{d}\theta$, normalized to the incoming current density $|\mathbf{j}_{\mathrm{in}}| = \hbar k/\mu$,

$$\mathrm{d}\lambda = \left|f(\theta)\right|^2\mathrm{d}\theta, \qquad \frac{\mathrm{d}\lambda}{\mathrm{d}\theta} = \left|f(\theta)\right|^2. \tag{4.197}$$

The integrated scattering cross section is

$$\lambda = \int_{-\pi}^{\pi}\frac{\mathrm{d}\lambda}{\mathrm{d}\theta}\mathrm{d}\theta = \int_{-\pi}^{\pi}\left|f(\theta)\right|^2\mathrm{d}\theta. \tag{4.198}$$

Note that the differential and the integrated scattering cross sections have the physical dimension of a length. The differential cross section can be interpreted as the length perpendicular to the direction of incidence from which the incoming particles are scattered into the differential arc defined by $\mathrm{d}\theta$, while the integrated cross section corresponds to the length from which particles are scattered at all.

Particle conservation implies that the total flux through a circle, $\int_{-\pi}^{\pi}\mathbf{j}\cdot\hat{\mathbf{e}}_{\mathbf{r}}r\mathrm{d}\theta$ should vanish for large radius r. The contribution from the incoming wave $\mathrm{e}^{\mathrm{i}kz}$ vanishes on symmetry grounds, while the contribution from the outgoing circular wave is:

$$I_{\mathrm{out}} = \lim_{r\to\infty}\int_{-\pi}^{\pi}\mathbf{j}_{\mathrm{out}}(\mathbf{r})\cdot\hat{\mathbf{e}}_{\mathbf{r}}r\mathrm{d}\theta = \frac{\hbar k}{\mu}\int_{-\pi}^{\pi}\left|f(\theta)\right|^2\mathrm{d}\theta = \frac{\hbar k}{\mu}\lambda. \tag{4.199}$$

The contribution $\mathbf{j}_{\mathrm{int}}(\mathbf{r})$ of the interference of incoming "plane" and outgoing circular wave to the current density is,

$$\mathbf{j}_{\mathrm{int}}(\mathbf{r}) = \frac{\hbar k}{2\mu}f(\theta)\frac{\mathrm{e}^{\mathrm{i}k(r-z)}}{\sqrt{r}}(\hat{\mathbf{e}}_{\mathbf{r}} + \hat{\mathbf{e}}_z) + \mathrm{cc} + \cdots, \tag{4.200}$$

so the interference contribution to the flux through a circle of large radius r is

$$\mathbf{j}_{\text{int}}(\mathbf{r}) \cdot \hat{\mathbf{e}}_{\mathbf{r}} r \mathrm{d}\theta = \frac{\hbar k}{2\mu} f(\theta) \mathrm{e}^{\mathrm{i}kr(1-\cos\theta)} \sqrt{r}(1+\cos\theta) + \text{cc}. \tag{4.201}$$

The integral over the right-hand side of (4.201) can be evaluated by the method of stationary phase, since the integrand contributes only around $\cos\theta = 1$ for $r \to \infty$. This gives

$$I_{\text{int}} = \int_{-\pi}^{\pi} \mathbf{j}_{\text{int}}(\mathbf{r}) \cdot \hat{\mathbf{e}}_{\mathbf{r}} r \mathrm{d}\theta = 2\frac{\hbar k}{\mu} \sqrt{\frac{\pi}{k}} \big[\Re\big\{ f(\theta=0) \big\} - \Im\big\{ f(\theta=0) \big\} \big]. \tag{4.202}$$

Particle conservation requires $I_{\text{out}} + I_{\text{int}} = 0$, so with (4.199) we obtain the *optical theorem for scattering in two-dimensional space*,

$$\lambda = 2\sqrt{\frac{\pi}{k}} \big[\Im\big\{ f(\theta=0) \big\} - \Re\big\{ f(\theta=0) \big\} \big]. \tag{4.203}$$

4.3.2 Lippmann–Schwinger Equation and Born Approximation

Adapting the treatment of Sect. 2.2 to the case of two spatial dimensions leads to the Lippmann–Schwinger equation

$$\psi(\mathbf{r}) = \mathrm{e}^{\mathrm{i}kz} + \int \mathscr{G}_{\text{2D}}(\mathbf{r}, \mathbf{r}') V(\mathbf{r}') \psi(\mathbf{r}') \mathrm{d}\mathbf{r}', \tag{4.204}$$

which looks just like the corresponding equation (2.18) in 3D, except that the free-particle Green's function $\mathscr{G}_{\text{2D}}(\mathbf{r}, \mathbf{r}')$, defined by the 2D version of Eq. (2.16), is

$$\mathscr{G}_{\text{2D}}(\mathbf{r}, \mathbf{r}') = \frac{\mathrm{i}\mu}{2\hbar^2} H_0^{(1)}\big(k|\mathbf{r}-\mathbf{r}'|\big) \overset{k|\mathbf{r}-\mathbf{r}'|\to\infty}{\sim} \frac{\mathrm{i}\mu}{2\hbar^2} \mathrm{e}^{-\mathrm{i}\pi/4} \sqrt{\frac{2}{\pi k|\mathbf{r}-\mathbf{r}'|}} \mathrm{e}^{\mathrm{i}k|\mathbf{r}-\mathbf{r}'|}. \tag{4.205}$$

Here $H_0^{(1)}$ stands for the zero-order Hankel function of the first kind, see Eqs. (B.32) and (B.33) in Appendix B.4. In the asymptotic region $|\mathbf{r}| \gg |\mathbf{r}|'$ the Green's function in (4.204) can be replaced by

$$\mathscr{G}_{\text{2D}}(\mathbf{r}, \mathbf{r}') = \frac{\mu \mathrm{e}^{\mathrm{i}\pi/4}}{\hbar^2 \sqrt{2\pi k}} \frac{\mathrm{e}^{\mathrm{i}kr}}{\sqrt{r}} \left[\mathrm{e}^{-\mathrm{i}\mathbf{k}_{\mathbf{r}} \cdot \mathbf{r}'} + O\left(\frac{r'}{r}\right) \right]. \tag{4.206}$$

This is the 2D version of (2.19); $\mathbf{k}_{\mathbf{r}}$ again stands for $k\hat{\mathbf{e}}_{\mathbf{r}}$, but $\hat{\mathbf{e}}_{\mathbf{r}}$ is now the radial unit vector in the y–z plane. Inserting (4.206) in (4.204) gives the asymptotic form (4.195) with

$$f(\theta) = \frac{\mu \mathrm{e}^{\mathrm{i}\pi/4}}{\hbar^2 \sqrt{2\pi k}} \int \mathrm{e}^{-\mathrm{i}\mathbf{k}_{\mathbf{r}} \cdot \mathbf{r}'} V(\mathbf{r}') \psi(\mathbf{r}') \mathrm{d}\mathbf{r}'. \tag{4.207}$$

The Born approximation is defined by replacing the exact solution $\psi(\mathbf{r}')$ in the integrand in (4.207) by the incoming "plane" wave $\mathrm{e}^{\mathrm{i}kz'} = \mathrm{e}^{\mathrm{i}(k\hat{\mathbf{e}}_z)\cdot\mathbf{r}'}$,

$$f^{\mathrm{Born}}(\theta) = \frac{\mu \mathrm{e}^{\mathrm{i}\pi/4}}{\hbar^2\sqrt{2\pi k}} \int \mathrm{d}\mathbf{r}' \mathrm{e}^{-\mathrm{i}\mathbf{k}_\mathbf{r}\cdot\mathbf{r}'} V(\mathbf{r}') \mathrm{e}^{\mathrm{i}kz'} = \frac{\mu \mathrm{e}^{\mathrm{i}\pi/4}}{\hbar^2\sqrt{2\pi k}} \int \mathrm{d}\mathbf{r}' \mathrm{e}^{-\mathrm{i}\mathbf{q}\cdot\mathbf{r}'} V(\mathbf{r}'), \tag{4.208}$$

where $\hbar\mathbf{q}$ is the momentum transferred from the incoming wave travelling in the direction of $\hat{\mathbf{e}}_z$ to the outgoing wave travelling in the direction of $\hat{\mathbf{e}}_\mathbf{r}$,

$$\mathbf{q} = k(\hat{\mathbf{e}}_\mathbf{r} - \hat{\mathbf{e}}_z), \qquad q = |\mathbf{q}| = 2k\sin(\theta/2). \tag{4.209}$$

For a radially symmetric potential $V(\mathbf{r}) = V(r)$, Eq. (4.208) can be simplified via an expansion of the exponential $\mathrm{e}^{-\mathrm{i}\mathbf{q}\cdot\mathbf{r}'}$ in polar variables [compare (4.219) below],

$$f^{\mathrm{Born}}(\theta) = \frac{\mu \mathrm{e}^{\mathrm{i}\pi/4}}{\hbar^2\sqrt{2\pi k}} 2\pi \int_0^\infty V(r) J_0\big(2kr\sin(\theta/2)\big) r\,\mathrm{d}r. \tag{4.210}$$

4.3.3 Partial-Waves Expansion and Scattering Phase Shifts

For planar motion in the y–z plane, there is only one relevant component of angular momentum, namely $\hat{L} = y\hat{p}_z - z\hat{p}_y$, and in terms of the angle θ,

$$\hat{L} = \frac{\hbar}{\mathrm{i}} \frac{\partial}{\partial\theta}. \tag{4.211}$$

The eigenfunctions of $\hat{L}$ are $\mathrm{e}^{\mathrm{i}m\theta}$ with $m = 0, \pm1, \pm2, \ldots$, and the corresponding eigenvalues are $m\hbar$. Any wave function $\Psi(\mathbf{r}) \equiv \Psi(r,\theta)$ can be expanded in the complete basis of eigenfunctions of $\hat{L}$,

$$\Psi(\mathbf{r}) = \sum_{m=-\infty}^{\infty} \frac{u_m(r)}{\sqrt{r}} \mathrm{e}^{\mathrm{i}m\theta}. \tag{4.212}$$

From the polar representation of the Laplacian in 2D, we can write the kinetic energy operator in (4.194) as,

$$-\frac{\hbar^2}{2\mu}\Delta = -\frac{\hbar^2}{2\mu}\left(\frac{\partial^2}{\partial r^2} + \frac{1}{r}\frac{\partial}{\partial r}\right) + \frac{\hat{L}^2}{2\mu r^2}. \tag{4.213}$$

We assume a radially symmetric potential, $V(\mathbf{r}) = V(r)$. Inserting the expansion (4.212) into the Schrödinger equation (4.194) then gives, with the help of (4.213), an uncoupled set of radial equations for the radial wave functions $u_m(r)$,

$$\left[-\frac{\hbar^2}{2\mu}\frac{\mathrm{d}^2}{\mathrm{d}r^2} + \frac{(m^2 - \frac{1}{4})\hbar^2}{2\mu r^2} + V(r)\right] u_m(r) = E u_m(r). \tag{4.214}$$

The 2D radial Schrödinger equation looks similar to the 3D radial Schrödinger equation (2.35) in Sect. 2.3.2. In fact, Eqs. (4.214) and (2.35) are identical, if we equate $|m| - \frac{1}{2}$ with the 3D angular momentum quantum number l:

$$l \equiv |m| - \frac{1}{2}. \tag{4.215}$$

Many results derived for the 3D radial waves in Sect. 2.3 can be carried over to the 2D radial waves simply via (4.215), but integer values of m imply half-integer values of l, so the results of Sect. 2.3.2 have to be checked to see whether they hold in these cases. This is particularly important for s-waves in 2D ($m = 0$), which correspond to $l = -\frac{1}{2}$.

For the free-particle case $V(r) \equiv 0$, two linearly independent solutions of the radial equation (4.214) are

$$u_m^{(\mathrm{s})}(kr) = \sqrt{\frac{\pi}{2}kr}\, J_{|m|}(kr), \qquad u_m^{(\mathrm{c})}(kr) = -\sqrt{\frac{\pi}{2}kr}\, Y_{|m|}(kr), \tag{4.216}$$

where $J_{|m|}$ and $Y_{|m|}$ stand for the *ordinary Bessel functions* of the first and second kind, respectively [see Appendix B.4]. Their asymptotic behaviour is given by[2]

$$\begin{aligned} u_m^{(\mathrm{s})}(kr) &\overset{kr\to\infty}{\sim} \sin\left[kr - \left(|m| - \frac{1}{2}\right)\frac{\pi}{2}\right], \\ u_m^{(\mathrm{c})}(kr) &\overset{kr\to\infty}{\sim} \cos\left[kr - \left(|m| - \frac{1}{2}\right)\frac{\pi}{2}\right]. \end{aligned} \tag{4.217}$$

The influence of a potential $V(r)$ is manifest in the asymptotic phase shifts δ_m of the regular solutions of the radial Schrödinger equation (4.214). When $V(r)$ falls off faster than $1/r^2$ at large distances the effective potential in (4.214) is dominated by the centrifugal term at large distances, and the regular solution can be taken to be a superposition of the two radial free-particle wave functions (4.216) obeying (4.217),

$$u_m(r) \overset{r\to\infty}{\propto} A u_m^{(\mathrm{s})}(kr) + B u_m^{(\mathrm{c})}(kr) \overset{r\to\infty}{\propto} \sin\left[kr - \left(|m| - \frac{1}{2}\right)\frac{\pi}{2} + \delta_m\right], \tag{4.218}$$

with $\tan\delta_m = B/A$.

In order to relate the scattering phase shifts to the scattering amplitude, we first expand the incoming "plane" wave of (4.195) in partial waves,

$$\mathrm{e}^{\mathrm{i}kz} = \sum_{m=-\infty}^{\infty} \mathrm{i}^m J_m(kr)\mathrm{e}^{\mathrm{i}m\theta} \overset{kr\to\infty}{\sim} \sum_{m=-\infty}^{\infty} \frac{1}{\sqrt{2\pi \mathrm{i}kr}}\left(\mathrm{e}^{\mathrm{i}kr} + (-1)^m \mathrm{i}\mathrm{e}^{-\mathrm{i}kr}\right). \tag{4.219}$$

[2] Due to the m-independent term $\frac{\pi}{4}$ appearing in the arguments both of $u_m^{(\mathrm{s})}(kr)$ and of $u_m^{(\mathrm{c})}(kr)$ in (4.217), there is no *a priori* preference for the assignment of an asymptotic "sine-" or "cosine-like" behaviour. The present nomenclature is chosen to make the connection to the 3D case as transparent as possible.

The appropriate partial-waves expansion for the scattering amplitude is

$$f(\theta) = \sum_{m=-\infty}^{\infty} f_m \mathrm{e}^{\mathrm{i}m\theta}, \tag{4.220}$$

and the constant coefficients f_m are the partial-wave scattering amplitudes. Expressing the sum of "plane" and circular wave in the form (4.212) gives an explicit expression for the asymptotic behaviour of the radial wave functions,

$$\begin{aligned} u_m(r) &\overset{r\to\infty}{\sim} \frac{1}{\sqrt{2\pi\mathrm{i}k}}\left[(1+\sqrt{2\pi\mathrm{i}k}\,f_m)\mathrm{e}^{\mathrm{i}kr} + \mathrm{i}(-1)^m \mathrm{e}^{-\mathrm{i}kr}\right] \\ &= \frac{\mathrm{i}(-1)^m}{\sqrt{2\pi\mathrm{i}k}}\left[\mathrm{e}^{-\mathrm{i}kr} - \mathrm{i}(-1)^m(1+\sqrt{2\pi\mathrm{i}k}\,f_m)\mathrm{e}^{\mathrm{i}kr}\right]. \end{aligned} \tag{4.221}$$

We can rewrite the asymptotic form of the regular solution (4.218) as

$$\begin{aligned} u_m(r) &\overset{r\to\infty}{\propto} \sin\left[kr - \left(|m| - \frac{1}{2}\right)\frac{\pi}{2} + \delta_m\right] \\ &\propto \mathrm{e}^{-\mathrm{i}[kr-(|m|-\frac{1}{2})\frac{\pi}{2}+\delta_m]}\mathrm{e}^{-\mathrm{i}\delta_m} - \mathrm{e}^{\mathrm{i}[kr-(|m|-\frac{1}{2})\frac{\pi}{2}+\delta_m]}\mathrm{e}^{+\mathrm{i}\delta_m} \\ &\propto \mathrm{e}^{-\mathrm{i}kr} - \mathrm{e}^{-\mathrm{i}(|m|-\frac{1}{2})\pi}\mathrm{e}^{\mathrm{i}kr}\mathrm{e}^{2\mathrm{i}\delta_m}. \end{aligned} \tag{4.222}$$

Comparing the lower lines of Eqs. (4.221) and (4.222) gives

$$\mathrm{e}^{2\mathrm{i}\delta_m} = 1 + \sqrt{2\pi\mathrm{i}k}\,f_m, \quad f_m = \frac{1}{\sqrt{2\pi\mathrm{i}k}}\left(\mathrm{e}^{2\mathrm{i}\delta_m} - 1\right) = \sqrt{\frac{2\mathrm{i}}{\pi k}}\mathrm{e}^{\mathrm{i}\delta_m}\sin\delta_m. \tag{4.223}$$

Equation (4.223) can be used to express the scattering cross sections in terms of the scattering phase shifts,

$$\begin{aligned} \frac{\mathrm{d}\lambda}{\mathrm{d}\theta} &= \left|f(\theta)\right|^2 = \sum_{m,m'} f_m^* f_{m'} \mathrm{e}^{\mathrm{i}(m'-m)\theta} \\ &= \frac{2}{\pi k}\sum_{m,m'} \mathrm{e}^{\mathrm{i}(\delta_{m'}-\delta_m)}\sin\delta_{m'}\sin\delta_m \mathrm{e}^{\mathrm{i}(m'-m)\theta}, \end{aligned} \tag{4.224}$$

$$\lambda = \int_{-\pi}^{\pi}\left|f(\theta)\right|^2 \mathrm{d}\theta = 2\pi\sum_{m=-\infty}^{\infty}\left|f_m\right|^2 = \frac{4}{k}\sum_{m=-\infty}^{\infty}\sin^2\delta_m. \tag{4.225}$$

The scattering amplitude in forward direction is

$$f(\theta=0)=\sum_{m=-\infty}^{\infty} f_m=\sqrt{\frac{2\mathrm{i}}{\pi k}}\sum_{m=-\infty}^{\infty}\mathrm{e}^{\mathrm{i}\delta_m}\sin\delta_m$$

$$=\sqrt{\frac{2}{\pi k}}\sum_{m=-\infty}^{\infty}\sin\delta_m\mathrm{e}^{\mathrm{i}(\delta_m+\pi/4)},\quad\text{hence}\tag{4.226}$$

$$\Im\{f(0)\}-\Re\{f(0)\}=\frac{2}{\sqrt{\pi k}}\sum_{m=-\infty}^{\infty}\sin^2\delta_m=\frac{1}{2}\sqrt{\frac{k}{\pi}}\lambda,\tag{4.227}$$

which again yields the optical theorem (4.203).

4.3.4 Near-Threshold Behaviour of the Scattering Phase Shifts

The leading near-threshold behaviour of the phase shifts can be derived from the small-argument behaviour of the free-particle solutions (4.216),

$$u_m^{(\mathrm{s})}(kr)\overset{kr\to0}{\sim}\frac{\sqrt{\pi}}{\Gamma(|m|+1)}\left(\frac{kr}{2}\right)^{\frac{1}{2}+|m|},\tag{4.228}$$

$$u_m^{(\mathrm{c})}(kr)\overset{kr\to0}{\sim}\frac{\Gamma(|m|)}{\sqrt{\pi}}\left(\frac{kr}{2}\right)^{\frac{1}{2}-|m|}\quad\text{for } m\neq0.\tag{4.229}$$

The case $m=0$ is special, because the two powers of r appearing in (4.228) and (4.229), namely $\frac{1}{2}+|m|$ and $\frac{1}{2}-|m|$ are equal in this case. We focus first on the case $m\neq0$; the special case of s-waves in 2D is treated in Sect. 4.3.5 below.

At distances r beyond the range of the potential, the radial wave function $u_m(r)$ is a superposition of the free-particle wave functions (4.216); towards threshold, $k\to0$, the product kr tends to zero so we can make use of the small-argument expressions (4.228), (4.229),

$$u_m(r)\overset{kr\to0}{\propto}u_m^{(\mathrm{s})}(kr)+\tan\delta_m u_m^{(\mathrm{c})}(kr)$$

$$\sim\frac{\sqrt{\pi}}{\Gamma(|m|+1)}\left(\frac{k}{2}\right)^{\frac{1}{2}+|m|}\left[r^{|m|+\frac{1}{2}}+\tan\delta_m\left(\frac{k}{2}\right)^{-2|m|}\frac{\Gamma(|m|)\Gamma(|m|+1)}{\pi r^{|m|-\frac{1}{2}}}\right].\tag{4.230}$$

Directly at threshold, the radial Schrödinger equation (4.214) has a regular solution $u_m^{(0)}(r)$ which is defined up to a constant by the boundary condition $u_m^{(0)}(0)=0$ and is a function of r only. The wave function (4.230) must become proportional to this k-independent solution for $k\to0$, so in the second term in the square bracket in the

lower line of Eq. (4.230), the k-dependence of $\tan\delta_m$ must compensate the factor $(k/2)^{-2|m|}$, $\tan\delta \overset{k\to 0}{\propto} k^{2|m|}$. More explicitly,

$$\tan\delta_m \overset{k\to 0}{\sim} \mp\frac{\pi}{\Gamma(|m|)\Gamma(|m|+1)}\left(\frac{a_m k}{2}\right)^{2|m|}. \tag{4.231}$$

The characteristic length a_m appearing on the right-hand side of (4.231) is the *scattering length* in the partial wave $m \neq 0$. Equation (4.231) is essentially identical to Eq. (2.77) in Sect. 2.3.8 if we replace $|m|$ by $l + \frac{1}{2}$, except that the power $2|m|$ in (4.231) is always even for integer m, so the possibility of having positive or negative values on the right-hand side has to be explicitly included via the $\mp$ sign.

As in the 3D case, the threshold behaviour (4.231) is only valid in all partial waves if the potential $V(r)$ in the radial Schrödinger equation (4.214) falls off faster than any power of $1/r$ at large distances. For potentials falling off as $1/r^\alpha$, the considerations of Sect. 2.6 can be carried over to the 2D case, remembering that l now stands for $|m| - \frac{1}{2}$. In particular, the condition for the validity of Eq. (4.231) now reads $2|m| < \alpha - 2$. For $2|m| > \alpha - 2$, Eq. (2.274) in Sect. 2.6.1 is applicable, provided $l + \frac{1}{2}$ is replaced by $|m|$. The special case treated in Sect. 2.6.2 becomes the special case $2|m| = \alpha - 2$, and the (marginally) leading term of the near-threshold behaviour of $\tan\delta_m$ is given by Eq. (2.280).

4.3.5 The Case $m = 0$, s-Waves in Two Dimensions

The case of s-waves in two dimensions is special, because the radial Schrödinger equation (4.214) now reads

$$\left[-\frac{\hbar^2}{2\mu}\frac{\mathrm{d}^2}{\mathrm{d}r^2} - \frac{1}{4}\frac{\hbar^2}{2\mu r^2} + V(r)\right]u_{m=0}(r) = E u_{m=0}(r), \tag{4.232}$$

and the centrifugal potential is *attractive*. In the language of Sect. 2.7 on potentials with inverse-square tails, the 2D s-wave radial equation (4.232) corresponds to the "critically attractive case" treated in Sects. 2.7.1.3 and 2.7.2.3. This degree of attractivity of an inverse-square potential marks the boundary to the "over-critically attractive" case. If the factor $\frac{1}{4}$ in front of the inverse-square term in (4.232) were replaced by $\frac{1}{4} + \varepsilon$ with an ever so small positive ε, then the radial Schrödinger equation (4.232) would support an infinite dipole series of bound states, as described in Sect. 2.7.2.2.

The free-particle solutions, for $V(r) \equiv 0$ in (4.232), are

$$u^{(\mathrm{s})}_{m=0}(r) = \sqrt{\frac{\pi}{2}kr}\,J_0(kr), \qquad u^{(\mathrm{s})}_{m=0}(r) = -\sqrt{\frac{\pi}{2}kr}\,Y_0(kr), \tag{4.233}$$

compare (2.330) in Sect. 2.7.1.3 and (4.216). Their small-argument behaviour is

$$u^{(\mathrm{s})}_{m=0}(kr) \overset{kr\to 0}{\sim} \sqrt{\frac{\pi}{2}kr}, \qquad u^{(\mathrm{c})}_{m=0}(kr) \overset{kr\to 0}{\sim} -\sqrt{\frac{2}{\pi}kr}\left[\ln\left(\frac{kr}{2}\right) + \gamma_{\mathrm{E}} + O\big((kr)^2\big)\right]; \tag{4.234}$$

compare (2.332) in Sect. 2.7.1.3. Beyond the range of the interaction potential $V(r)$, the regular solution of the radial Schrödinger equation (4.232) is a superposition of the free-particle waves (4.233), and its asymptotic behaviour is,[3]

$$u_{m=0}(r) \overset{r\to\infty}{\propto} \sqrt{kr}\big[J_0(kr) - \tan\delta_{m=0} Y_0(kr)\big] \overset{kr\to\infty}{\propto} \sin\left(kr + \frac{\pi}{4} + \delta_{m=0}\right). \tag{4.235}$$

The leading near-threshold behaviour of the s-wave scattering phase shift is as already derived in Eq. (2.350),

$$\cot\delta_{m=0} \overset{k\to 0}{\sim} \frac{2}{\pi}\left(\ln\left(\frac{ka}{2}\right) + \gamma_{\mathrm{E}}\right). \tag{4.236}$$

Equation (4.236) defines the scattering length a for s-waves in two dimensions. In the limit $k \to 0$, the wave function (4.235) converges to a k-independent limit $u^{(0)}_{m=0}$,

$$u_{m=0}(r) \overset{k\to 0}{\propto} u^{(0)}_{m=0}(r) \overset{r\to\infty}{\propto} -\sqrt{r}\ln\left(\frac{r}{a}\right). \tag{4.237}$$

The wave function on the far right of (4.237) has exactly one node (beyond $r = 0$), and this node lies at $r = a$. For a potential falling off as $1/r^\alpha$ at large distances, a well-defined scattering length in the partial wave m exists as long as $2|m| < \alpha - 2$. For $m = 0$, this condition is fulfilled for all $\alpha > 2$. The scattering length a defined according to Eqs. (4.236), (4.237) is well defined for all interaction potentials which fall off faster than $1/r^2$ at large distances.

It is worthwhile to reflect a little on the remarkable situation of s-waves in 2D. At threshold, the regular free-particle wave is proportional to $\sqrt{r}$, corresponding to r^{l+1} when $l = -\frac{1}{2}$. The "irregular" solution, which we might expect to be proportional to r^{-l}, is actually proportional to $\sqrt{r}\ln r$, which seems only marginally less regular than the regular wave. An arbitrary superposition of these two free-particle waves can be written as

$$u(r) \propto A\sqrt{r} - \sqrt{r}\ln r = -\sqrt{r}\ln\left(\frac{r}{\mathrm{e}^A}\right), \tag{4.238}$$

which is just the form on the right-hand side of (4.237), with the scattering length given by $a = \mathrm{e}^A$. In two-dimensional scattering, the scattering length is never negative.

[3] Since $m = 0$ corresponds to $l = -\frac{1}{2}$, the phase shift $\tilde{\delta}$ in Sect. 2.7.2.3 is actually *the* scattering phase shift $\delta_{m=0}$ in the present case, see Eq. (2.341).

The leading near-threshold behaviour of the s-wave phase shift (4.236) was already given in Ref. [87], together with the next term of the effective-range expansion in two dimensions,

$$\cot\delta_{m=0} \overset{k\to 0}{\sim} \frac{2}{\pi}\left[\ln\left(\frac{ka}{2}\right) + \gamma_{\mathrm{E}} + \frac{(kr_{\mathrm{eff}})^2}{2}\right]; \tag{4.239}$$

the effective range in 2D is defined by

$$r_{\mathrm{eff}}^2 = 2\int_0^\infty \left(\left[w^{(0)}(r)\right]^2 - \left[u^{(0)}(r)\right]^2\right)\mathrm{d}r, \tag{4.240}$$

see also [5]. Here $u^{(0)}(r)$ is the regular solution, at threshold, of (4.232), which behaves as the right-hand side of (4.237) asymptotically, and $w^{(0)}(r)$ is the free-particle solution which has this form for all r,

$$w^{(0)}(r) = -\sqrt{r}\ln\left(\frac{r}{a}\right), \qquad u^{(0)}(r) \overset{r\to\infty}{\sim} -\sqrt{r}\ln\left(\frac{r}{a}\right). \tag{4.241}$$

In contrast to the similar-looking definition of the effective range in 3D, see Eq. (2.103) in Sect. 2.3.8, the right-hand side of (4.240) has the physical dimension of a length squared. Note that r_{eff}^2 defined in this way can be negative. The integral on the right-hand side of (4.240) converges to a well defined limit for interaction potentials falling off faster than $1/r^4$ at large distances [5].

The leading near-threshold behaviour of the scattering cross sections is, naturally, dominated by the contribution from the s-wave. From (4.220), (4.223) and (4.236) we obtain

$$f(\theta) \overset{k\to 0}{\sim} f_0 \overset{k\to 0}{\sim} \frac{\sqrt{\pi\,\mathrm{i}/(2k)}}{\ln(\frac{ka}{2}) + \gamma_{\mathrm{E}}}, \tag{4.242}$$

so

$$\frac{\mathrm{d}\lambda}{\mathrm{d}\theta} \overset{k\to 0}{\sim} \frac{\pi/(2k)}{|\ln(\frac{ka}{2}) + \gamma_{\mathrm{E}}|^2} \quad \text{and} \quad \lambda \overset{k\to 0}{\sim} \frac{\pi^2/k}{|\ln(\frac{ka}{2}) + \gamma_{\mathrm{E}}|^2}. \tag{4.243}$$

The quantum mechanical scattering cross sections in two dimensions diverge at threshold. This divergence is essentially as $1/k$, moderated marginally by the logarithmic factor. Note that the expressions in (4.242) and (4.243), where the leading behaviour contains the logarithm in the expression $\ln(ka/2) + \gamma_{\mathrm{E}}$, are only meaningful when $ka/2$ is so small, that $\ln(ka/2) < -\gamma_{\mathrm{E}}$, i.e., for

$$ka < 2\exp(-\gamma_{\mathrm{E}}). \tag{4.244}$$

For a reference potential $V_{\mathrm{tail}}(r)$, which is attractive and more singular than $1/r^2$ at short distances, and falls off faster than $1/r^2$ at large distances, the radial Schrödinger equation

$$\left[-\frac{\hbar^2}{2\mu}\frac{\mathrm{d}^2}{\mathrm{d}r^2} - \frac{1}{4}\frac{\hbar^2}{2\mu r^2} + V_{\mathrm{tail}}(r)\right]u_{m=0}(r) = E u_{m=0}(r) \tag{4.245}$$

can be solved with incoming boundary conditions, which describes absorption in the close region $r \to 0$. At large distances, the radial wave function still has the form given in the bottom line of (4.222), but the phase shift is now complex. With $m = 0$,

$$u(r) \overset{r\to\infty}{\propto} \mathrm{e}^{-\mathrm{i}kr} - \mathrm{i}\mathrm{e}^{2\mathrm{i}\delta}\mathrm{e}^{\mathrm{i}kr} \propto \mathrm{e}^{-\mathrm{i}(kr+\frac{\pi}{4})} - \mathrm{e}^{2\mathrm{i}\delta}\mathrm{e}^{\mathrm{i}(kr+\frac{\pi}{4})}. \tag{4.246}$$

The right-hand side(s) of (4.246) represent an incoming radial wave together with an outgoing radial wave, which is generated by *quantum reflection* in the nonclassical part of coordinate space. Defining the coefficient of $\mathrm{e}^{\mathrm{i}(kr+\pi/4)}$ as the quantum reflection amplitude gives

$$R = -\mathrm{e}^{2\mathrm{i}\delta}, \tag{4.247}$$

similar to Eq. (4.81) for s-waves in 3D.

The leading near-threshold behaviour of the complex phase shift $\boldsymbol{\delta}$ is given by a formula similar to (4.236), except that the real scattering length a is replaced by a complex scattering length $\mathscr{A}$, which is defined through the zero-energy solution $u^{(0)}(r)$ of (4.245) obeying incoming boundary conditions for $r \to 0$:

$$u^{(0)}(r) \overset{r\to\infty}{\propto} -\sqrt{r}\ln\left(\frac{r}{\mathscr{A}}\right) = -\sqrt{r}\ln\left(\frac{r}{|\mathscr{A}|}\right) + \sqrt{r}\mathrm{i}\arg(\mathscr{A}). \tag{4.248}$$

For the complex phase shift $\boldsymbol{\delta}$ we have

$$\cot\boldsymbol{\delta} \overset{k\to 0}{\sim} \frac{2}{\pi}\left[\ln\left(\frac{k\mathscr{A}}{2}\right) + \gamma_{\mathrm{E}}\right], \tag{4.249}$$

which, for the quantum reflection amplitude (4.247), implies

$$R \overset{k\to 0}{\sim} -1 - \frac{\mathrm{i}\pi}{\ln(\frac{k\mathscr{A}}{2}) + \gamma_{\mathrm{E}} + \mathrm{i}(\arg(\mathscr{A}) - \frac{\pi}{2})}. \tag{4.250}$$

The results (4.249) and (4.250) are derived in Ref. [5], where further terms up to and including $O(k^2)$ are also given. (Note that the quantum reflection amplitude in [5] is i times the amplitude R defined above.)

For *near-threshold quantization* in a deep potential which is well described at large distances by the singular reference potential $V_{\mathrm{tail}}(r)$, the quantization rule $\upsilon_{\mathrm{D}} - \upsilon = F(E)$ is determined by the quantization function $F(E)$, and the universal near-threshold behaviour of this quantization function for s-states in 2D is

$$F(E) \overset{\kappa\to 0}{\sim} \frac{1}{\pi}\arctan\left(\frac{\arg\mathscr{A}}{\ln(\frac{k|\mathscr{A}|}{2}) + \gamma_{\mathrm{E}}}\right) + O\big(\kappa^2\big). \tag{4.251}$$

The complex scattering length $\mathscr{A}$ is as defined in (4.248), and it is a property of the reference potential $V_{\mathrm{tail}}(r)$. The relation connecting the threshold quantum number υ_{D} with the scattering length a reads

$$a = |\mathscr{A}|\exp\left(-\frac{\arg(\mathscr{A})}{\tan(\upsilon_{\mathrm{D}}\pi)}\right), \tag{4.252}$$

so, for a bound-sate energy $E_\mathrm{b} = -\hbar^2\kappa_\mathrm{b}^2/(2\mu)$ very close to threshold,

$$a \overset{\kappa_\mathrm{b}\to 0}{\sim} \frac{2\exp(-\gamma_\mathrm{E})}{\kappa_\mathrm{b}} + O(\kappa_\mathrm{b}). \tag{4.253}$$

For further details, see Ref. [5].

4.3.6 Rutherford Scattering in Two Dimensions

An instructive example showing interesting differences to the well-studied case of scattering in 3D is the case of Rutherford scattering in two dimensions, which was first treated comprehensively by Barton [7]. The potential is

$$V(\mathbf{r}) = \frac{C}{r}. \tag{4.254}$$

This could be the interaction between two point particles whose motion is restricted to a two-dimensional plane embedded in three-dimensional space. It is worth remembering, however, that the Coulomb interaction in a genuinely two-dimensional space does not have this r-dependence. In terms of the scaled coordinate $\boldsymbol{\rho} = k\mathbf{r}$, the Schrödinger equation reads

$$\left[-\Delta_{\boldsymbol{\rho}} + \frac{2\eta}{\rho}\right]\psi = \psi, \tag{4.255}$$

where η is the Sommerfeld parameter

$$\eta = \frac{\mu C}{\hbar^2 k}. \tag{4.256}$$

As in Sect. 2.5.1, we introduce the quantum mechanical length a_C, which does not exist in classical mechanics,

$$a_C = \frac{1}{|\eta|k} = \frac{\hbar^2}{\mu|C|}, \quad |\eta| = \frac{1}{a_C k}. \tag{4.257}$$

For an attractive potential, $C < 0$ in (4.254), a_C is the usual Bohr radius.

As in the 3D case, the Schrödinger equation (4.255) has analytical solutions in 2D as well. Equations (2.190), (2.191) and (2.192) in Sect. 2.5.1 are replaced in 2D by

$$\psi_\mathrm{C}(\mathbf{r}) = \mathrm{e}^{-\frac{\pi}{2}\eta}\frac{\Gamma(\frac{1}{2}+\mathrm{i}\eta)}{\Gamma(\frac{1}{2})}\mathrm{e}^{\mathrm{i}kz}F\left(-\mathrm{i}\eta, \frac{1}{2}; \mathrm{i}k[r-z]\right), \tag{4.258}$$

$$\psi_\mathrm{C}(\mathbf{r}) = \mathrm{e}^{\mathrm{i}[kz+\eta\ln(k[r-z])]}\left[1 + O\left(\frac{1}{k[r-z]}\right)\right] + f_\mathrm{C}(\theta)\frac{\mathrm{e}^{\mathrm{i}(kr-\eta\ln 2kr)}}{\sqrt{r}}\left[1 + O\left(\frac{1}{k[r-z]}\right)\right] \tag{4.259}$$

and

$$f_{\mathrm{C}}(\theta) = -\frac{\eta \mathrm{e}^{\mathrm{i}\pi/4}}{\sqrt{2k\sin^2(\theta/2)}} \frac{\Gamma(\frac{1}{2}+\mathrm{i}\eta)}{\Gamma(1-\mathrm{i}\eta)} \mathrm{e}^{-\mathrm{i}\eta \ln[\sin^2(\theta/2)]}, \tag{4.260}$$

respectively. The function F in (4.258) again denotes the confluent hypergeometric function, see Appendix B.5. With the identities

$$\left|\Gamma\left(\frac{1}{2}+\mathrm{i}\eta\right)\right|^2 = \frac{\pi}{\cosh(\pi\eta)}, \qquad \left|\Gamma(1-\mathrm{i}\eta)\right|^2 = \frac{\pi\eta}{\sinh(\pi\eta)}, \tag{4.261}$$

we obtain the differential cross section for Rutherford scattering in two dimensions,

$$\frac{\mathrm{d}\lambda}{\mathrm{d}\theta} = \left|f_{\mathrm{C}}(\theta)\right|^2 = \frac{\eta\tan(\pi\eta)}{2k\sin^2(\theta/2)} = \frac{|C|}{4E}\frac{\tanh(\pi|\eta|)}{\sin^2(\theta/2)} = \left(\frac{\mathrm{d}\lambda}{\mathrm{d}\theta}\right)_{\mathrm{Ruth}}^{\mathrm{qm}}. \tag{4.262}$$

In contrast to the 3D case, the quantum mechanical result (4.262) does *not* agree with the classical Rutherford cross section in two dimensions,

$$\left(\frac{\mathrm{d}\lambda}{\mathrm{d}\theta}\right)_{\mathrm{Ruth}}^{\mathrm{class}} = \frac{|C|}{4E}\frac{1}{\sin^2(\theta/2)}, \tag{4.263}$$

see Eq. (1.55) in Sect. 1.4. On the other hand, evaluating Eq. (4.210) gives the corresponding result in Born approximation,

$$\left(\frac{\mathrm{d}\lambda}{\mathrm{d}\theta}\right)_{\mathrm{Ruth}}^{\mathrm{Born}} = \left(\frac{\mu C}{\hbar^2}\right)^2 \frac{\pi}{2k^3\sin^2(\theta/2)} = \frac{|C|}{4E}\frac{\pi|\eta|}{\sin^2(\theta/2)}. \tag{4.264}$$

In terms of the quantum mechanical length a_C (the "Bohr radius") defined in (4.257),

$$\left(\frac{\mathrm{d}\lambda}{\mathrm{d}\theta}\right)_{\mathrm{Ruth}}^{\mathrm{qm}} = \frac{a_C/2}{(a_C k)^2}\frac{\tanh[\pi/(a_C k)]}{\sin^2(\theta/2)}, \tag{4.265}$$

$$\left(\frac{\mathrm{d}\lambda}{\mathrm{d}\theta}\right)_{\mathrm{Ruth}}^{\mathrm{class}} = \frac{a_C/2}{(a_C k)^2}\frac{1}{\sin^2(\theta/2)}, \qquad \left(\frac{\mathrm{d}\lambda}{\mathrm{d}\theta}\right)_{\mathrm{Ruth}}^{\mathrm{Born}} = \frac{a_C/2}{(a_C k)^2}\frac{\pi/(a_C k)}{\sin^2(\theta/2)}. \tag{4.266}$$

Comparing Eqs. (4.265) and (4.266) shows that the coincidence of Rutherford scattering in 3D, namely that classical mechanics, the Born approximation and the full quantum mechanical treatment all yield the same result (1.42) for the differential scattering cross section [see also (2.194) and (2.196) in Sect. 2.5.1], is lifted in two spatial dimensions. The angular dependence, $\mathrm{d}\lambda/\mathrm{d}\theta \propto 1/\sin^2(\theta/2)$, is the same in all three cases, but the energy-dependent prefactors of the classical cross section and of the Born approximation differ from the exact quantum mechanical result. This is illustrated in Fig. 4.18, where the respective differential cross sections, multiplied by $\sin^2(\theta/2)$, are plotted as a functions of the dimensionless product $ka_C = 1/|\eta|$.

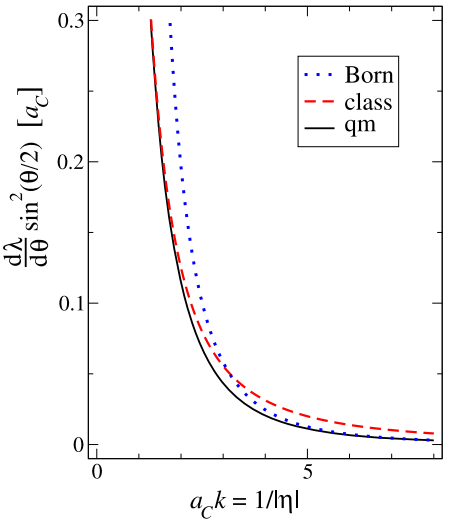

Fig. 4.18 Rutherford scattering in two spatial dimensions. The *solid black line* shows the exact quantum mechanical differential cross section (4.265) [in units of the "Bohr radius" a_C] multiplied by $\sin^2(\theta/2)$ as function of the dimensionless product $a_C k = 1/|\eta|$. The *dashed red line* and the *dotted blue line* show the corresponding classical result and the result of the Born approximation (4.266)

Both the classical cross section and the Born approximation overestimate the exact quantum mechanical cross sections (4.262), (4.265). As already observed by Barton [7], the Born approximation becomes accurate in the high-energy limit, whereas the classical result becomes exact in the low-energy limit,

$$\left(\frac{d\lambda}{d\theta}\right)^{\text{Born}}_{\text{Ruth}} \overset{k\to\infty}{\sim} \left(\frac{d\lambda}{d\theta}\right)^{\text{qm}}_{\text{Ruth}}, \qquad \left(\frac{d\lambda}{d\theta}\right)^{\text{class}}_{\text{Ruth}} \overset{k\to 0}{\sim} \left(\frac{d\lambda}{d\theta}\right)^{\text{qm}}_{\text{Ruth}}. \tag{4.267}$$

The example is a nice illustration of the fact that, for homogeneous potentials of degree -1, i.e., of the Coulomb type, the classical limit is at the threshold $E = 0$, and the classical treatment becomes increasingly inaccurate for large values of $|E|$. This is well accepted for bound states at negative energies, where $E \to 0$ corresponds to the limit of infinite quantum numbers, but it is not so widely appreciated for the regime of positive energies.

References

1. Adhikari, S.K.: Quantum scattering in two dimensions. Am. J. Phys. **54**, 362 (1986)
2. Anderson, M.H., Ensher, J.R., Matthews, M.R., Wieman, C.E., Cornell, E.A.: Observation of Bose–Einstein condensation in a dilute atomic vapor. Science **269**, 198 (1995)
3. Arnecke, F., Friedrich, H., Madroñero, J.: Effective-range expansion for quantum reflection amplitudes. Phys. Rev. A **74**, 062702 (2006)
4. Arnecke, F., Friedrich, H., Madroñero, J.: Scattering of ultracold atoms by absorbing nanospheres. Phys. Rev. A **75**, 042903 (2007)
5. Arnecke, F., Friedrich, H., Raab, P.: Near-threshold scattering, quantum reflection, and quantization in two dimensions. Phys. Rev. A **78**, 052711 (2008)
6. Ball, P.: Lost correspondence. Nature (1999). doi:10.1038/news991202-2, http://www.nature.com/news/1999/991126/full/news991202-2.html

7. Barton, G.: Rutherford scattering in two dimensions. Am. J. Phys. **51**, 420 (1982)
8. Boisseau, C., Audouard, E., Vigué, J.: Comment on "Breakdown of Bohr's correspondence principle". Phys. Rev. Lett. **86**, 2694 (2001)
9. Barton, G.: Frequency shifts near an interface: inadequacy of two-level atomic models. J. Phys. B **7**, 2134 (1974)
10. Böheim, J., Brenig, W., Stutzki, J.: On the low energy limit of reflection and sticking coefficients in atom-surface scattering II: Long range forces. Z. Phys. B **48**, 43 (1982). Erratum: Z. Phys. B **49**, 362 (1983)
11. Berry, M.V., Mount, K.E.: Semiclassical approximations in wave mechanics. Rep. Prog. Phys. **35**, 315 (1972)
12. Brenig, W.: Low-energy limit of reflection and sticking coefficients in atom surface scattering: 1. Short-range forces. Z. Phys. B **36**, 227 (1980)
13. Bodo, E., Zhang, P., Dalgarno, A.: Ultra-cold ion–atom collisions: near resonant charge exchange. New J. Phys. **10**, 033024 (2008)
14. Chin, C., Grimm, R., Julienne, P., Tiesinga, E.: Feshbach resonances in ultracold gase. Rev. Mod. Phys. **82**, 1225 (2010)
15. Côté, R., Heller, E.J., Dalgarno, A.: Quantum suppression of cold atomic collisions. Phys. Rev. A **53**, 234 (1996)
16. Carbonell, J., Lasauskas, R., Delande, D., Hilico, L., Kiliç, S.: A new vibrational level of the H_2^+ molecular ion. Europhys. Lett. **64**, 316 (2003)
17. Crubellier, A., Luc-Koenig, E.: Threshold effects in the photoassociation of cold atoms: R-6 model in the Milne formalism. J. Phys. B **39**, 1417 (2006)
18. Clougherty, D.P., Kohn, W.: Quantum theory of sticking. Phys. Rev. B **46**, 4921 (1992)
19. Casimir, H.B.G., Polder, D.: The influence of retardation on the London–van der Waals forces. Phys. Rev. **73**, 360 (1948)
20. Côté, R., Segev, B.: Quantum reflection engineering: the bichromatic evanescent-wave mirror. Phys. Rev. A **67**, 041604(R) (2003)
21. Druzhinina, V., DeKieviet, M.: Experimental observation of quantum reflection far from threshold. Phys. Rev. Lett. **91**, 193202 (2003)
22. Del Giudice, E., Galzenati, E.: On singular potential scattering I. Nuovo Cimento **38**, 435 (1965)
23. Dalfovo, F., Giorgini, S., Guilleumas, M., Pitaevskii, L., Stringari, S.: Collective and single-particle excitations of a trapped Bose gas. Phys. Rev. A **56**, 3840 (1997)
24. Dickinson, A.S.: Quantum reflection model for ionization rate coefficients in cold metastable helium collisions. J. Phys. B **40**, F237 (2007)
25. Davis, K.B., Mewes, M.-O., Andrews, M.R., van Druten, N.J., Durfee, D.S., Kurn, D.M., Ketterle, W.: Bose–Einstein condensation in a gas of sodium atoms. Phys. Rev. Lett. **75**, 3969 (1995)
26. Dashevskaya, E.I., Maergoiz, A.I., Troe, J., Litvin, I., Nikitin, E.E.: Low-temperature behavior of capture rate constants for inverse power potentials. J. Chem. Phys. **118**, 7313 (2003)
27. Damburg, R.J., Propin, R.K.: On asymptotic expansions of electronic terms of the molecular ion H_2^+. J. Phys. B **1**, 681 (1968)
28. Docenko, O., Tamanis, M., Zaharova, J., Ferber, R., Pashov, A., Knöckel, H., Tiemann, E.: The coupling of the $X^1\Sigma^+$ and $a^3\Sigma^+$ states of the atom pair Na + Cs and modelling cold collisions. J. Phys. B **39**, S929 (2006)
29. Eltschka, C., Friedrich, H., Moritz, M.J.: Comment on "Breakdown of Bohr's correspondence principle". Phys. Rev. Lett. **86**, 2693 (2001)
30. Fink, M., Eiglsperger, J., Madroñero, J., Friedrich, H.: Influence of retardation in the scattering of ultracold atoms by conducting nanowires. Phys. Rev. A **85**, 040702(R) (2012); Fink, M.: Scattering and Absorption of Ultracold Atoms by Nanotubes. Doctoral thesis, Technical University Munich (2013): http://mediatum.ub.tum.de/doc/1141600/1141600.pdf
31. Flambaum, V.V., Gribakin, G., Harabati, C.: Analytical calculation of cold-atom scattering. Phys. Rev. A **59**, 1998 (1999)

32. Friedrich, H., Jurisch, A.: Quantum reflection times for attractive potential tails. Phys. Rev. Lett. **92**, 103202 (2004)
33. Friedrich, H., Jacoby, G., Meister, C.G.: Quantum reflection by Casimir van der Waals potential tails. Phys. Rev. A **65**, 032902 (2002)
34. Friedrich, H.: Theoretical Atomic Physics, 2nd edn. Springer, Berlin (1998). 3rd. Ed. 2006
35. Friedrich, H., Trost, J.: Working with WKB waves far from the semiclassical limit. Phys. Rep. **397**, 359 (2004)
36. Gribakin, G.F., Flambaum, V.V.: Calculation of the scattering length in atomic collisions using the semiclassical approximation. Phys. Rev. A **48**, 546 (1993)
37. Gao, B.: Quantum-defect theory of atomic collisions and molecular vibration spectra. Phys. Rev. A **58**, 4222 (1998)
38. Gao, B.: Breakdown of Bohr's correspondence principle. Phys. Rev. Lett. **83**, 4225 (1999)
39. Gao, B.: General form of the quantum-defect theory for $-1/r^{\alpha}$ type of potentials with $\alpha > 2$. Phys. Rev. A **78**, 012702 (2008)
40. Gao, B.: Universal properties in ultracold ion–atom interactions. Phys. Rev. Lett. **104**, 231201 (2010)
41. Greene, C., Fano, U., Strinati, G.: General form of quantum defect theory. Phys. Rev. A **19**, 1485 (1979)
42. Giusti, A.: A multichannel quantum defect approach to dissociative recombination. J. Phys. B **13**, 3867 (1980)
43. Greene, C.H., Rau, A.R.P.: General form of the quantum-defect theory. II. Phys. Rev. A **26**, 2441 (1982)
44. Gao, B., Tiesinga, E., Williams, C.J., Julienne, P.S.: Multichannel quantum-defect theory for slow atomic collisions. Phys. Rev. A **72**, 042719 (2005)
45. Hilico, L., Billy, N., Grémaud, B., Delande, D.: Ab initio calculation of the $J = 0$ and $J = 1$ states of the H_2^+, D_2^+ and HD^+ molecular ions. Eur. Phys. J. D **12**, 449 (2000)
46. Huang, K., Yang, C.N.: Quantum-mechanical many-body problem with hard-sphere interaction. Phys. Rev. A **105**, 767 (1957)
47. Johnson, S.: Life of Abraham Cowley. In: Lonsdale, R. (ed.) The Lives of the Most Eminent English Poets. Oxford University Press, Oxford (2006). (First published 1781)
48. Khuri, N.N., Martin, A., Richard, J.-M., Wu, T.T.: Low-energy potential scattering in two and three dimensions. J. Math. Phys. **50**, 072105 (2009)
49. Kaiser, A., Müller, T.-O., Friedrich, H.: Influence of higher-order dispersion coefficients on near-threshold bound and continuum states: application to $^{88}Sr_2$. J. Chem. Phys. **135**, 214302 (2011)
50. Kaiser, A., Müller, T.-O., Friedrich, H.: Quantisation rule for highly excited vibrational states of H_2^+. Mol. Phys. **111**, 878 (2013)
51. Lapidus, I.R.: Quantum-mechanical scattering in two dimensions. Am. J. Phys. **50**, 45 (1982)
52. LeRoy, R.J., Bernstein, R.B.: Dissociation energy and long-range potential of diatomic molecules from vibrational spacings of higher levels. J. Chem. Phys. **52**, 3869 (1970)
53. Lemeshko, M., Friedrich, B.: Rotational and rotationless states of weakly bound molecules. Phys. Rev. A **79**, 050501 (2009)
54. Lemeshko, M., Friedrich, B.: Rotational structure of weakly bound molecular ions. J. At. Mol. Sci. **1**, 39 (2010)
55. Landau, L.D., Lifschitz, E.M.: Quantenmechanik. Theoretische Physik, vol. 3, p. 81. Akademie-Verlag, Berlin (1965)
56. Laue, T., Tiesinga, E., Samuelis, C., Knöckel, H., Tiemann, E.: Magnetic-field imaging of weakly bound levels of the ground-state Na_2 dimer. Phys. Rev. A **65**, 023412 (2002)
57. Marinescu, M., Dalgarno, A., Babb, J.F.: Retarded long-range potentials for the alkali-metal atoms and a perfectly conducting wall. Phys. Rev. A **55**, 1530 (1997)
58. Moritz, M.J., Eltschka, C., Friedrich, H.: Threshold properties of attractive and repulsive inverse-square potentials. Phys. Rev. A **63**, 042101 (2001)
59. Moritz, M.J., Eltschka, C., Friedrich, H.: Near-threshold quantization and level densities for potential wells with weak inverse-square tail. Phys. Rev. A **64**, 022101 (2001)

60. Madroñero, J., Friedrich, H.: Influence of realistic atom wall potentials in quantum reflection traps. Phys. Rev. A **75**, 022902 (2007)
61. Mody, A., Haggerty, M., Doyle, J.M., Heller, E.J.: No-sticking effect and quantum reflection in ultracold collisions. Phys. Rev. B **64**, 085418 (2001)
62. Müller, T.-O., Friedrich, H.: Near-threshold quantization for potentials with inverse-cube tails. Phys. Rev. **83**, 022701 (2011)
63. Mies, F.: A multichannel quantum defect analysis of diatomic predissociation and inelastic atomic scattering. J. Chem. Phys. **80**, 2514 (1984)
64. Mies, F., Julienne, P.S.: A multichannel quantum defect analysis of two-state couplings in diatomic molecules. J. Chem. Phys. **80**, 2526 (1984)
65. Müller, T.-O., Kaiser, A., Friedrich, H.: s-Wave scattering for deep potentials with attractive tails falling off faster than $-1/r^2$. Phys. Rev. **84**, 032701 (2011)
66. Müller, T.-O., Kaiser, A., Friedrich, H.: Addendum to "s-Wave scattering for deep potentials with attractive tails falling off faster than $-1/r^2$". Phys. Rev. **84**, 054702 (2011)
67. Müller, T.-O.: Threshold law far attractive inverse-cube interactions. Phys. Rev. Lett. **110**, 260401 (2013)
68. Moerdijk, A.J., Verhaar, B.J., Axelsson, A.: Resonances in ultracold collisions of ^{6}Li, ^{7}Li, and ^{23}Na. Phys. Rev. A **51**, 4852 (1995)
69. Madison, K.W., Wang, Y., Rey, A.M., Bongs, K. (eds.): Annual Review of Cold Atoms and Molecules, vol. 1. World Scientific, Singapore (2013)
70. Oberst, H., Kouznetsov, D., Shimizu, K., Fujita, J., Shimizu, F.: Fresnel diffraction mirror for an atomic wave. Phys. Rev. Lett. **94**, 013203 (2005)
71. Peek, J.M.: Eigenparameters for the $1s\sigma g$ and $2p\sigma u$ orbitals of H_2^+. J. Chem. Phys. **43**, 3004 (1965)
72. Paulsson, R., Karlsson, F., LeRoy, R.J.: Reliability of high-order phase integral eigenvalues for single and double minimum potentials. J. Chem. Phys. **79**, 4346 (1983)
73. Phys. Rev. Focus: Apply quantum principle with caution, http://prlo.aps.org/story/v4/st26 (1999)
74. Pasquini, T., Shin, Y., Sanner, C., Saba, M., Schirotzek, A., Pritchard, D.E., Ketterle, W.: Quantum reflection from a solid surface at normal incidence. Phys. Rev. Lett. **93**, 223201 (2004)
75. Quémener, G., Julienne, P.S.: Ultracold molecules under control. Chem. Rev. **112**, 4949 (2012)
76. Raab, P., Friedrich, H.: Quantization function for deep potentials with attractive tails. Phys. Rev. A **78**, 022707 (2008)
77. Raab, P., Friedrich, H.: Quantization function for potentials with $-1/r^4$ tails. Phys. Rev. A **80**, 052705 (2009)
78. Shimizu, F.: Specular reflection of very slow metastable neon atoms from a solid surface. Phys. Rev. Lett. **86**, 987 (2001)
79. Stein, A., Knöckel, H., Tiemann, E.: Fourier-transform spectroscopy of Sr_2 and revised ground-state potential. Phys. Rev. A **78**, 042508 (2008)
80. Steinke, M., Knöckel, H., Tiemann, E.: (X)1 $^1\Sigma^+$ state of LiNa studied by Fourier-transform spectroscopy. Phys. Rev. A **85**, 042720 (2012)
81. Schwarz, F., Müller, T.-O., Friedrich, H.: Near-threshold Feshbach resonances in interatomic collisions and spectra. Phys. Rev. A **85**, 052703 (2012)
82. Schuster, T., Scelle, R., Trautmann, A., Knoop, S., Oberthaler, M.K., Haverhals, M.M., Goosen, M.R., Kokkelmans, S.J.J.M.F., Tiemann, E.: Feshbach spectroscopy and scattering properties of ultracold Li + Na mixtures. Phys. Rev. A **85**, 042721 (2012)
83. Samuelis, C., Tiesinga, E., Laue, T., Elbs, M., Knöckel, H., Tiemann, E.: Cold atomic collisions studied by molecular spectroscopy. Phys. Rev. A **63**, 012710 (2000)
84. Stwalley, W.: The dissociation energy of the hydrogen molecule using long-range forces. Chem. Phys. Lett. **6**, 241 (1970)
85. Trost, J., Eltschka, C., Friedrich, H.: Quantisation in molecular potentials. J. Phys. B **31**, 361 (1998)

86. Ticknor, C.: Two-dimensional dipolar scattering. Phys. Rev. A **80**, 052702 (2009)
87. Verhaar, B.J., van den Eijnde, P.H.W., Voermans, M.A., Schaffrath, M.M.J.: Scattering length and effective range in two dimensions: application to adsorbed hydrogen atoms. J. Phys. A **17**, 595 (1984)
88. Voronin, A.Y., Froelich, P.: Quantum reflection of ultracold antihydrogen from a solid surface. J. Phys. B **38**, L301 (2005)
89. Voronin, A.Y., Froelich, P., Zygelman, B.: Interaction of ultracold antihydrogen with a conducting wall. Phys. Rev. A **72**, 062903 (2005)
90. Yu, I.A., Doyle, J.M., Sandberg, J.C., Cesar, C.L., Kleppner, D., Greytak, T.J.: Evidence for universal quantum reflection of hydrogen from liquid ^{4}He. Phys. Rev. Lett. **71**, 1589 (1993)
91. Zhao, B.S., Meijer, G., Schöllkopf, W.: Quantum reflection of He_2 several nanometers above a grating surface. Science **331**, 892 (2011)